Unclassified

Security Classification of this page

REPORT DOCUMENTATION PAGE

1a Report Security Classification Unclassified	1b Restrictive Markings
2a Security Classification Authority N/A	3 Distribution Availability of Report Approved for public release; distribution is unlimited.
2b Declassification/Downgrading Schedule N/A	
4 Performing Organization Report Number(s) N/A	5 Monitoring Organization Report Number(s) N/A
6a Name of Performing Organization: Naval Postgraduate School 6b Office Symbol: 55	7a Name of Monitoring Organization Naval Postgraduate School
6c Address *(city, state, and ZIP code)* Monterey, CA 93943-5000	7b Address *(city, state, and ZIP code)* Monterey, CA 93943-5000
8a Name of Funding/Sponsoring Organization: N/A 8b Office Symbol	9 Procurement Instrument Identification Number N/A
8c Address *(city, state, and ZIP code)*	10 Source of Funding Numbers Program Element Number / Project No / Task No / Work Unit Accession No

11 Title *(Include Security Classification)*
Thermodynamic Air/Sea Feedback Mechanisms in the Equatorial Pacific

12 Personal Author(s)
Robert S. Steadley

13a Type of Report	13b Time Covered	14 Date of Report *(year, month,day)*	15 Page Count
Master's Thesis		1992 September 15	105

16 Supplementary Notation The views expressed in this thesis are those of the author and do not reflect the official policy or position of the Department of Defense or the U.S. Government.

17 Cosati Codes			18 Subject Terms *(continue on reverse if necessary and identify by block number)*
Field	Group	Subgroup	Mixed Layer, Kraus-Turner, El Nino, Equatorial Pacific

19 Abstract

The occurrence of the El Nino Southern Oscillation (ENSO) has been studied from numerous air-ocean interaction aspects, yielding theories implying a positive-only correlation between the time rate of change of sea surface temperature anomaly ($\partial T's/\partial t$) and the corresponding change in the depth of the ocean mixed layer (h'). However, an alternate proposal by Chu (1991a,b, 1992) holds that there are both positive and negative correlations between $\partial T's/\partial t$ and h'. Chu's proposal, based upon the modified Kraus-Turner ocean mixed layer (OML) thermodynamic model, goes further to say that the regions occupied by these positive and negative correlation values correspond roughly to those occupied by positive and negative values of a surface forcing function, P, that is an indication of the strength of the counteracting surface forcings of wind work and buoyant damping. The model-generated fields of surface wind stress, net heat flux, sea surface temperature, and primary (mixed) layer depth are analyzed for a two year ENSO event, 1986 - 87, covering the region of the equatorial Pacific, 10N to 10S and to 140E to 80W, in order to determine the validity of these theories. The results shows a fairly uniform P-field over the entire period, consisting of a negative P-field (indicative of a shallowing regime) in most of the western Pacific and in the far eastern part of the eastern Pacific with a positive P-field (indicative of an entrainment regime) in between. The correlations between $\partial T's/\partial t$ and h' show that there exists both positive and negative correlations between $\partial T's/\partial t$ and h', however, there is no appreciable similarity between the regions occupied by positive and negative correlations and those occupied by positive and negative P-values.

20 Distribution/Availability of Abstract	21 Abstract Security Classification
[X] unclassified/unlimited [ ] same as report [ ] DTIC users	Unclassified
22a Name of Responsible Individual: Peter C. Chu	22b Telephone *(Include Area code)*: (408) 646-3257 / 22c Office Symbol

DD FORM 1473, 84 MAR 83 APR edition may be used until exhausted

All other editions are obsolete

security classification of this page

Unclassified

Approved for public release; distribution is unlimited.

Thermodynamic Air/Ocean Feedback Mechanisms in the Equatorial Pacific.

by

Robert S Steadley
Lieutenant , United States Navy
B.S., United States Naval Academy, 1985

Submitted in partial fulfillment of the requirements for the degree of

MASTER OF SCIENCE IN PHYSICAL OCEANOGRAPHY

from the

NAVAL POSTGRADUATE SCHOOL
September 1992

ABSTRACT

The occurrence of the El Nino Southern Oscillation (ENSO) has been studied from numerous air-ocean interaction aspects, yielding theories implying a positive-only correlation between the time rate of change of sea surface temperature anomaly ($\partial T'_s/\partial t$) and the corresponding change in the depth of the ocean mixed layer (h'). However, an alternate proposal by Chu (1991a,b, 1992) holds that there are both positive and negative correlations between $\partial T'_s/\partial t$ and h'. Chu's proposal, based upon the modified Kraus-Turner ocean mixed layer (OML) thermodynamic model, goes further to say that the regions occupied by these positive and negative correlation values correspond roughly to those occupied by positive and negative values of a surface forcing function, P, that is an indication of the strength of the counteracting surface forcings of wind work and buoyant damping. The model-generated fields of surface wind stress, net heat flux, sea surface temperature, and primary (mixed) layer depth are analyzed for a two year ENSO event, 1986 - 87, covering the region of the equatorial Pacific, 10N to 10S and to 140E to 80W, in order to determine the validity of these theories. The results shows a fairly uniform P-field over the entire period, consisting of a negative P-field (indicative of a shallowing regime) in most of the western Pacific and in the far eastern part of the eastern Pacific with a positive P-field (indicative of an entrainment regime) in between. The correlations between $\partial T'_s/\partial t$ and h' show that there exists both positive and negative correlations between $\partial T'_s/\partial t$ and h', however, there is no appreciable similarity between the regions occupied by positive and negative correlations and those occupied by positive and negative P-values.

TABLE OF CONTENTS

LIST OF FIGURES

I. INTRODUCTION

A. RATIONALE FOR STUDY

Currently, there are several significant theories containing simple ocean thermodynamics that have been developed to study the phenomenon of the El Nino Southern Oscillation (ENSO). Certain theories differ, however, concerning the correlation between the time rate of change of sea surface temperature anomaly ($\partial T'_s/\partial t$) and the anomaly of upper layer thickness (η), or mixed layer depth anomaly (h'). The relationship between η and h' will be explained in the following background section, but for now, it is sufficient to say that they are interchangeable.

Numerous published theories (Wyrtki, 1975; McCreary, 1983; Cane and Zebiak, 1985; Battisti, 1988,1989; and Hirst, 1986 among others) show a positive-only correlation between $\partial T'_s/\partial t$ and η. The modified Kraus-Turner (K-T) ocean mixed layer (OML) thermodynamic model proposed by Chu (1991a,b, 1992) holds, conversely, that there are both positive and negative correlations between these two parameters depending on the physical process being considered. The purpose of this study is to analyze data to establish the proper correlation between these parameters and thus establish a correct basis for the study of the El Nino phenomenon.

1. Upwelling Physics

The theories based on upwelling physics are repesented by the follwing thermodynamic equation (Hirst, 1986):

$$\partial T'_s/\partial t + \bar{\mathbf{u}} \bullet \bar{T}_x = k(\sigma\eta - T'_s), k > 0, \sigma > 0 \qquad (1)$$

which implies a positive correlation between $\partial T'_s/\partial t$ and η'. In the limit of large k, this equation reduces to $T'_s = \sigma\eta$, indicating a positive-only correlation between T'_s and η.

2. Ocean Mixed Layer Physics

Chu (1991a,b, 1992) draws a distinction between "upwelling physics" and "OML physics" in dealing with the correlation between $\partial T'_s/\partial t$ and h'. When considering "upwelling physics," based upon a cooling upper layer where the outgoing heat flux from the base of the mixed layer is greater than the incoming heat flux, the following relationship is valid:

$$\partial T'_{s/} \partial t \sim h'_w \qquad (2)$$

where there is a positive correlation between $\partial T's / \partial t$ and h'. Based upon this type of physics, equation (1) of the Hirst model is valid. However, when considering "OML physics", where the upper layer may be under either strong or weak wind forcing, there exist both positive and negative correlations between these two parameters

$$\partial T'_s / \partial t \sim (+/-) h'_w \qquad (3)$$

where there exists a positive correlation for strong wind forcing and negative correlation for weak wind forcing. Chu takes this relationship one step further, relating these positive and negative correlations to corresponding positive and negative values of a surface forcing function, P. This function will be discussed further in the following section.

B. BACKGROUND

1. Relationship of Mixed Layer Depth to Upper Layer Thickness Anomalies

The value of the upper layer thickness anomaly, η, is based on the position of the main thermocline, and is defined as:

$$\eta = p / g' - d \qquad (4)$$

where $g' = g\Delta\rho / \bar{\rho}$, η is the instantaneous change in the depth of the thermocline, and d is the initial depth of the mixed layer. Figure 1 illustrates the physical relationship between h and η.

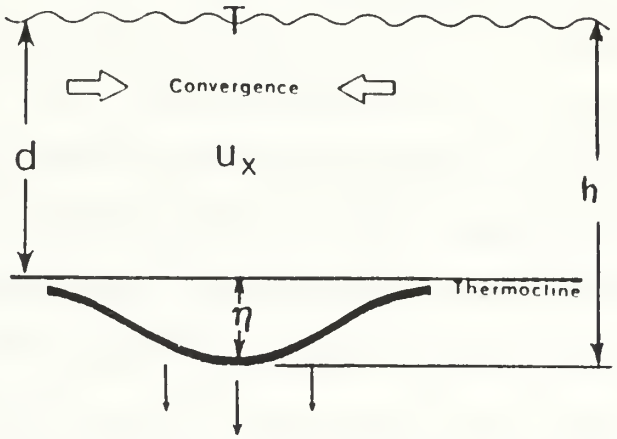

Figure 1. Illustration of upper layer anomaly, η, where d represents the initial thickness, and h represents the instantaneous mixed layer depth (from Yamagata, 1985).

Essentially, η represents the change in the depth of the thermocline lying just below the mixed layer, and therefore corresponds to the mixed layer depth anomaly, h'.

2. Significance of Surface Forcing function, *P*

A discussion of P should begin with the modified K-T model that introduced P as a surface forcing function. The value of P, whether positive or

negative, is indicative of the predominant surface forcing, wind work or buoyant damping respectively, on the OML, and is defined by the following equation:

$$P = C_1 u_{w*}^3 - C_2 \alpha g h_w Q_0 / \rho_{w0} c_{pw} \qquad (5)$$

(a) (b)

where C_1 and C_2 are tuning coefficients, u_{w*} is the water surface friction velocity defined as $(C_D \rho_{ao}/\rho_{wo})^{1/2} | V_b |$, V_b is the surface wind velocity, h_w is the thickness of the OML, Q_o is the net surface heat flux, ρ_{a0} and ρ_{w0} are characteristic values of surface air density and water density, and α is the thermal expansion coefficient. The values used for the tuning coefficients, C_1 and C_2, are 1.0 and 0.5 respecitively (Schneider and Muller, 1990). Term (a) represents the surface forcing due to wind work, and term (b) defines the surface forcing due to buoyant forcing/damping. Wind work acts to increase turbulence in the mixed layer, and thus increase the depth of the mixed layer. Buoyant damping is caused by downward heat flux, $+Q_o$, which acts to stabilize the mixed layer by heating the upper portion of the mixed layer leading to stratification and thus a shallowing of the mixed layer. Strong surface wind forcing, u_{w*}, will result in a positive value for P. Likewise, strong downward heat flux, Q_o, accompanied by moderate to weak wind forcing, will result in a negative value for P. Generally, the value of P varies from positive to negative throughout the ocean basin based on the diurnal and seasonal variations in Q_o and the synoptic and seasonal variations in u_{w*}.

The modified K-T model incorporates this P-value in the following equation:

$$\partial T'_s / \partial t + \bar{\mathbf{u}}_{\mathbf{w}} \bullet \nabla T_s = \frac{Q_0 - \Lambda_w(P) Q_{-h}}{\rho_{w0} c_{pw} h_w} \qquad (6)$$

(a) (b) (c)

where term (a) is the rate of change for T_s, term (b) the horizontal advection of T_s, and term (c) the thermodynamic forcing, including the heat flux at the base of the mixed layer, Q_{-h}. Of significance in term (c) is the heavyside step function, $\Lambda_w(P)$. This function is referred to as an OML "switcher." For positive values of P, the value of the switcher is 1, and for zero or negative values of P, the value of the switcher is 0. These two cases have the following effect on the modified K-T model in equation (6):

a. $P \leq 0$

In this case, the value of $\Lambda(P)$ is 0, yielding the following equation:

$$\partial T'_s / \partial t + \vec{u}_w \bullet \nabla T_s = \frac{Q_o}{\rho_{w0} c_{pw} h_w} \qquad (7)$$

Here, a negative P-value results from weak wind forcing and/or strong downward heat flux, causing a shallowing in the OML. Since the mixed layer will heat more rapidly as its depth decreases, there will be a positive correlation between h' and $\partial T'_s \partial t$. This case is illustrated in figure 2.

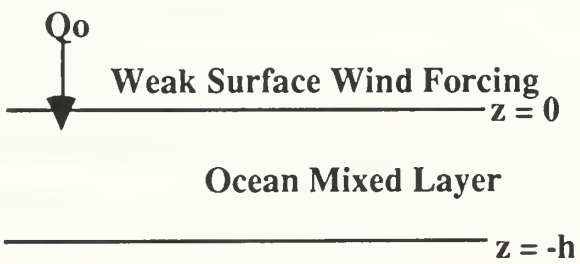

Figure 2. Kraus-Turner OML Thermodynamics under weak wind forcing, P≤0 (from Chu, 1991a).

b. $P > 0$

In this case, the value of $\Lambda(P)$ is 1, yielding:

$$\partial T'_s / \partial t + \vec{u}_w \bullet \nabla T_s = \frac{Q_o - Q_{-h}}{r_{w0} c_{pw} h_w} \qquad (8)$$

As noted before, a positive P-value results from strong wind forcing, which causes entrainment of deep water into the OML, as indicated by the presence of the Q_{-h} term. Since Q_{-h} is greater than Q_o, the OML is referred to as a "cooling layer" (Miller, 1976), and an increase in the mixed layer depth will be accompanied by a corresponding increase in $\partial T'_s/\partial t$. Thus, there would be a positive correlation between h' and $\partial T'_s/\partial t$. In physical terms, the thicker the layer becomes the less rapidly it will cool. This case is illustrated in figure 3.

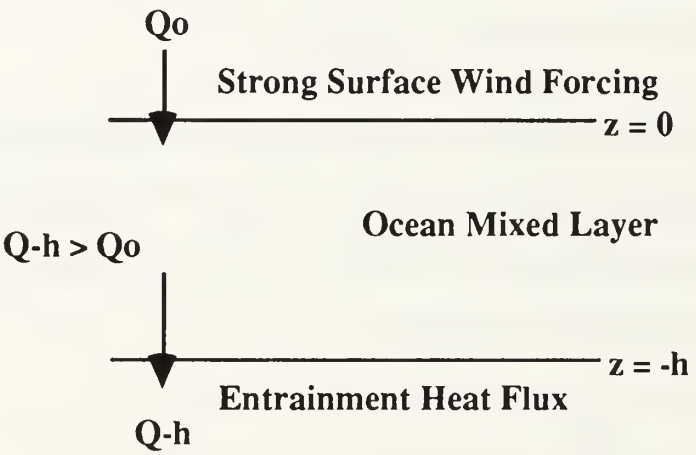

Figure 3. Kraus-Turner OML thermodynamics under strong wind forcing, P>0 (from Chu, 1991a).

II. DATA COLLECTION AND PROCESSING

A. DATA COLLECTION

In order to effectively study the correlation between $\partial T'_s/\partial t$ and h' and its relationship to the P-value, the following data sets are required: monthly mean net surface heat flux (Q_{net}), monthly mean surface wind stress (τ_w), daily mean sea surface temperature(T_s), and daily mean mixed layer depth (h). The area of coverage includes the majority of the equatorial Pacific. Therefore, the study area is chosen as 140 E to 80 W and 10N to 10S inclusive. Figure 4 is a map of the equatorial Pacific region. The time period is chosen to span a designated ENSO event, January 1986 - December 1987. Data was collected for this study from two sources, Fleet Numerical Oceanography Center (FNOC) in Monterey, California, and the National Center for Atmospheric Research (NCAR) in Boulder, Colorado. The data products received from FNOC, T_s and h, were generated by the Thermodynamic Ocean Prediction System (TOPS) - coupled Expanded Ocean Thermal Structure (EOTS) Analysis model. The data products received from NCAR were Q_{net}, τ_w, and T_s, and were archived from the European Center for Medium Range Weather Forecasting (ECMWF) synoptic forecasts. A description of these data sets and their forecasting and modeling methods is provided below.

1. FNOC Archive Data Sets

Data was acquired through FNOC from the archives of the Data Base Management Division. During the time period of 1986-87, the data products of sea surface temperature and primary (mixed) layer depth were generated by the TOPS- coupled EOTS (TEOTS) analysis technique. A discussion of the FNOC

data will include a section on TEOTS analysis methods and another section on TEOTS data product output.

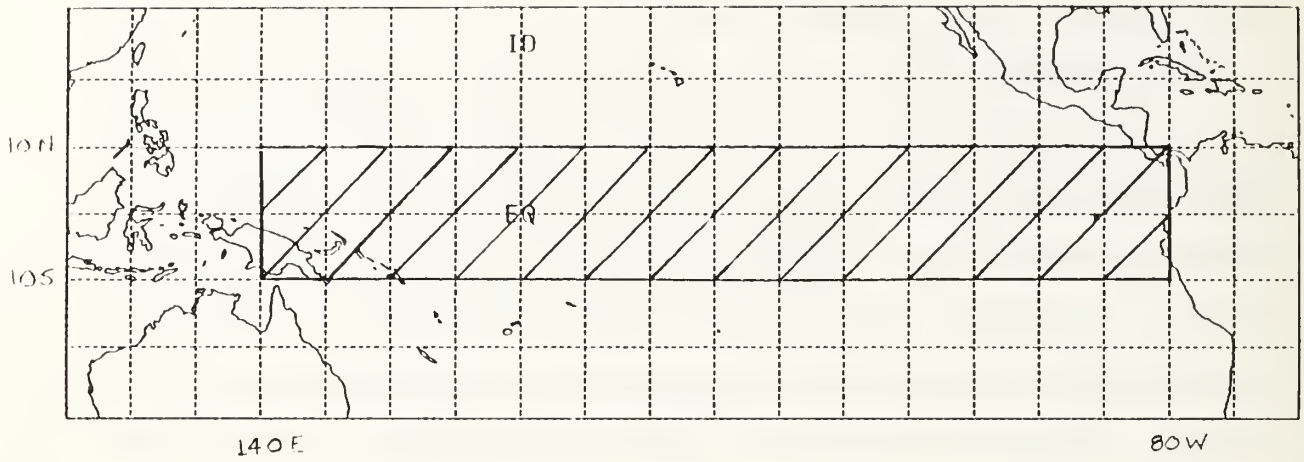

Figure 4. Equatorial Pacific region

a. TEOTS Analysis Method

The EOTS analysis scheme combines ocean thermal climatology with real time thermal observations, applying a series of corrections via the Fields-by-Information-Blending (FIB) analysis technique. The ocean climatology is drawn from an archive of coarse resolution (320 km) monthly climatology. The observations are provided by real time ship and satellite data. Daily Ship observations consist of about 150-200 XBT's , and 1200-2000 ship injection/ bucket temperature measurements. Daily Satellite measurements consist of 50,000-80,000 Multi-Channel Sea Surface Temperature (MCSST) retrievals from NOAA. This system is limited, however, since local bursts of atmospheric forcing, which cause considerable change in the mixed layer depth and sea surface temperature are often neglected by using such a sparse number of real time measurements. For this reason, FNOC adapted a system, endorsed by Elsberry and Garwood (1980) and Clancy and Martin (1981), coupling a synoptic mixed

layer model (TOPS) to the basic EOTS analysis to generate a continuously updated, real-time, analysis-forecast-analysis system. The gist of the system is to initialize the TOPS model daily using the EOTS analysis fields, produce a forecast field driven by observed and forecasted atmospheric forcing, and subsequently feed this field back into the EOTS analysis as a first-guess for the following analysis day. This system is collectively referred to as TEOTS, and appears in the form of a flow chart in figure 5 (FNOC, 1987).

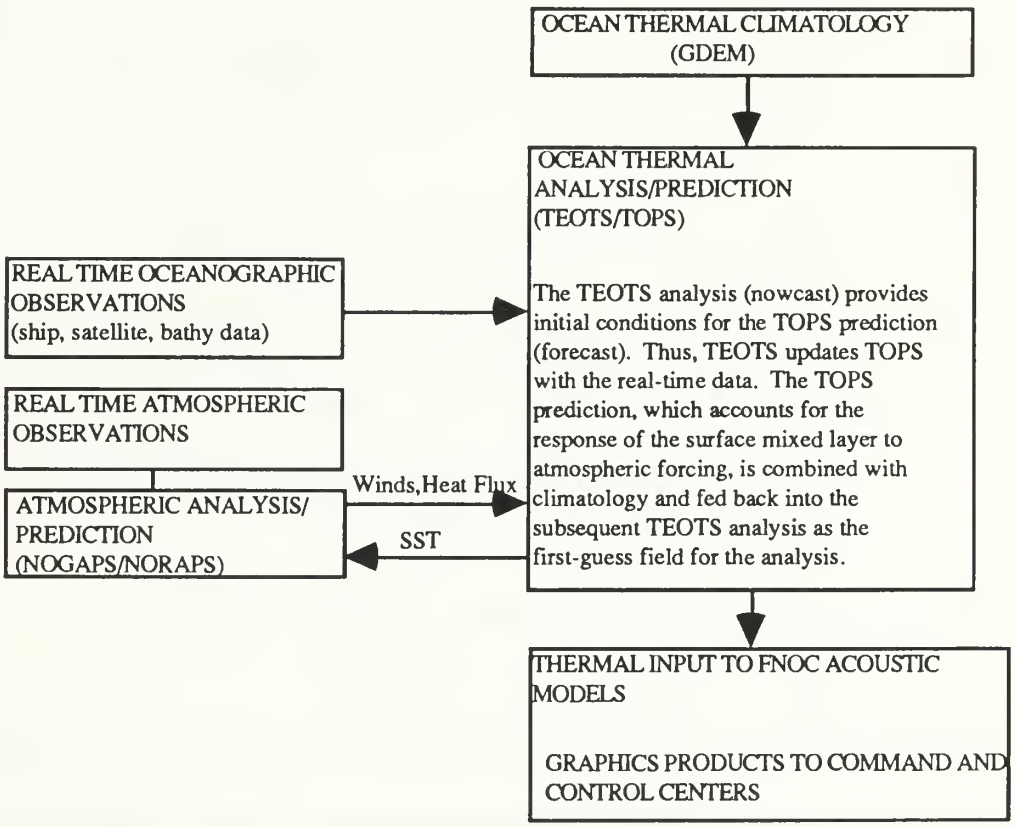

Figure 5. TEOTS Flow Chart (from FNOC, 1987)

One concern in deciding whether or not to use the TEOTS-generated data involves the relationship between Ts and h. One of main goals of this study is to determine a correlation between these two parameters, and therefore it is necessary to establish that there are no physical assumptions

concerning this correlation within the TOPS forecast that might bias the results of this study. The following is a brief discussion of the physics used in TOPS.

The TOPS consists of four prognostic equations representing the conservation of temperature, salinity, and momentum in the upper ocean (FNOC, 1987).

$$\frac{\partial \bar{T}}{\partial t} = \frac{\partial}{\partial z}(-\overline{w' T'} + \upsilon \frac{\partial \bar{T}}{\partial z}) + \frac{1}{\rho_w c}\frac{\partial \bar{F}}{\partial z} - \frac{\partial}{\partial x}(u_a \bar{T}) - \frac{\partial}{\partial y}(v_a \bar{T}) - \frac{\partial}{\partial z}(w_a \bar{T}) + A(\frac{\partial^2 \bar{T}}{\partial x^2} + \frac{\partial^2 \bar{T}}{\partial y^2}) \tag{9}$$

$$\frac{\partial \bar{S}}{\partial t} = \frac{\partial}{\partial z}(-\overline{w' S'} + \upsilon \frac{\partial \bar{S}}{\partial z}) - \frac{\partial}{\partial x}(u_a \bar{S}) - \frac{\partial}{\partial y}(v_a \bar{S}) - \frac{\partial}{\partial z}(w_a \bar{S}) + A(\frac{\partial^2 \bar{S}}{\partial x^2} + \frac{\partial^2 \bar{S}}{\partial y^2}) \tag{10}$$

$$\frac{\partial \bar{u}}{\partial t} = f\bar{v} + \frac{\partial}{\partial z}(-\overline{w' u'} + \upsilon \frac{\partial \bar{u}}{\partial z}) - D\bar{u} \tag{11}$$

$$\frac{\partial \bar{v}}{\partial t} = -f\bar{u} + \frac{\partial}{\partial z}(-\overline{w' v'} + \upsilon \frac{\partial \bar{v}}{\partial z}) - D\bar{v} \tag{12}$$

where T is the temperature, S is the salinity, u, v, and w are the x, y, and z components of the current velocity, F is the solar radiation flux (positive downward), ρ_w is the reference density, c is the specific heat of seawater, D is a damping coefficient, ν is a diffusion coefficient, z is the vertical coordinate (positive upward from the surface), and u_a, v_a, and w_a are the x, y, and z components of the "advection" current. The parameter A is a horizontal eddy

diffusion coefficient whose value depends on the horizontal grid spacing. Equations (9) - (12) exclude the effects of geostrophic flow, which was determined to have a negligible effect on mixed layer dynamics.

These equations were parameterized by the following boundary conditions (Mellor and Durbin, 1975 and Clancy and Martin, 1981):

$$\overline{w' T'} = -\ell q S_H \frac{\partial \bar{T}}{\partial z} \tag{13}$$

$$\overline{w' S'} = -\ell q S_H \frac{\partial \bar{S}}{\partial z} \tag{14}$$

$$\overline{w' u'} = -\ell q S_M \frac{\partial \bar{u}}{\partial z} \tag{15}$$

$$\overline{w' v'} = -\ell q S_M \frac{\partial \bar{v}}{\partial z} \tag{16}$$

where ℓ is the turbulence length scale, q is the square of twice the turbulent kinetic energy and is defined by the following equation:

$$\ell q S_M \left(\left(\frac{\partial u}{\partial z} \right)^2 + \left(\frac{\partial v}{\partial z} \right)^2 \right) + \ell q S_H \left(\frac{g}{\rho_w} \frac{\partial \rho}{\partial z} \right) - \frac{q^3}{15\ell} = 0 \tag{17}$$

The three terms in equation (17) represent wind forcing, or shear production, buoyant damping, and viscous dissipation respectively. The variables S_M and S_H are functions of the gradient Richardson number, Ri, defined as follows:

$$Ri = \frac{-\frac{g}{\rho_w} \frac{\partial \rho}{\partial z}}{\left[\left(\frac{\partial u}{\partial z} \right)^2 + \left(\frac{\partial v}{\partial z} \right)^2 \right]} \tag{18}$$

The Richardson number basically indicates the predominant forcing between shear production and buoyant damping. If the Richardson number exceeds a critical number, Ri = .23, buoyant damping stratifies the mixed layer sufficiently enough to inhibit the turbulent mixing of shear production, and the layer enters a shallowing regime (Miles, 1961 and LeBlond and Mysak, 1978). Conversely, if Ri $\leq$ .23, shear production dominates, resulting in entrainment and a deepening of the mixed layer. The extent to which the mixed layer deepens is dependent on the magnitude of the turbulent length scale, ℓ, defined as follows:

$$\ell = 0.1 \frac{\int_{-\infty}^{0} |z| q dz}{\int_{-\infty}^{0} q dz} \tag{19}$$

As seen in the progression through the prognostic equations (9) - (12) to the closure of equation (19), there are no assumptions made regarding the direct relationship of mixed layer depth to sea surface temperature. The TOPS model is a very meticulous mixed layer forecasting system whose only assumption excludes the presence of geostrophic flow. For this reason, the TEOTS analysis system was determined to be unbiased regarding the objective of this study.

b. TEOTS Analysis Output Description

The output of the TEOTS analysis took the form of two different grid schemes, one for T_s and one for h. Mixed layer depth is output on a grid using a polar stereographic projection. This type of scheme consists of 63 X 63 grids overlaid on maps of the Northern and Southern Hemispheres whose origins are the poles. The grid spacing is approximately 320 kilometers. A disadvantage of this grid scheme, when dealing with equatorial data, is that the resolution of the data decreases radially outward from the polar origin, yielding the worst resolution at the equator. Sea surface temperature is output on a grid using a

spherical, or Mercator, plot. This type of scheme consists of a 73 X 144 grid overlaid on a Mercator projection of the globe. The grid spacing for the spherical plot is approximately 2.5°, or 280 kilometers. The contoured plots of monthly mean mixed layer depth are found in Appendix D. The contoured plots of monthly sea surface temperature are found in Appendix C.

2. NCAR/ECMWF Archived Data Sets

As previously mentioned, the ECMWF data sets were received from NCAR. A description of the numerical models used to generate this data will be quite brief due to the emphasis on mixed layer dynamics rather than the physics of the processes driving atmospheric forcing.

a. ECMWF Numerical Weather Prediction

The wind and surface flux fields provided by ECMWF are generated by an operational model using numerical weather prediction. The model used for wind analysis and prediction produces 6-hourly forecasts on 15 standard levels in the vertical and on a 1.125° horizontal grid. The model combines observations obtained within a six hour window of the analysis time with a multivariate height, wind, and thickness system (Lorenc, 1981) from the preceding analysis period to produce a forecast for the following period. The method used to combine these two inputs, statistical interpolation, assigns weights to the these inputs, and uses geostrophy and other error checking criteria to smooth the results (Lonnberg, 1982). A system flow chart is shown in figure 8.

Once the surface wind field has been generated, the surface wind stress fields are computed using the relation:

$$\tau_0 = \rho C_D U^2 \qquad (20)$$

where ρ is the density of air in the planetary boundary layer, C_D is the drag coefficient over the surface, and U is the 10 meter wind provided by the foregoing model.

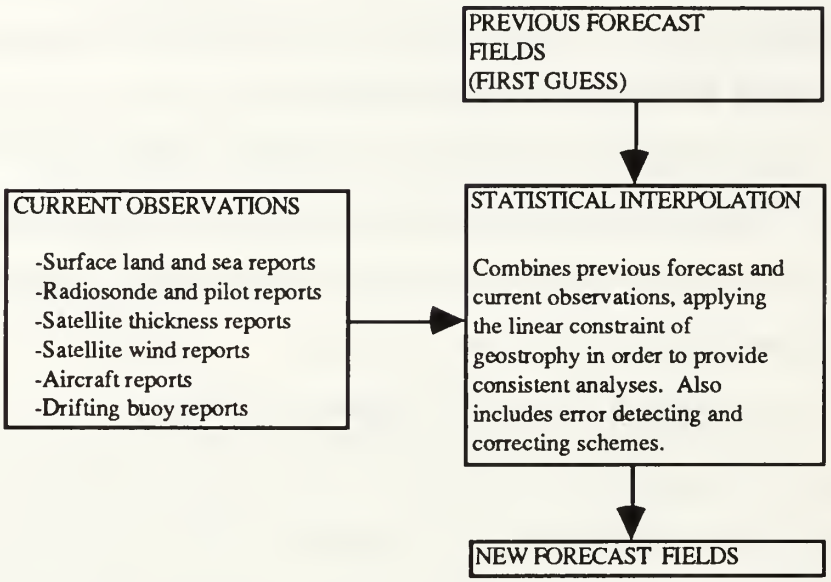

Figure 6. ECMWF analysis / forecast flowchart

Surface flux fields are simply a byproduct of the standard outputs (winds, temperature, potential temperature, and humidity) of the ECMWF model. Shortwave and longwave radiation are computed using straightforward atmospheric physics combined with satellite cloud imagery to form an algorithm modeling the behavior of the radiation budget. Radiation affects the ocean mixed layer both directly, by increasing or decreasing the heat flux driving the buoyant damping on the layer, and indirectly, by affecting the development of clouds and weather patterns which have a local effect on shear production. A schematic of these radiative processes is shown in figure 9. Longwave radiation

emitted by the surface is computed using the modified Stefan-Boltzman law

$$R_L = -\varepsilon\sigma T^4 \tag{21}$$

where ε is the emissivity of water, σ is the Stefan-Boltzman constant, and T is the temperature of the surface in degrees K. Since longwave radiation is emitted not only by the surface but by clouds and the atmosphere, the estimation of longwave radiation is a fairly complicated function of the earth and satellite-based soundings. Shortwave radiation at the top of the atmosphere is computed using an inverse square law coupled with Lambert's cosine law to yield

$$R_0 = S_0(d_m / d)^2 \cos\gamma \tag{22}$$

where S_0 is the solar constant, d_m/d is the ratio of the mean to the actual distance from the sun, and γ is the solar zenith angle. In order to obtain the actual surface value of shortwave radiation, absorption and scattering predominantly by clouds are also considered.

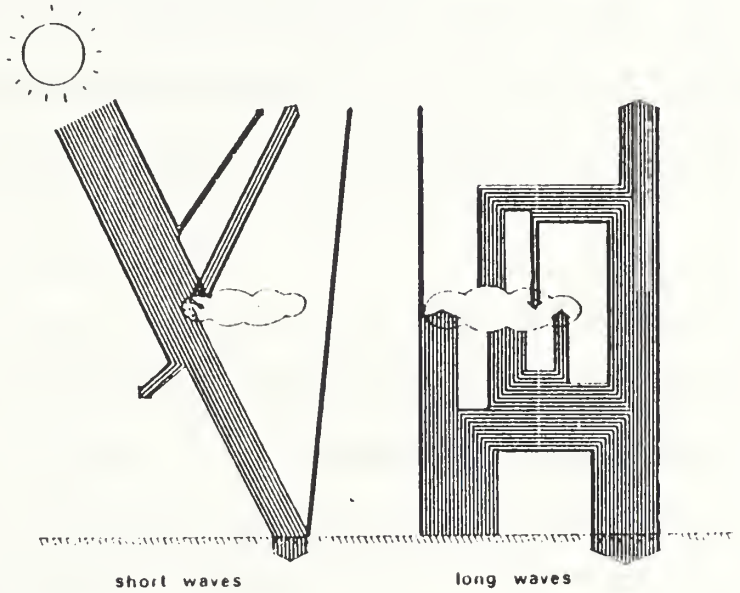

Figure 7. Radiative Processes in the Planetary Boundary Layer (from Wergen, 1982)

Latent heat flux is computed from the basic equation

$$H_L = L_e E \tag{23}$$

where L_e is the latent heat of evaporation/condensation and E is the rate of evaporation/condensation determined by the soundings. Sensible heat flux is calculated using the bulk aerodynamic approach based on the Monin-Obukhov similarity theory. This theory assumes that near the surface, vertical wind and potential temperature gradients depend only upon height, surface sensible heat flux, surface momentum flux, and the thermal expansion coefficient of air. Accordingly, ECMWF uses the temperature and winds at their lowest sounding level (33 m) and the surface temperature to compute the sensible heat flux at the surface as

$$H_s = [\frac{k}{\ln(h/z_0)}]^2 \bullet G(h/z_0, Ri)|V_h|\Delta\theta_h \qquad (24)$$

where k is von Karman's constant, h/z_0 is the ratio of height to roughness length, V_h is the wind velocity at the 33 m level, $\Delta\theta_h$ is the change in potential temperature between the surface and the 33 m level, and $G(h/z_0,Ri)$ is an analytical function that is continuously updated based on observations and performance of the model (Wergen, 1982). The Richardson number, Ri, is given by

$$Ri = \frac{gh\Delta\theta_h}{\theta|V_h|^2} \qquad (25)$$

and is an indication of stability within the surface boundary layer.

b. ECMWF Output Description

The ECMWF data fields accessed through NCAR were archived in grid-in-binary (GRIB) format. In order to compute the surface friction velocity, the following data sets were extracted: u-component of surface wind stress, and v-component of surface wind stress. In order to compute the net surface heat flux, the following data sets were extracted: net surface shortwave radiation, net

surface longwave radiation, surface sensible heat flux, and surface latent heat flux. The data fields are derived from 6 hour forecasts valid for 0 Z and 12 Z, and are plotted on a 1.125° grid. The contoured plots of monthly mean net surface heat flux are found in Appendix A. The contoured plots of monthly mean water surface friction velocity are found in Appendix B.

B. DATA PROCESSING

Data processing consisted of two basic steps. First, wind and heat flux data fields are combined with mixed layer data to compute values for the surface forcing function, P. Sea surface temperature and mixed layer depth were then analyzed to determine the correlation between $\partial T'_s/\partial t$ and h'.

1. P-Value Computation

The P-value fields were computed by equation (4). Since the majority of the data required for this computation came from the ECMWF forecasts, a 1.125° grid was chosen to represent the P-field. One P-field was calculated per month from January 1986 - December 1987. The following equation was used to compute the value of the net surface heat flux, Q_0:

$$Q_0 = Q_{sw} + Q_{lw} + Q_s + Q_l \tag{26}$$

where Q_{sw} is the shortwave radiative flux, Q_{lw} is the longwave radiative flux, Q_s is the sensible heat flux, and Q_l is the latent heat flux. All fluxes are in the units of watts per meter squared (W/m^2). These terms were defined as positive downwards and vice versa as archived, and thus the terms were simply added together to yield Q_0.

In order to obtain the value of water surface friction velocity, u_w^* the u and v-components of surface wind stress were first combined into a scalar value of surface wind stress, in units of N/m^2. This value of wind stress was then

converted to wind speed in the planetary boundary layer, V_b, in units of meters per second (m/s). The following equation was then used to calculate u_w*:

$$u_{w}^{*} \equiv (C_D \rho_{a0} / \rho_{w0})^{1/2} |V_b| \qquad (27)$$

The only remaining variable in the calculation of P is h. The only modification required here was to convert the depth from units of feet to meters. However, since the grid spacing for mixed layer depth was irregular and greater than that of winds and heat flux, a bivariable interpolation routine was used to interpolate the polar stereographic mixed layer depth grid field to the 1.125 Mercator grid. Contoured plots of monthly mean P-values are shown in Appendix E.

2. Correlation Computation

The first step in calculating the correlation between $\partial T'_s/\partial t$ and h' was to match the grids between T_s and h. For ease of plotting, the 2.5° grid for T_s was chosen. Here again a bivarible interpolation routine was used to interpolate the polar stereographic mixed layer depth grid field to the spherical T_s grid field. The objective of the data processing here is to obtain a correlation field based on daily trends of $\partial T'_s/\partial t$ and h' over each of the 24 months. Contoured plots of these correlations are shown in Appendix F.

III. SURFACE FIELDS

The daily surface data sets were averaged over each of the 24 months of the two year period to yield monthly mean averages.

A. HEAT BUDGET

In order to see the time variation of net surface heat flux, we plot the zonal values of net surface heat flux versus time for latitudes 5N, 0, and 5S (figure 7).

1. Western Equatorial Pacific

The heat budget in the western equatorial Pacific is characterized by a downward net surface heat flux throughout 1986-87. The highest downward heat flux occurs in the southwestern equatorial Pacific during the period of September -November 86 (225 W/m^2). In the northwestern equatorial Pacific, the downward heat flux values oscillate between strong during the spring and early fall to weak during the summer and winter. In the southwestern equatorial Pacific, downward heat flux values range between high in the early spring and late fall to weak during the summer months.

2. Mid Equatorial Pacific

The heat budget in the mid-equatorial Pacific is characterized by a predominantly upward net surface heat flux over the course of the two year study. The maximum upward heat flux occurs during Aug 86 (255.9 W/m^2) in the southern portion of the mid equatorial Pacific. North of the equator, heat fluxes are strongest during the winter, diminishing elsewhere. South of the equator, fluxes are again predominantly strongest in the winter, but proceeding further south, fluxes increase strongly in the summer.

3. Eastern Equatorial Pacific

The heat budget in the eastern equatorial Pacific has a typically downward net surface heat flux over a period of two years. The maximum downward heat flux occurs during Feb 87 (199.2 W/m^2) in the north. There is, however, no distinct seasonal pattern in the temporal fluctuation of heat flux in this region.

B. SURFACE FRICTION VELOCITY

The water surface friction velocity, u_w* as described by equation (5) will be referred to as wind speed since it is proportional to wind speed for a constant drag coefficient. The time evolution of zonal winds are plotted in the same manner as net surface heat flux and are shown in figure 8. Meridional winds are not plotted due to their low relative correlation with sea surface temperature change as shown by McPhaden and Hayes (1991).

1. Western Equatorial Pacific

a. North Equatorial Latitudes

The western equatorial Pacific is dominated by easterly winds over most of the two year period. The maximum easterly wind speed in the north (.26 cm/s) occur in December 1986. The trend in the north is typically strong easterlies during the winter and early spring.

b. South Equatorial Latitudes

The maximum easterly winds in the south (.23 cm/s) occur in June 1986. The trend in the south is typically strong easterlies during the summer months diminishing to weak during the winter months.

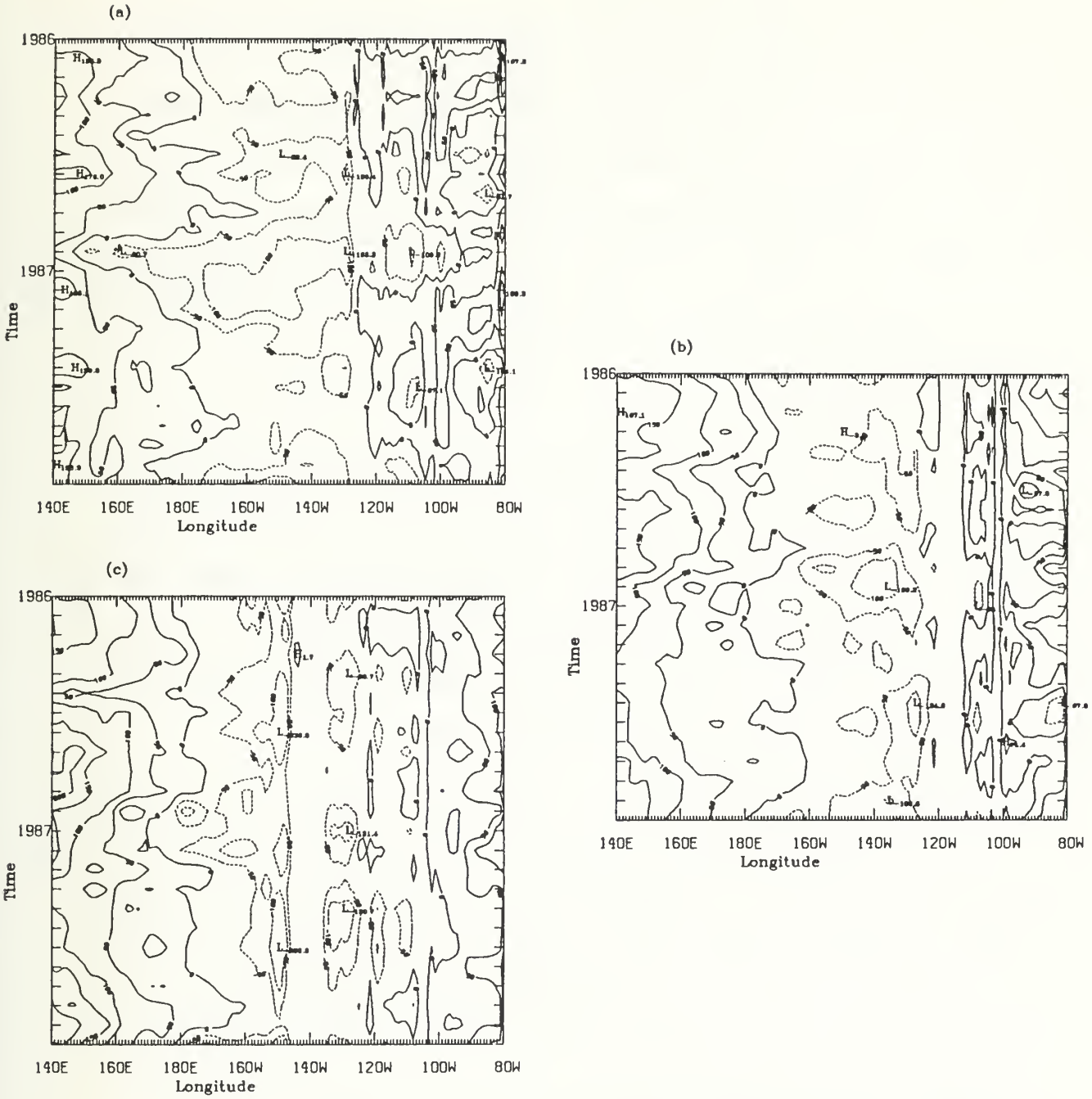

Figure 8. Time evolution of net surface heat flux (Q_o) for latitudes (a) 5N, (b) 0, and (c) 5S across the equatorial Pacific. The value of Q_o is defined as positive (solid) downwards, and negative (dashed) upwards.

2. Mid Equatorial Pacific

a. North Equatorial Latitudes

The mid equatorial Pacific is a region of seasonal wind variability. In the north the easterly winds dominate in late winter to early spring with the maximum wind speed (.36 cm/s) occurring in January 1987, and the westerlies dominate in the fall with maximum wind speed (.38 cm/s) occurring in September 1986. The summer months represent the transition between the easterlies and westerlies and thus the near-zero wind speeds are fairly consistent with the occurrence of the doldrums.

b. South Equatorial Latitudes

In the south, the seasonal shifts between easterlies and westerlies, differ from those in the north. Easterlies dominate in the early spring to late summer, with the maximum value (.26 cm/s) occurring in May 1987. The transition between easterlies and westerlies occur here in the early fall and late spring. The westerlies dominate during the late fall and winter months, with maximum value (.28 cm/s) occurring during March 1987.

3. Eastern Equatorial Pacific

The eastern equatorial Pacific follows the general patterns and trends of the mid equatorial Pacific. In the north, however, the shift between easterlies and westerlies occurs earlier, in the spring, and thus the maximum westerlies (.61 cm/s) occur in the summer, specifically July 1986. The maximum easterlies (.35 cm/s) occur in the early winter, specifically December 1986. In the south, the winds are fairly weak over the the two year period.

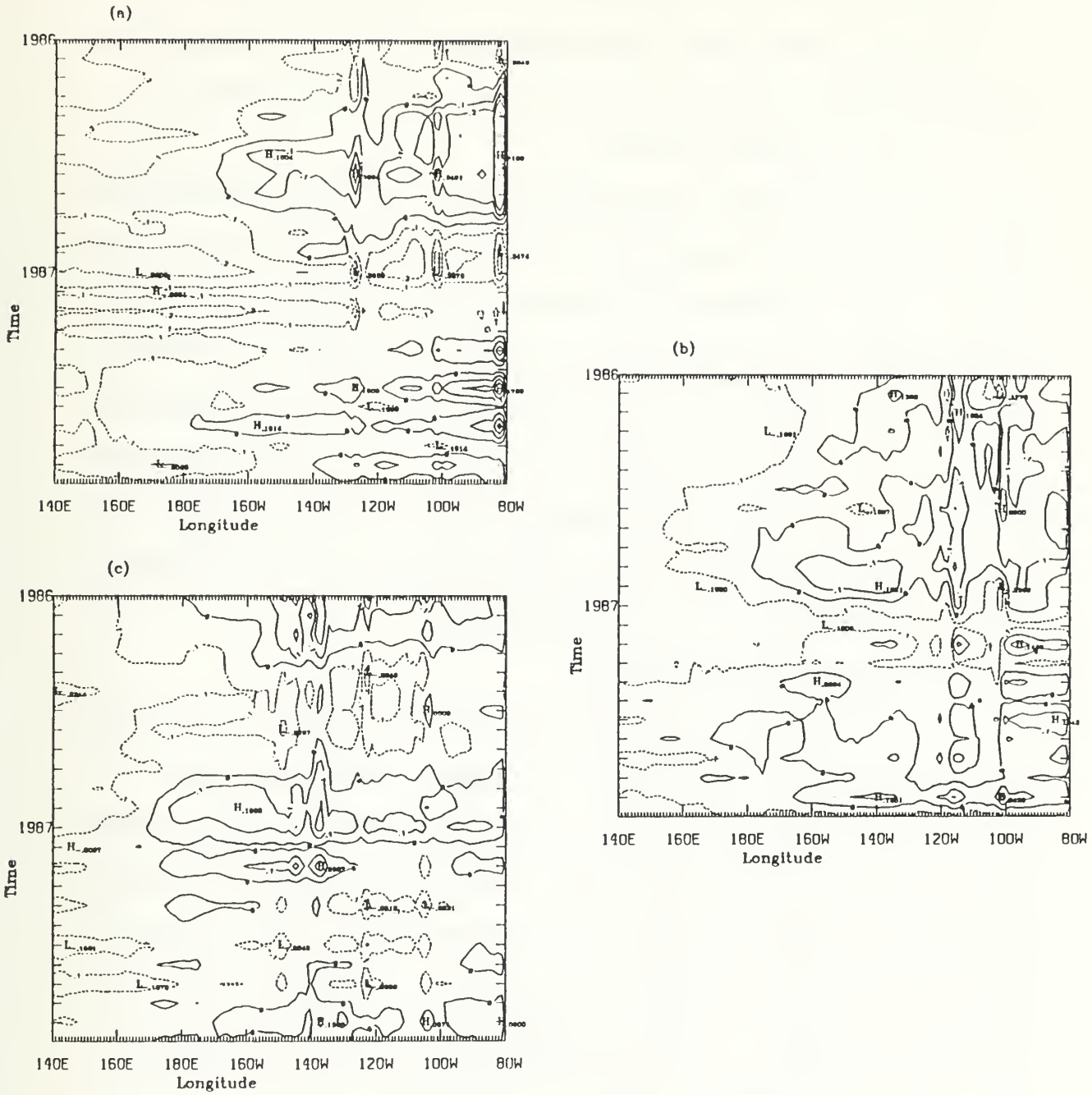

Figure 9. Time evolution of water surface friction velocity (u_w*) for latitudes (a) 5N, (b) 0, and (c) 5S across the equatorial Pacific. The value of u_w* is defined as positive (solid) for westerly winds and negative (dashed) for easterly winds.

C. SEA SURFACE TEMPERATURE

The time evolution of sea surface temperature, T_s, is plotted using the time-longitude plots used in the previous two sections and is shown in figure 9.

1. Western Equatorial Pacific

The western equatorial pacific possesses the highest values of sea surface temperature throughout the equatorial Pacific. These high values typically increase to the south. The highest values of sea surface temperature occur during the period October-December 1986 and March-July 87 (in excess of 30º C) in the southern portion of the mid-western equatorial Pacific. Temporally, the western equatorial Pacific has by far the lowest sea surface temperature variability (1º C). These findings are consistent with values obtained from Reynolds NMC/CAC Surface Temperature Analysis and the findings of McPhaden and Hayes (1991) and McPhaden (1988).

2. Eastern Equatorial Pacific

The eastern equatorial Pacific has the lowest values of sea surface temperature, generally decreasing to the southeast. The lowest values occur during September 1986 and August-September 1987 (about 20° C). The general trend of sea surface temperature shows warm values propagating eastward, peaking in March-April of each year, and propagating westward, peaking in September-October of each year. The temporal variability of temperature anomaly was also plotted versus time in the same manner as the latter. The results show that the eastern equatorial Pacific has the highest variability in sea surface temperature [O(1 C)], with the highest variability occurring in the far southeastern equatorial Pacific in March 1986 (3° C) and March 1987 (5º C).

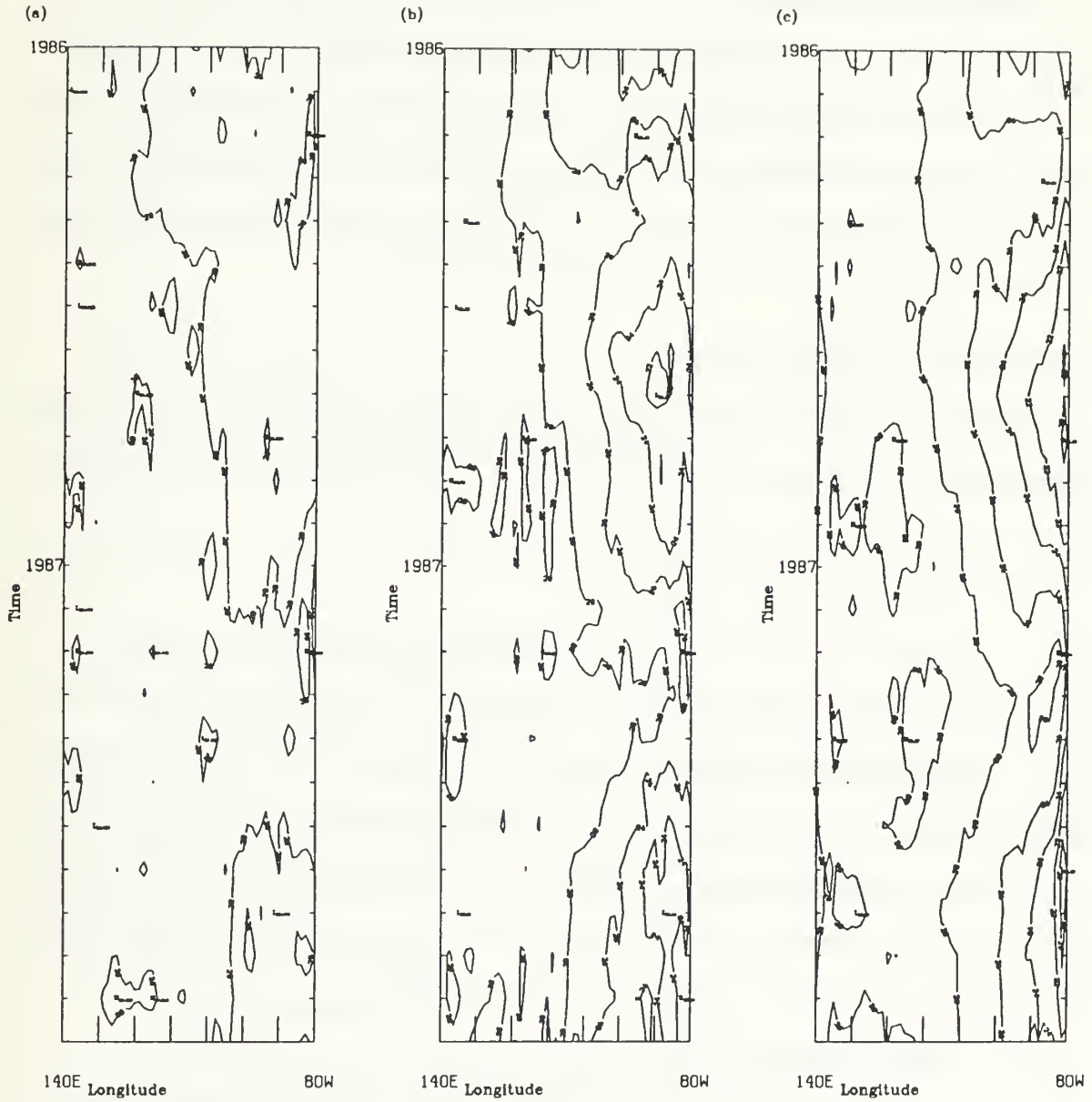

Figure 10. Time evolution of sea surface temperature (T_S) for latitudes (a) 5N, (b) 0, and (c) 5S across the equatorial Pacific.

IV. TWO REGIMES OF THE OML

The surface forcing function, or P-value is an indication of the dominant regime of the ocean mixed layer, whether entrainment (deepening), or shallowing. As mentioned previously, the surface forcing impacting these regimes are wind shear, or shear production, and heat flux, or buoyancy damping. These fields have been described in the chapter III. In addition to these variables, the mixed layer depth is also used in the calculation of the P-value.

A. MIXED LAYER DEPTH

Mixed layer depth is plotted and analyzed as per the previous sections. The plot of time evolution of mixed layer depth versus longitude is shown in figure 10.

1. Western Equatorial Pacific

The western equatorial Pacific has an intermediate range of mixed layer values, with higher values increasing to the east. The northern region has the largest values of mixed layer depth during the spring of each year (30 m). The lowest values of mixed layer depth occur during late summer each year (20 m) with values increasing toward the equator. The southern region has the largest values of mixed layer depth during late fall of each year (30 m), with the lowest values occurring during the spring of each year (17-19 m).

2. Mid Equatorial Pacific

The western portion of the mid-equatorial Pacific has largest values of mixed layer depth. The highest values of mixed layer depth occur just below the equator (50 m) and are sustained throughout the two year period with a comparatively low temporal variability (3-4 m).

3. Eastern Equatorial Pacific

The eastern equatorial Pacific maintains the lowest values of mixed layer depth, particularly in the far eastern portion. The lowest values (5 m) occur in the north (7.5 N) during the spring of each year. The lower latitudes (south of the equator) tend to have the highest values of mixed layer depth. The temporal trend reveals a deepening mixed layer in the fall and winter, returning to a shallow mixed layer depth during the spring and summer. This trend is more pronounced in the region south of the equator.

B. P-VALUE

Based on equation (5), the value of the surface forcing function, or P-value, is computed using the water surface friction velocity, u_{w*}, the mixed layer depth, h, and the net surface heat flux, Q_0. A plot of P-value, averaged over two years at each grid point, versus time is shown in figure 11 for latitude 5N, the equator, and 5S.

1. Western Equatorial Pacific

The western equatorial Pacific is dominated by negative P-values. In terms of the mixed layer, this would tend to indicate a shoaling regime. The largest negative value (2.3 $(cm/s)^3$) occurs to the far west (150 E) at the equator in February 1986. Although there is some temporal variability in the P-value in this region, there is no marked trend.

2. Mid Equatorial Pacific

The mid equatorial Pacific is characterized by positive P-values. In terms of the mixed layer, this would indicate an entrainment regime. The largest positive value (2.49 $(cm/s)^3$) occurs in the middle (150 W) just south of the

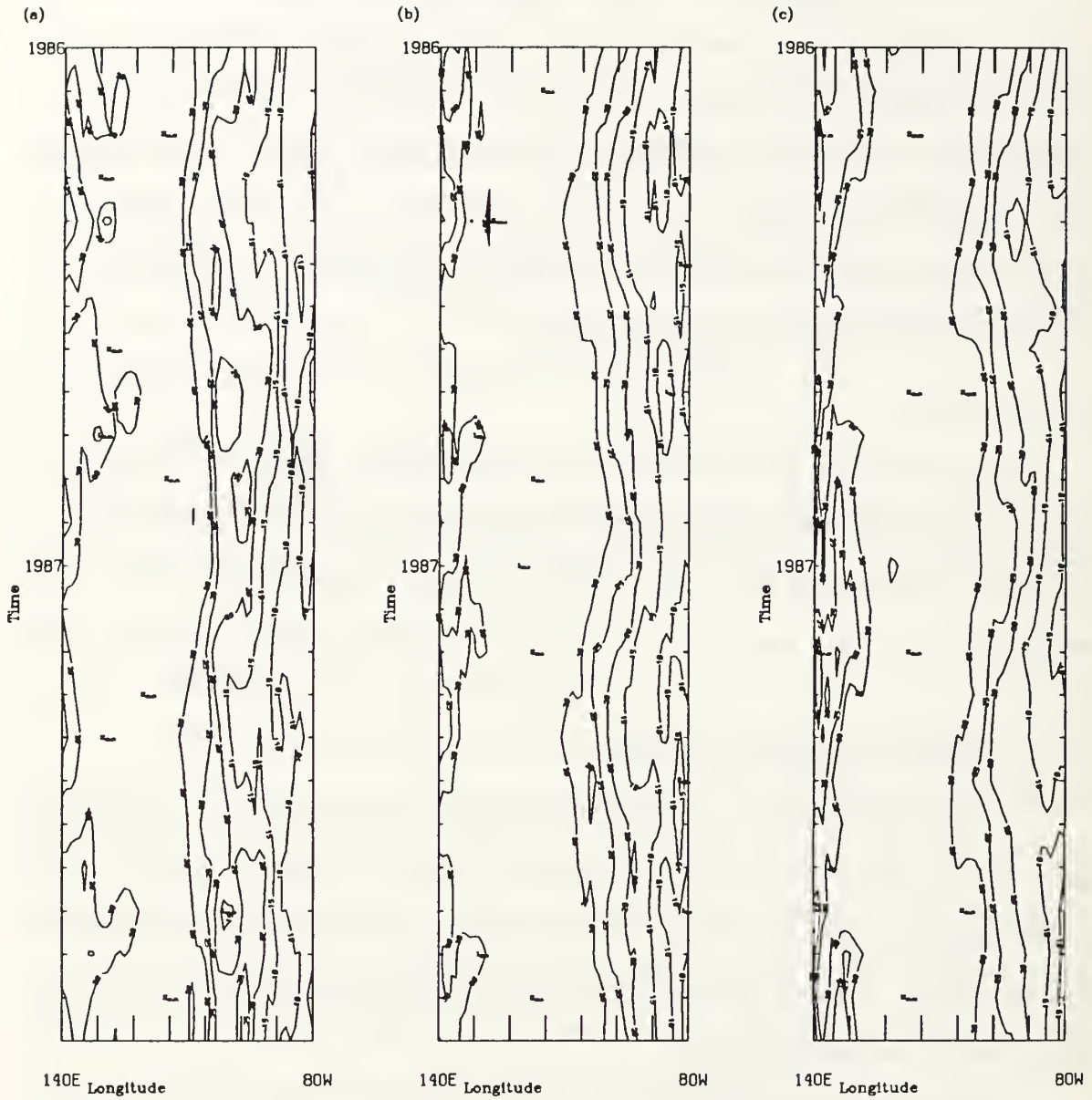

Figure 11. Time evolution of mixed layer depth (h) at latitudes (a) 5N, (b) 0, and (c) 5N across the equatorial Pacific.

equator in August 1986. There is no temporal trend in the magnitude of the P-value.

3. Eastern Equatorial Pacific

The eastern equatorial Pacific has both positive and negative P-values. The positive values of P occur toward the west, blending in with the positive values from the mid equatorial Pacific. The negative values occur to the southeast. The largest negative value (-0.58 $(cm/s)^3$) occurs to the far south in December 1986.

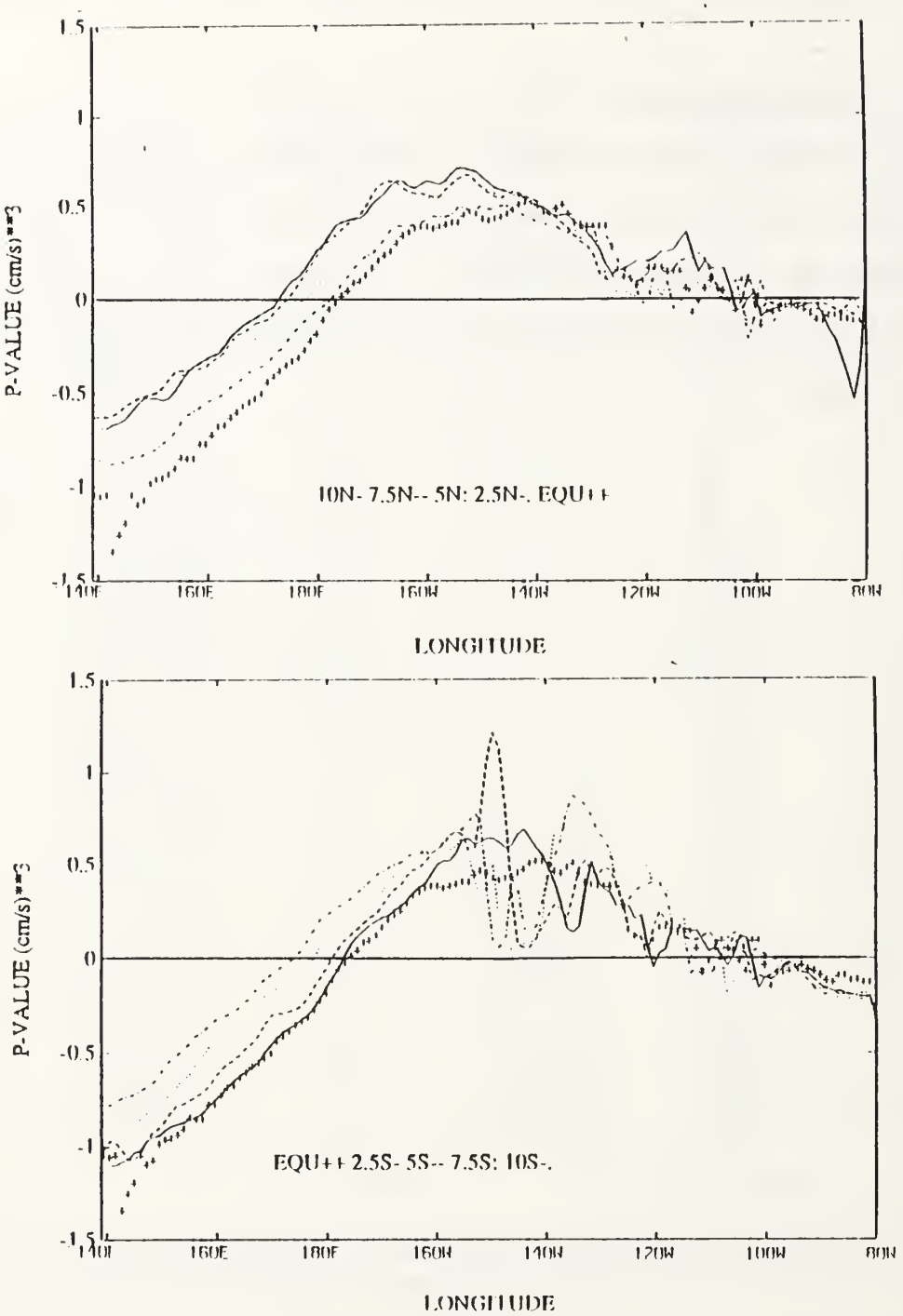

Figure 12. Average P-values for latitudes (a) 10N through 0, and (b) 0 through 10S across the equatorial Pacific.

V. CORRELATIONS BETWEEN $\partial T'_S/\partial T$ AND H'

Correlations between $\partial T'_s/\partial t$ and h' are computed with h' leading $\partial T'_s/\partial t$ by one day. Why is this lag time used? McPhaden and Hayes (1991) showed that the strongest correlation between sea surface temperature and wind forcing occurred with wind forcing leading temperature by one day (figure 11). It can therefore be assumed that mixed layer depth, which is driven by turbulence created by wind mixing, must therefore lead temperature on the same time scale.

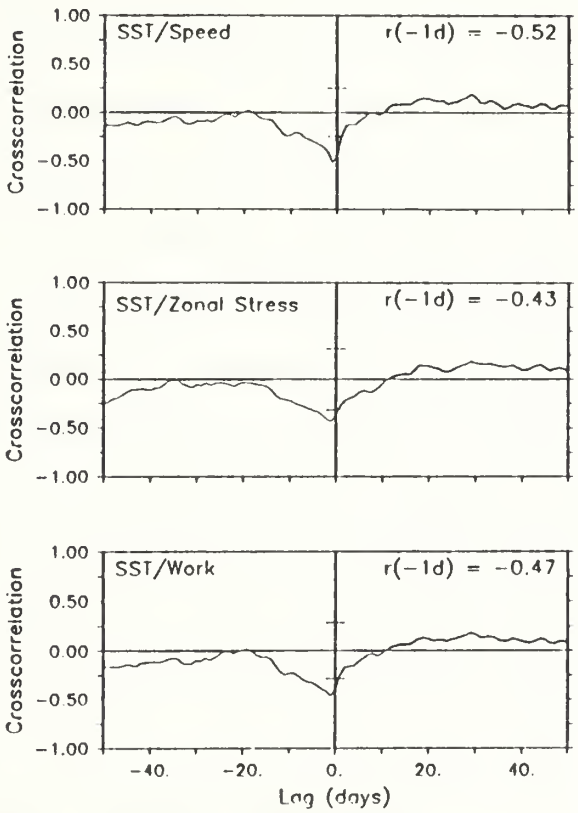

Figure 13. Cross correlations between SST and wind speed, zonal wind pseudostress, and wind pseudowork. Cross correlation extrema (r) and the lag (in days) at which they occur are shown. In each case, the lag indicates that cold SST follows high winds by 1 day (from McPhaden and Hayes, 1991).

In order to study this correlation and its relationship to P-value, the following process was used. First, $\partial T'_s/\partial t$ and h' were correlated based on daily values over the course of each of the 24 months, yielding monthly correlation fields. These fields, shown in Appendix F, are shaded dark for regions having negative correlations and light for regions having positive correlations. Comparing these fields to the P-fields shown in Appendix E, it is clear on the whole that there is no similarity between respective positive and negative regions as would be expected by "switching" theory.

The emphasis now shifts to choosing regions in the equatorial Pacific that exhibit typically strong entrainment and shallowing tendencies, based upon positive and negative P-values respectively. The regions chosen, based upon figure 11, are latitudes (10N-10S) along 165W for entrainment, and latitiudes along 160E for shallowing. The monthly correlations at these points are plotted over time, and are shown in figures 12 and 13. The result here is that over time, both of these regions undergo positive and negative correlations between $\partial T'_s/\partial t$ and h', regardless of the region chosen for its entrainment/shallowing tendency. It is clear from the apparently random oscillatory behavior of these correlations that the correlations between $\partial T'_s/\partial t$ and h' that we would expect from the modified Kraus-Turner model are not dominant on time scales of a day or more.

It is possible, however, that although the correlations between $\partial T'_s/\partial t$ and h' are not significant on these time scales, that the correlations between simply T'_s and h' might be significant. A test of this hypothesis is meaningful since the correlation between these two variables, T'_s and h' is also commonly accepted as being only positive. Correlations between daily values of T'_s and h' are computed over the two year period at 5S and longitudes 160E and 90W (shoaling regions)

and 165W (entrainment region) with the results plotted in figure 16. At 90W, the highest correlation (-0.8) occurs with h' leading T'_s by several days. The difference at this longitude is that instead of a negative maximum correlation for h' leading T'_s, the maximum correlation is positive (.35) and occurs with h' leading T'_s by nearly 100 days. Of importance here is that negative correlations are expected between temperature and mixed layer depth in regions of negative P-values (90W and 165E) and conversely positive correlations in regions of positive P-values (160E).

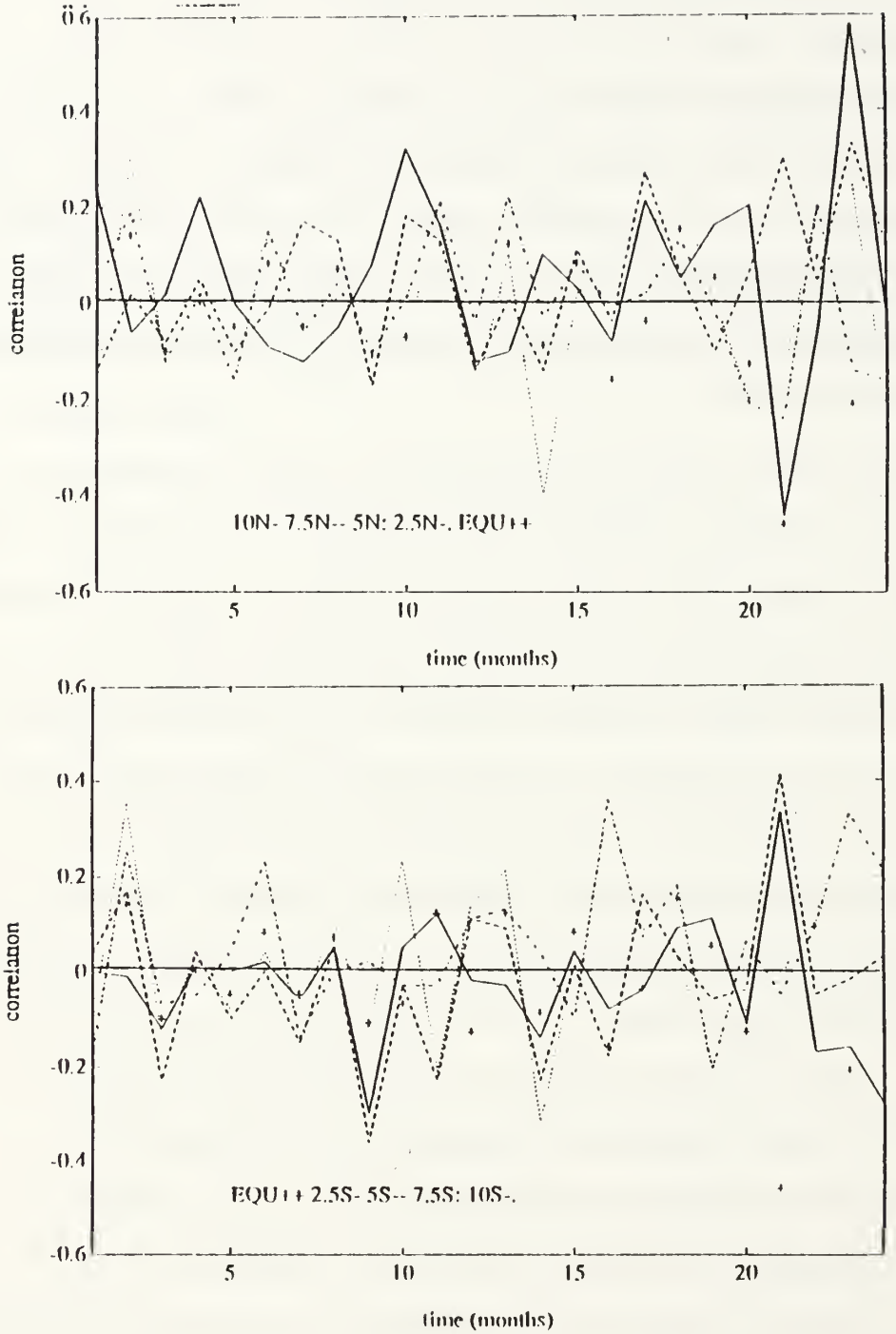

Figure 14. Monthly correlation of $\partial T'_s/\partial t$ and h' versus time for longitude 165W and (a) latitudes 10N - 0, (b) latitudes 0-10S.

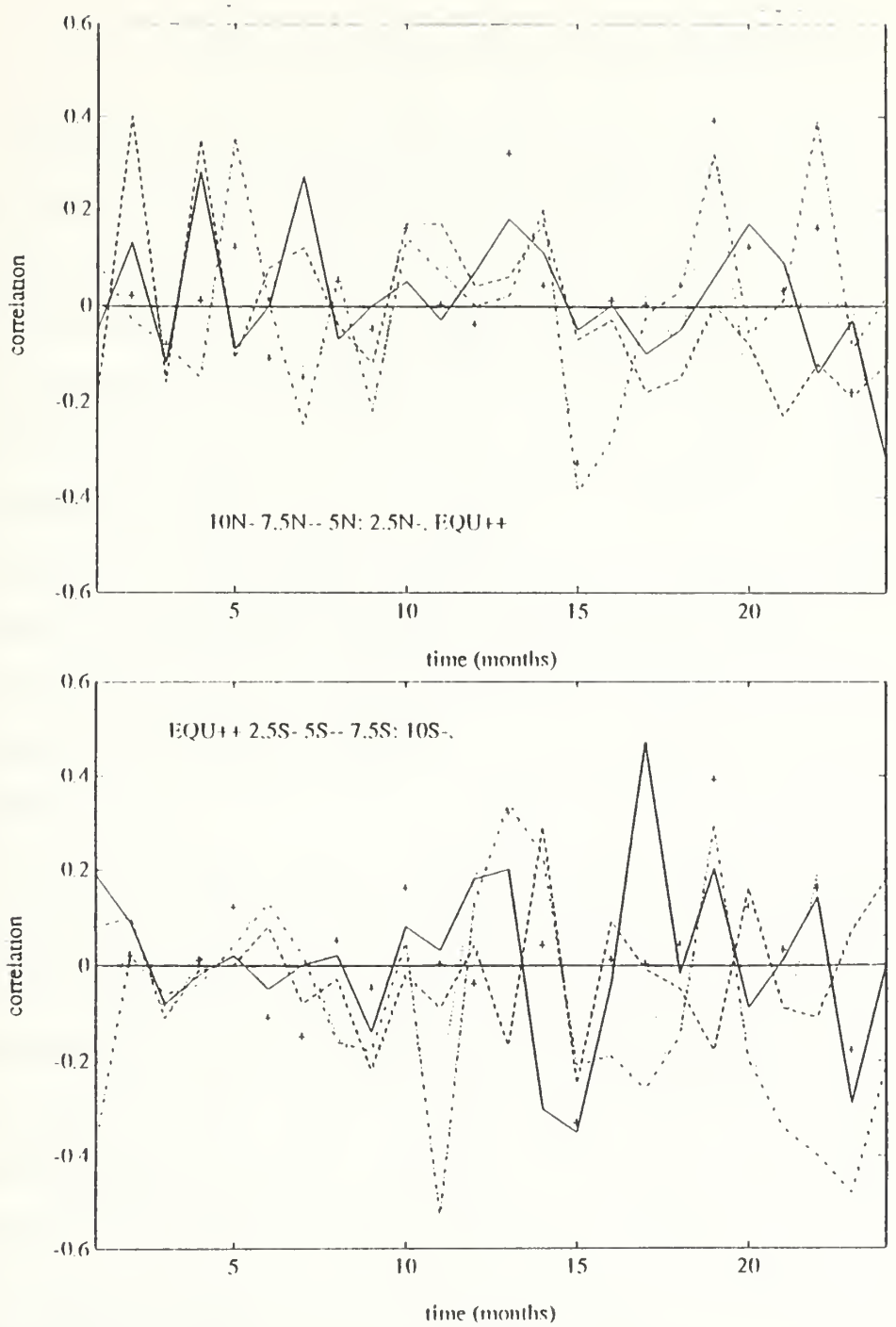

Figure 15. Monthly correlation of $\partial T'_s/\partial t$ and h' versus time for longitude 160E and (a) latitudes 10N - 0, (b) latitudes 0-10S.

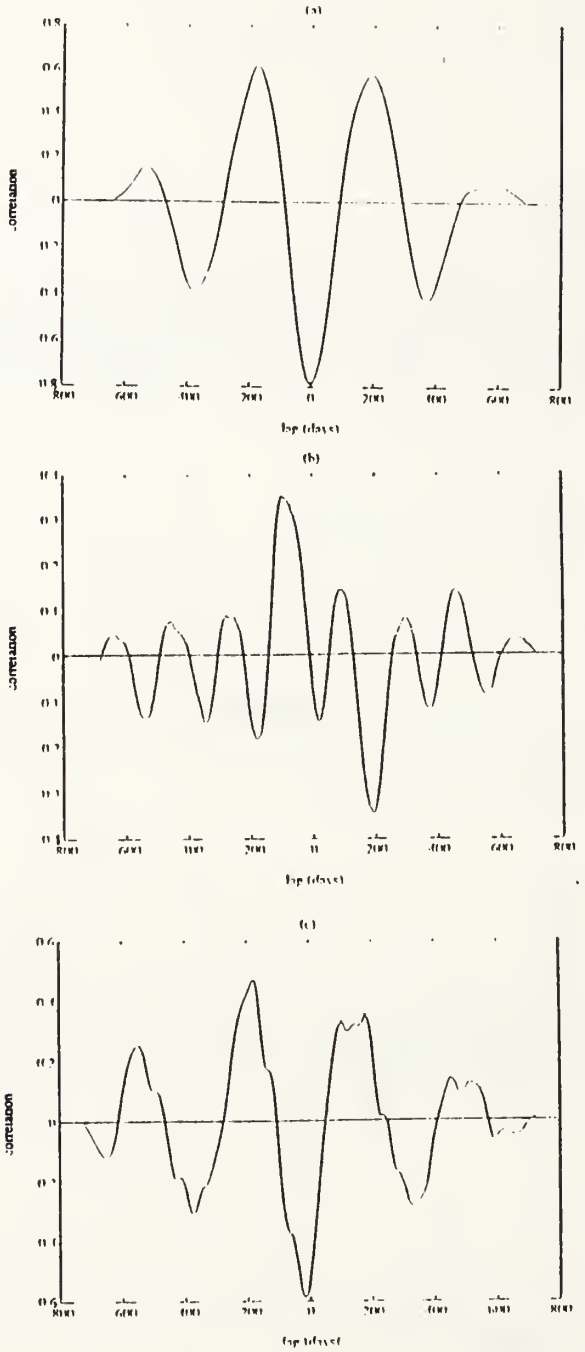

Figure 16. Correlation between daily values of T'_s and h' for the period 1986-87 with normalized values of correlation plotted against the lag(days) at latitude 5S and longitudes (a) 90W, (b)165W, and (c)160E.

VI. SUMMARY AND DISCUSSION

In studying the correlation between the time rate of change of sea surface temperature anomaly, $\partial T'_s/\partial t$, and the mixed layer depth anomaly, h', several findings are apparent. The most significant finding is that there exist both positive and negative correlations between $\partial T'_s/\partial t$ and h' at the various grid points chosen across the equatorial Pacific. This finding runs contrary to the upwelling physics theory showing a positive-only correlation. Since forward differencing was used in calculating $\partial T'_s/\partial t$, the correlations were based on a one day lead of h'. The reason for using this lead time is that mixed layer depth and sea surface temperature vary with mesoscale atmospheric variability (Elsberry and Garwood, 1978), and mixed layer depth changes caused by wind stress induced turbulence lead sea surface temperature changes by about one day (McPhaden and Hayes, 1991).

A second finding is that in the western equatorial Pacific (140E-180E) the monthly averaged values of the surface forcing function, P, are typically negative throughout the course of the two year period, indicating that this region is predominantly a shoaling regime. This is due largely to the strong downward net surface heat flux in this region. In the mid-equatorial Pacific (180E-120W), the monthly averaged values of the surface forcing function, P, are typically positive indicating that this region is predominantly an entrainment regime. Finally, the eastern equatorial Pacific is characterized by both positive and negative values, with negative values typically to the east indicating a general shallowing regime.

Although the correlation patterns between $\partial T'_s/\partial t$ and h' do not fit the P-value distribution with any degree of confidence, there is some similarity between

the correlations of T'_s and h' and P-values. It is found that h' leads T'_s by several days with a strong negative correlations (-0.8, -0.6) in regions of significantly negative P-values (90W, 160E). The converse is not so conclusive in that h' leads T'_s by nearly 100 days with a relatively strong positive correlation (0.35) in a region of positive P-values (165W).

VII. CONCLUSIONS AND RECOMMENDATIONS

A positive-only correlation between $\partial T'_s/\partial t$ and h' is commonly accepted in current thermodynamic theories regarding the El Nino phenomenon. In order for these theories to be valid, this relationship must hold true, particularly in the equatorial Pacific. Based on the results of this study, this positive-only correlation is not true in the equatorial Pacific. It would be premature at this point, though, to discount the validity of these theories based solely on the results of this study. To more sufficiently study this correlation and its relation to the P-value, the following study is recommended. First, the equatorial Pacific should be broken up into three regions, western, mid, and eastern, to investigate the unique surface forcings occurring in each. In each of these regions, thermistor chains or current meters should be utilized at, above (about 5N), and below (about 5S) the equator to measure hourly surface and subsurface temperatures. The subsurface temperatures could then be analyzed to determine mixed layer depth anomaly and subsequently correlated with the time rate of change of sea surface temperature anomaly. This finer time scale would not only conform more closely to the time scale of turbulence in the mixed layer, but would allow more flexibility in adjusting the lead time used in the correlations between mixed layer depth and sea surface temperature. The conflicting theories regarding this correlation could then be better resolved.

REFERENCES

Chu, P.C., An El Nino/ La Nina switcher, *TOGA Notes*, 16-21, 1991a.

Chu, P.C., Air-ocean surface heat exchange model and low frequency unstable modes in atmosphere and ocean, *Climate Variation, 5*, 484-487, 1991b.

Chu, P.C., Generation of low frequency unstable modes in a coupled equatorial troposhere and ocean mixed layer model, *Journal of Atmospheric Science, 49*, in press, 1992.

Clancy, R.M. and P.J. Martin, Synoptic forecasting of the oceanic mixed layer using the Navy's Operational Environmental Data Base: present capabilities and future applications", *Bulletin of the American Meteorological Society, 62*, 770-784, 1981.

Elsberry, R.L. and R.W. Garwood, Sea surface temperature anomaly generation in relation to atmospheric storms, *Bulletin of the American Meteorological Society, 59*, 786-789, 1978.

Elsberry, R. L. and R.W. Garwood, Numerical ocean prediction models - goals for the 1980's, *Bulletin of the American Meteorological Society, 61, 1556-1566*,1980.

Lonnberg, P., The ECMWF analysis system, ECMWF Seminar Proceedings on "Interpretation of numerical weather prediction products", 1-29, 1982.

Lorenc, A.C., A global three-dimensional multivariate statistical interpolation scheme, *Monthly Weather Review, 109*, 701-721, 1981.

McCreary, Julian P. Jr., A model of tropical ocean-atmospheric interaction, *Monthly Weather Review, 111*, 370-387.

McCreary, Julian P. Jr., and Anderson, David L. T., An overview of coupled ocean-atmosphere models of El Nino and the Southern Oscillation, *Journal of Geophysical Research, 96*, 3125ff, 1991.

Mellor, G.L. and T. Yamada, A hierarchy of turbulence closure models for geophysical fluid problems, *Reviews of Geophysics and Space Physics, 20*, 851-875, 1974.

Miles,J.W., On the stablility of heterogeneous shear flows, *Journal of Fluid Mechanics*, 10, 496-508, 1961.

McPhaden, Michael J. and Stanley P. Hayes, Variablility in eastern equatorial Pacific Ocean during 1986 - 1988, *Journal of Geophysical Research, 95, 13*, 195-208, 1990.

McPhaden, Michael J. and Stanley P. Hayes, On the variability of winds, sea surface temperature, and surface layer heat content in the western equatorial Pacific, *Journal of Geophysical Research*, 96, 3331-3342, 1991.

Ocean Modeling Workshop at Fleet Numerical Oceanography Center, Monterey, CA of 17-19 November 1987.

Price, J. F., C. N. K. Mooers and J. C. Van Leer, Observations and simulation of storm-induced mixed layer deepening, *Journal of Physical Oceanography*, *8*, 582-599, 1978.

Schneider, Niklas and Peter Muller, The meridional and seasonal structures of the mixed-layer depth and its diurnal amplitude during the hawaii-to-tahiti shuttle experiment, *Journal of Physical Oceanography*, 9, 1401, 1990.

Taft, B.A. and M.J. McPhaden, Diurnal cycle of sea surface temperature in the western tropical Pacific, paper presented at Symposium on Western Tropical Pacific Air-Sea Interactions, U.S. TOGA Project Office, Beijing, China, Nov. 15-17, 1988.

Wergen, W., 1982 Initialization, ECMWF Seminar/Workshop on Interpretation of Numerical Weather Prediction Products, 31-92, 1982.

Wyrtki, K., An estimate of equatorial upwelling in the Pacific, *Journal of Physical Oceanography*, *11*, 1205-1214, 1981.

Yamagata T., Stability of a simple air-sea coupled model in the tropics, in *Coupled Ocean-Atmospheric Models*, edited by J. C. J. Nihoul, pp. 637-658, Elsevier, New York, 1985.

APPENDIX A. MONTHLY NET SURFACE HEAT FLUX FIELDS

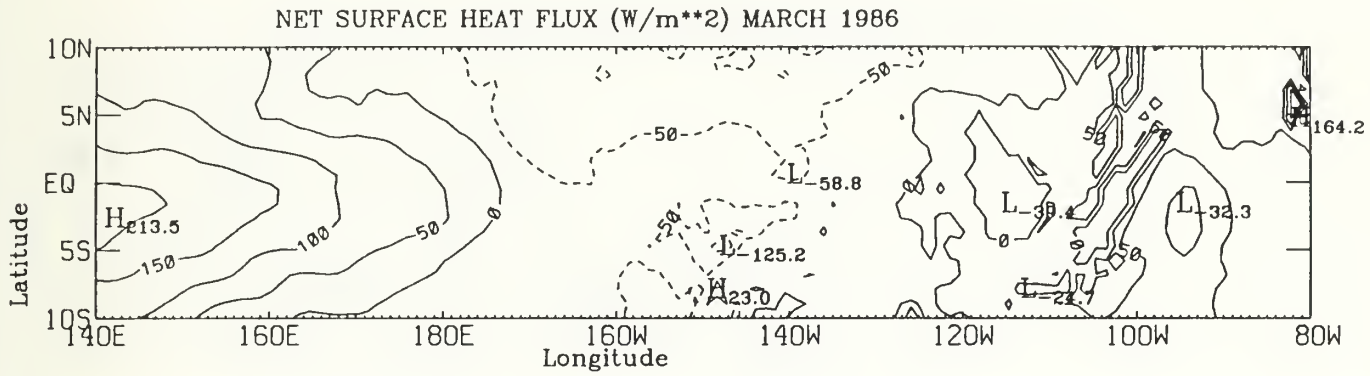
NET SURFACE HEAT FLUX (W/m**2) MARCH 1986
10N
5N
EQ
5S
10S
Latitude
140E
160E
180E
160W
140W
120W
100W
80W
Longitude
H213.5
L-58.8
L-125.2
H23.0
L-39.4
L-32.3
L-21.7
H164.2
50
0
-50
100
150

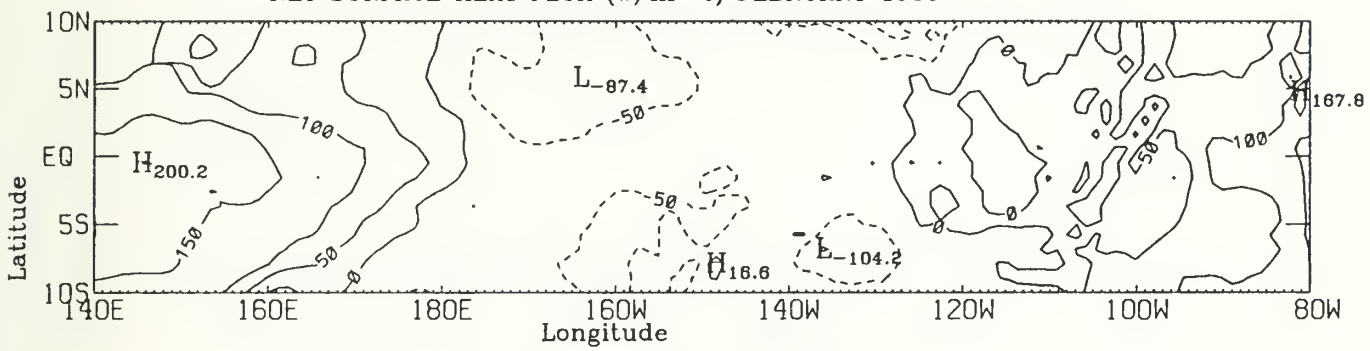
NET SURFACE HEAT FLUX (W/m**2) FEBRUARY 1986
10N
5N
EQ
5S
10S
Latitude
140E
160E
180E
160W
140W
120W
100W
80W
Longitude
H200.2
L-87.4
H16.6
L-104.2
H167.8
0
50
100
150

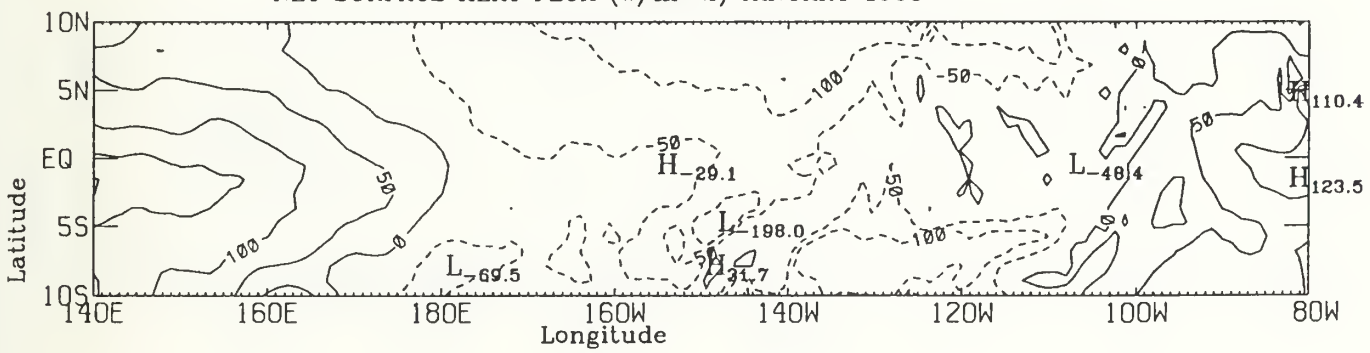
NET SURFACE HEAT FLUX (W/m**2) JANUARY 1986
10N
5N
EQ
5S
10S
Latitude
140E
160E
180E
160W
140W
120W
100W
80W
Longitude
H-29.1
L-198.0
L-69.5
H31.7
L-48.4
H110.4
H123.5
0
50
100
-50

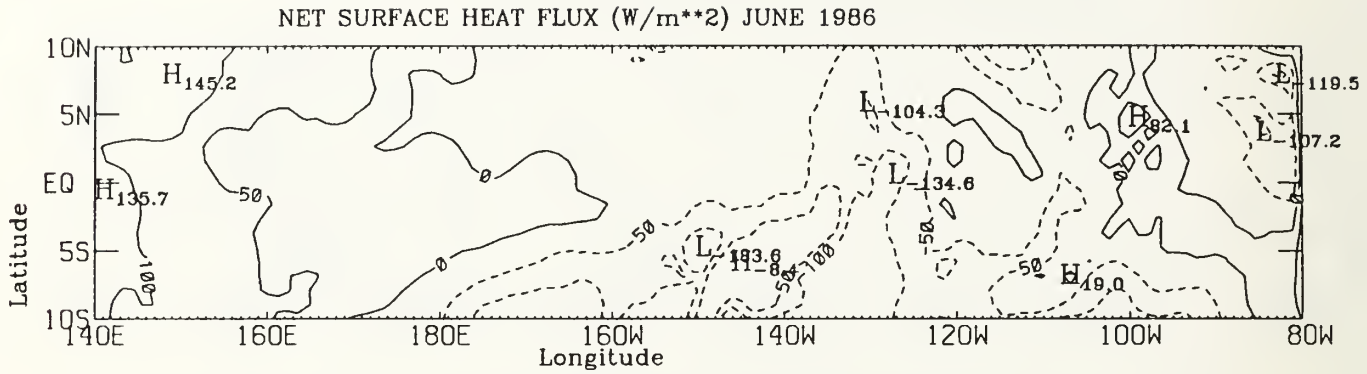
NET SURFACE HEAT FLUX (W/m**2) JUNE 1986
10N
5N
EQ
5S
10S
Latitude
140E
160E
180E
160W
140W
120W
100W
80W
Longitude
H145.2
H135.7
L104.3
L134.6
H82.1
L107.2
L119.5
L183.8
H19.0
50
0
100

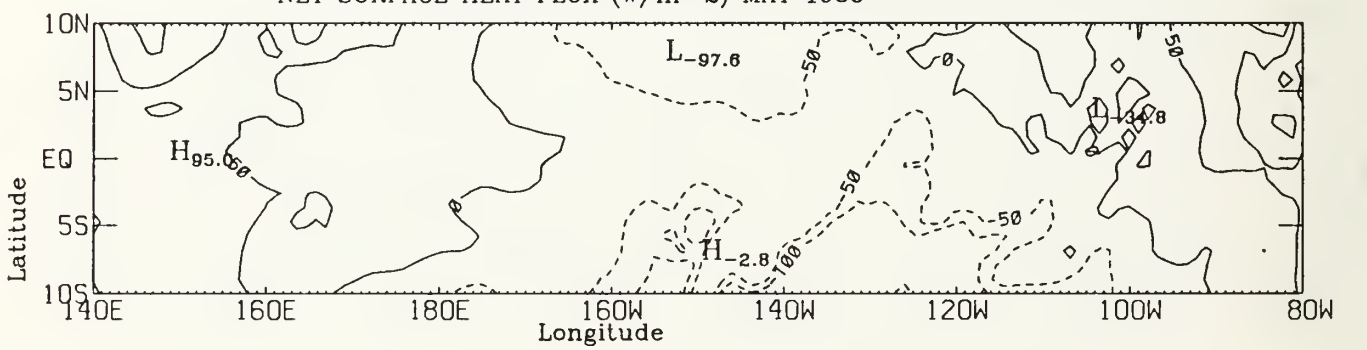
NET SURFACE HEAT FLUX (W/m**2) MAY 1986
10N
5N
EQ
5S
10S
Latitude
140E
160E
180E
160W
140W
120W
100W
80W
Longitude
L97.6
H95.6
H2.8
L34.8
50
0
100

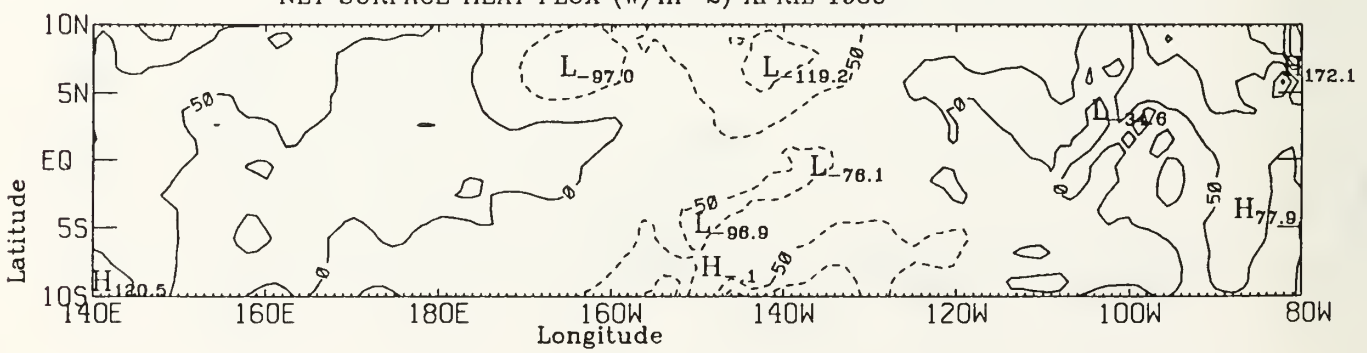
NET SURFACE HEAT FLUX (W/m**2) APRIL 1986
10N
5N
EQ
5S
10S
Latitude
140E
160E
180E
160W
140W
120W
100W
80W
Longitude
L97.0
L119.2
L76.1
L96.9
H1.1
H120.5
H77.9
L34.6
L172.1
50
0

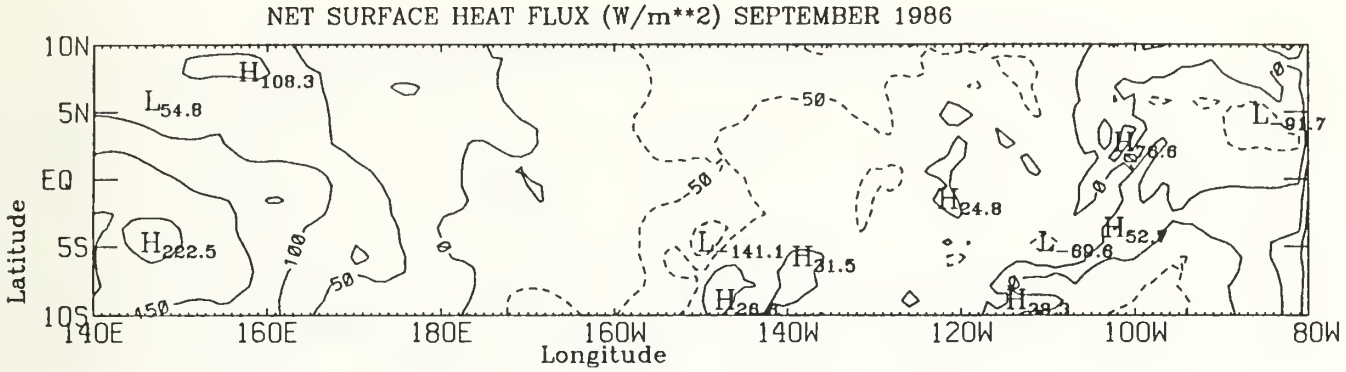
NET SURFACE HEAT FLUX (W/m**2) SEPTEMBER 1986
10N
5N
EQ
5S
10S
Latitude
140E
160E
180E
160W
140W
120W
100W
80W
Longitude
H108.3
L54.8
H222.5
L141.1
H31.5
H24.8
H52.7
L69.6
L91.7
50
0
100
150

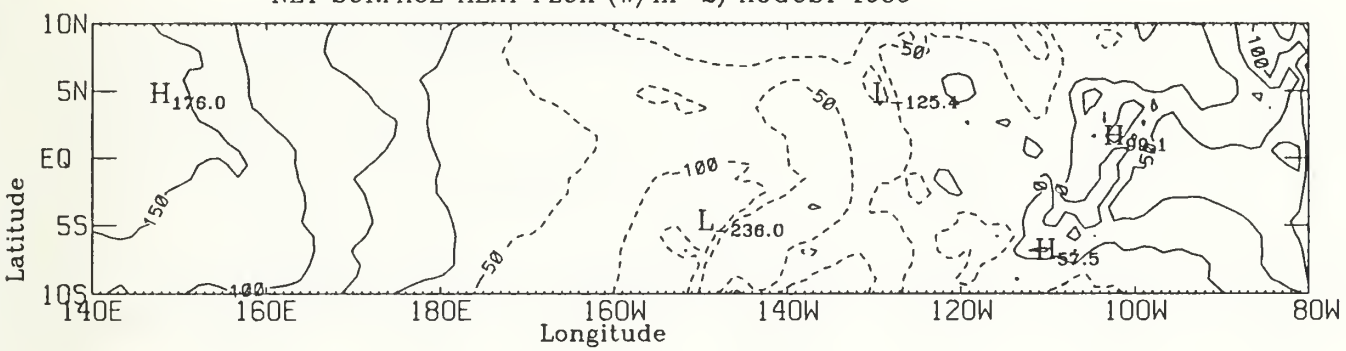
NET SURFACE HEAT FLUX (W/m**2) AUGUST 1986
10N
5N
EQ
5S
10S
Latitude
140E
160E
180E
160W
140W
120W
100W
80W
Longitude
H176.0
L125.4
H99.1
L236.0
H57.5
50
100
150

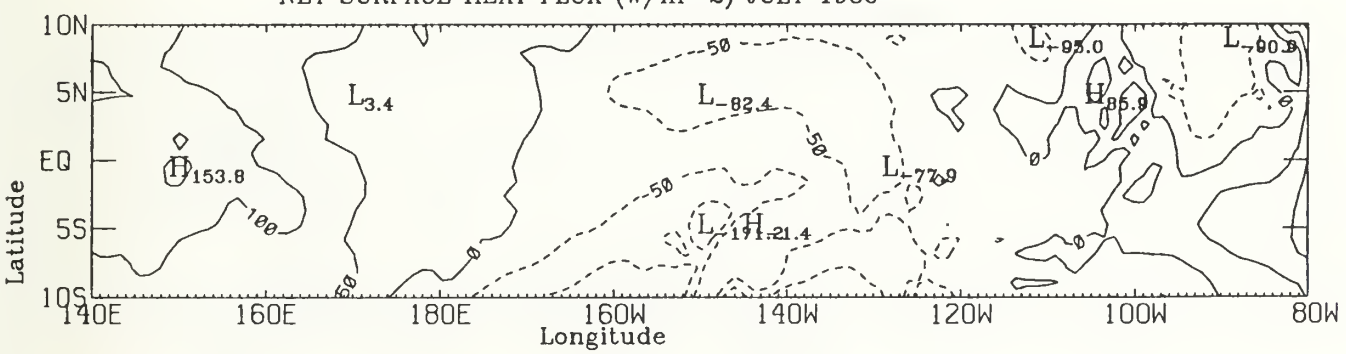
NET SURFACE HEAT FLUX (W/m**2) JULY 1986
10N
5N
EQ
5S
10S
Latitude
140E
160E
180E
160W
140W
120W
100W
80W
Longitude
L3.4
L82.4
L95.0
H85.9
H153.8
L77.9
L171.4
H21.4
50
0
100

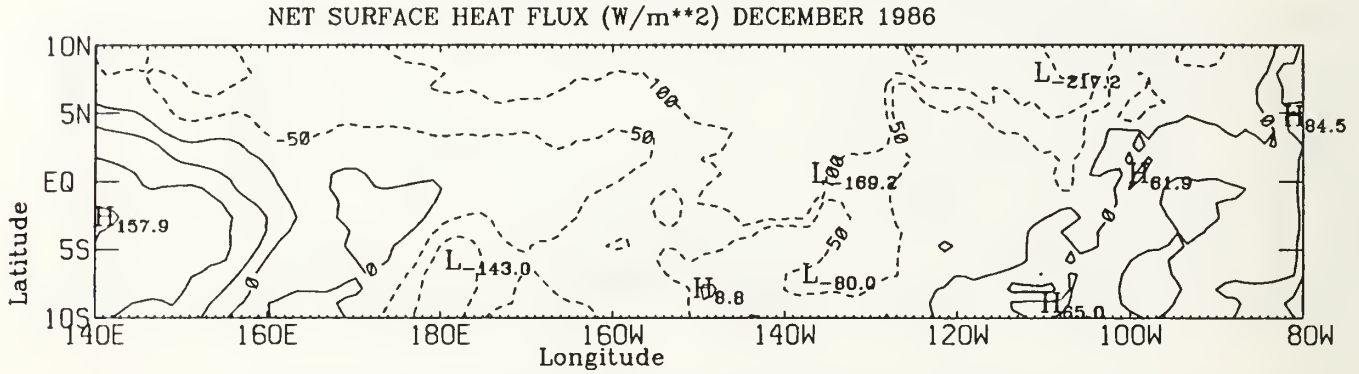
NET SURFACE HEAT FLUX (W/m**2) DECEMBER 1986
10N
5N
EQ
5S
10S
Latitude
140E
160E
180E
160W
140W
120W
100W
80W
Longitude
H157.9
L-143.0
H8.8
L-80.0
L-169.2
L-217.2
H84.5
H61.9
H65.0
-50
0
50
100

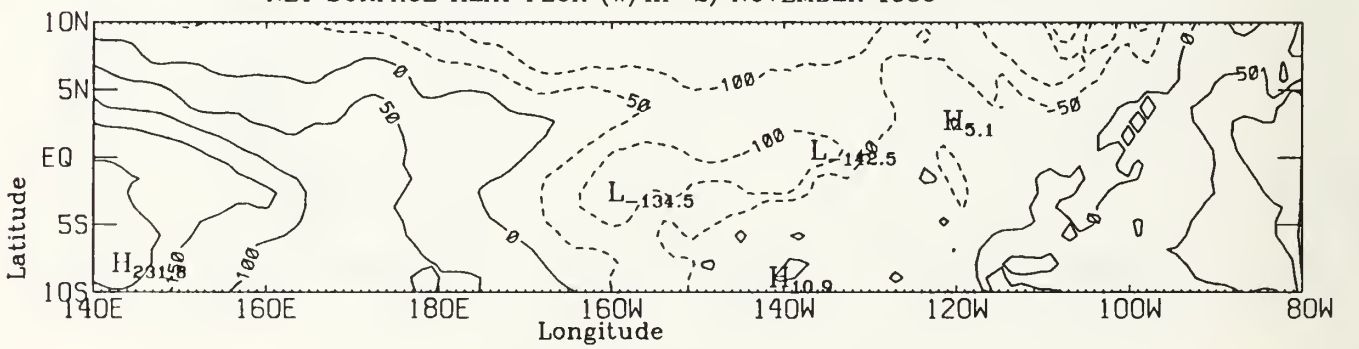
NET SURFACE HEAT FLUX (W/m**2) NOVEMBER 1986
10N
5N
EQ
5S
10S
Latitude
140E
160E
180E
160W
140W
120W
100W
80W
Longitude
H231.8
L-134.5
L-142.5
H5.1
H10.9
0
50
100

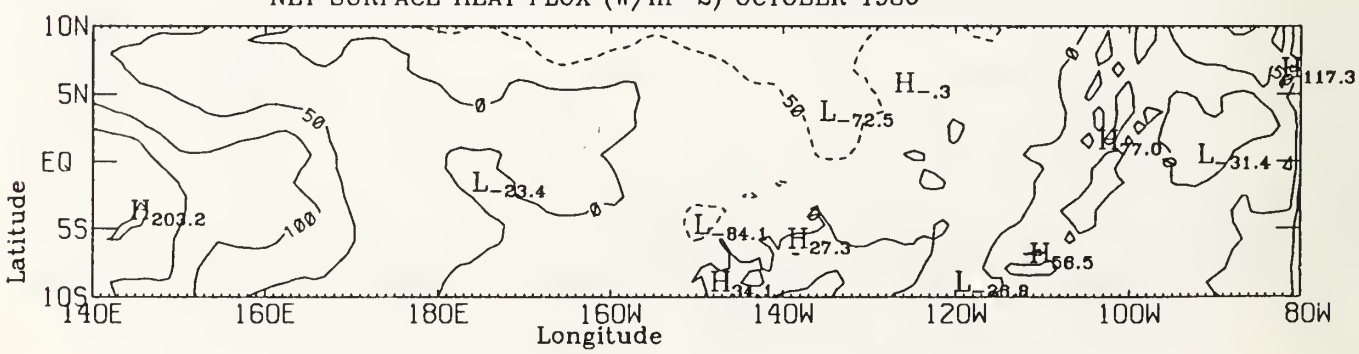
NET SURFACE HEAT FLUX (W/m**2) OCTOBER 1986
10N
5N
EQ
5S
10S
Latitude
140E
160E
180E
160W
140W
120W
100W
80W
Longitude
H203.2
L-23.4
L-84.1
H27.3
H34.1
L-72.5
H-.3
H117.3
H47.0
L-31.4
H56.5
L-28.8
0
50
100

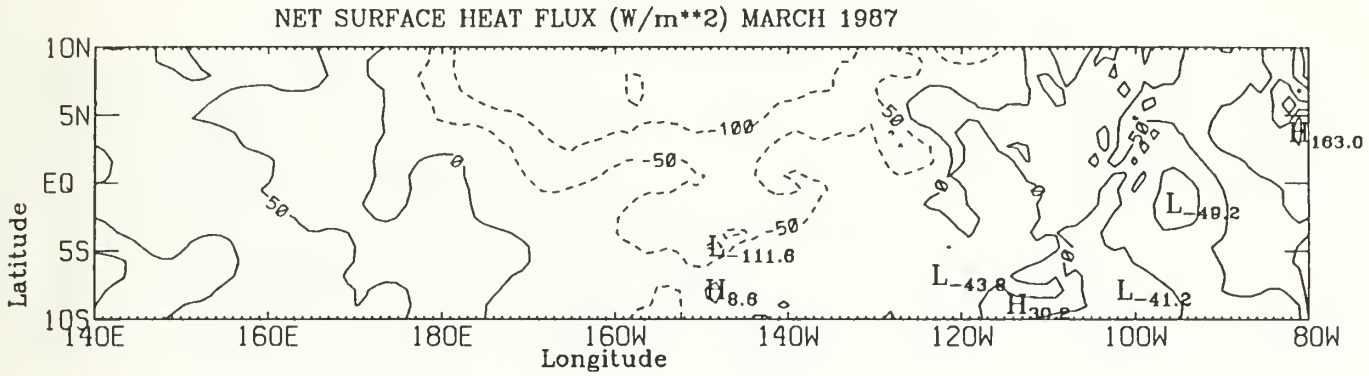
NET SURFACE HEAT FLUX (W/m**2) MARCH 1987
10N
5N
EQ
5S
10S
Latitude
140E
160E
180E
160W
140W
120W
100W
80W
Longitude
H163.0
L-49.2
L-111.6
H8.6
L-43.8
H30.2
L-41.2

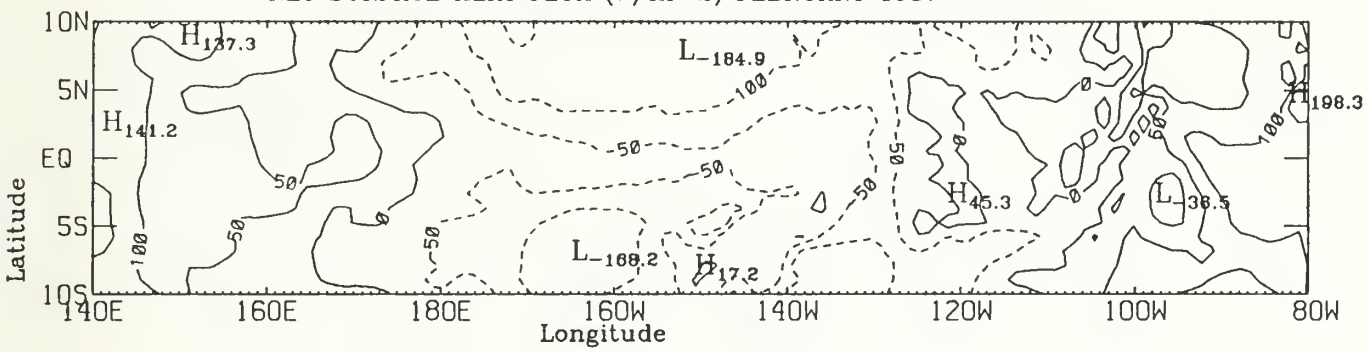
NET SURFACE HEAT FLUX (W/m**2) FEBRUARY 1987
10N
5N
EQ
5S
10S
Latitude
140E
160E
180E
160W
140W
120W
100W
80W
Longitude
H137.3
H141.2
L-184.9
H198.3
H45.3
L-36.5
L-168.2
H17.2

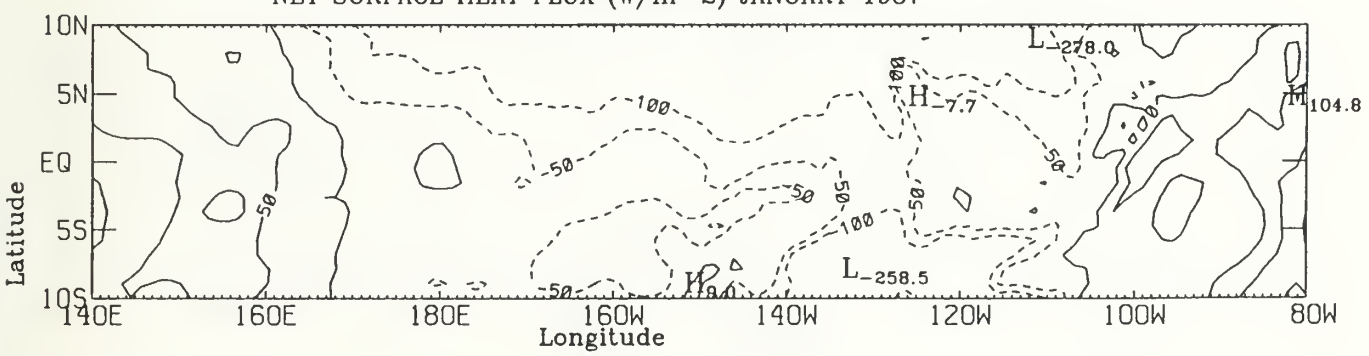
NET SURFACE HEAT FLUX (W/m**2) JANUARY 1987
10N
5N
EQ
5S
10S
Latitude
140E
160E
180E
160W
140W
120W
100W
80W
Longitude
L-278.0
H-7.7
H104.8
L-258.5

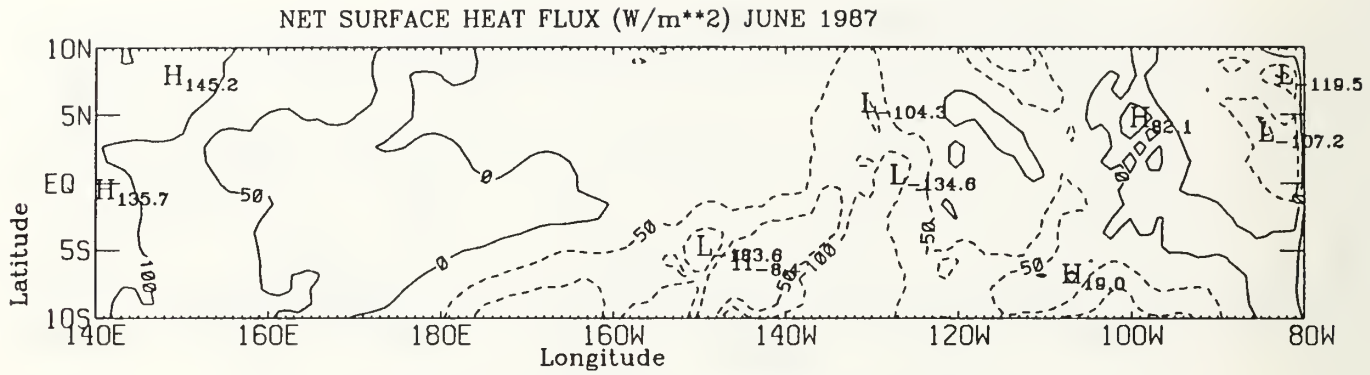
NET SURFACE HEAT FLUX (W/m**2) JUNE 1987
10N
5N
EQ
5S
10S
Latitude
140E
160E
180E
160W
140W
120W
100W
80W
Longitude
H145.2
H135.7
L104.3
L134.6
H82.1
L107.2
L119.5
H19.0
0
50
100

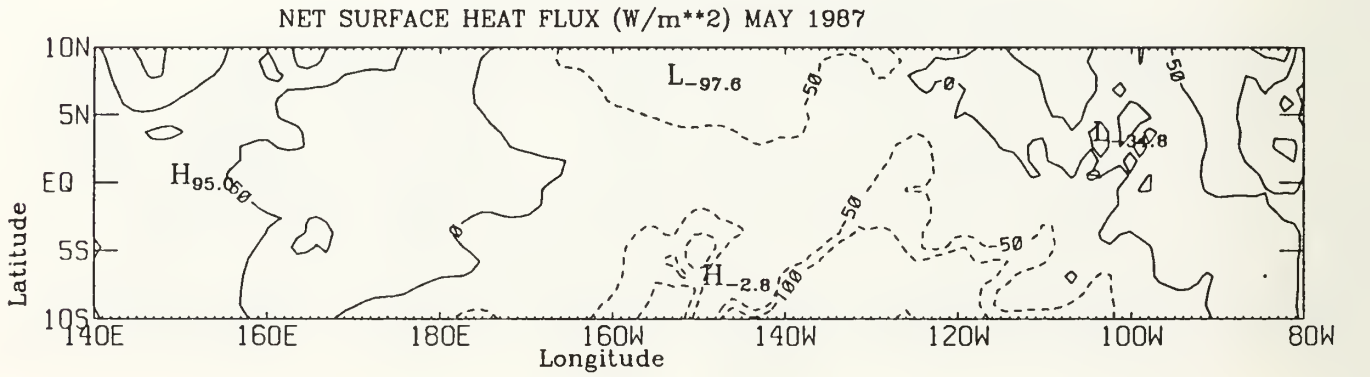
NET SURFACE HEAT FLUX (W/m**2) MAY 1987
10N
5N
EQ
5S
10S
Latitude
140E
160E
180E
160W
140W
120W
100W
80W
Longitude
L97.6
H95.6
H-2.8
0
50
100

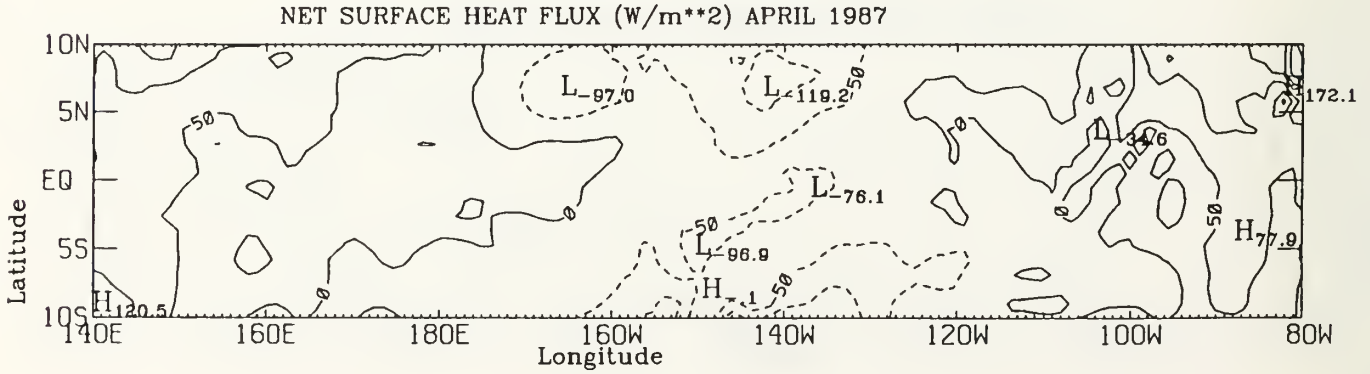
NET SURFACE HEAT FLUX (W/m**2) APRIL 1987
10N
5N
EQ
5S
10S
Latitude
140E
160E
180E
160W
140W
120W
100W
80W
Longitude
L97.0
L119.2
L76.1
L96.9
H120.5
H77.9
172.1
0
50

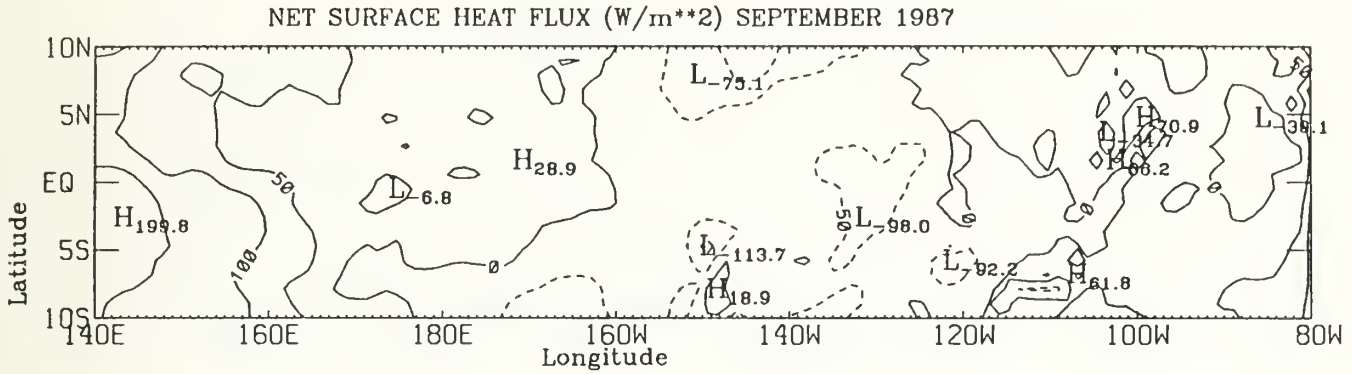
NET SURFACE HEAT FLUX (W/m**2) SEPTEMBER 1987
10N
5N
EQ
5S
10S
140E
160E
180E
160W
140W
120W
100W
80W
Latitude
Longitude
L-75.1
H28.9
L6.8
H199.8
L-98.0
L-113.7
H18.9
L-92.2
H61.8
H70.9
L-44.7
H66.2
L-35.1
50
0
-50
100

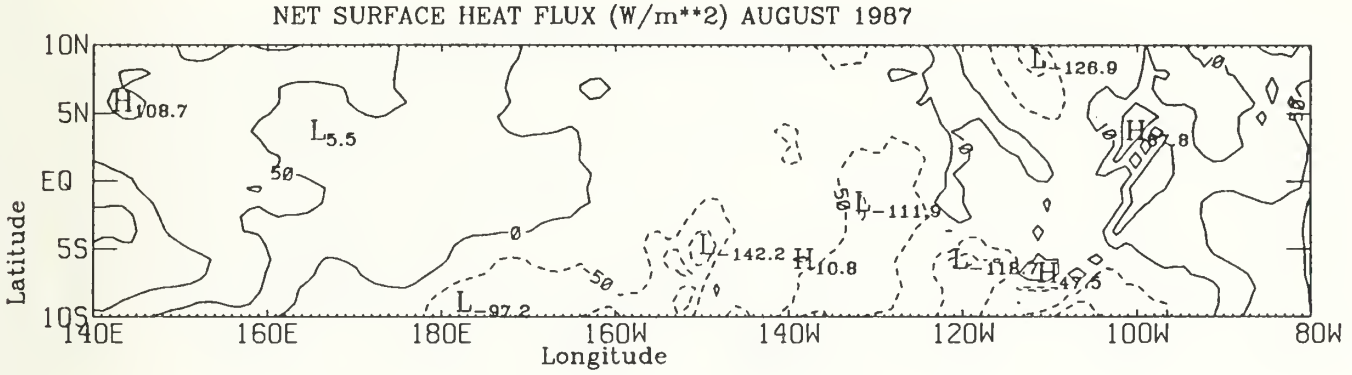
NET SURFACE HEAT FLUX (W/m**2) AUGUST 1987
10N
5N
EQ
5S
10S
140E
160E
180E
160W
140W
120W
100W
80W
Latitude
Longitude
L-126.9
H108.7
L5.5
L-111.9
L-142.2
H10.8
L-118.7
H47.5
L-97.2
H87.8
50
0
-50

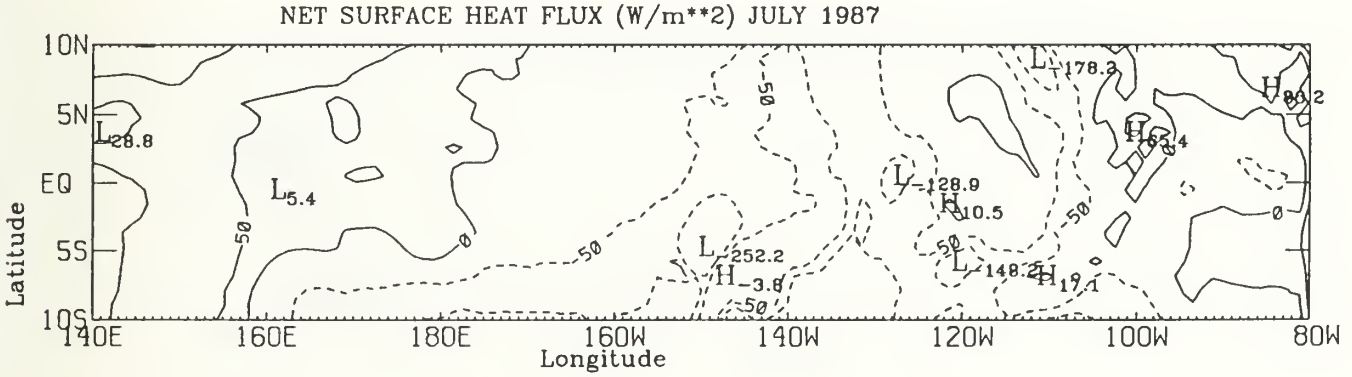
NET SURFACE HEAT FLUX (W/m**2) JULY 1987
10N
5N
EQ
5S
10S
140E
160E
180E
160W
140W
120W
100W
80W
Latitude
Longitude
L-178.3
L28.8
L5.4
L-128.9
H10.5
L-252.2
H-3.8
L-148.2
H19.1
H163.4
50
0
-50

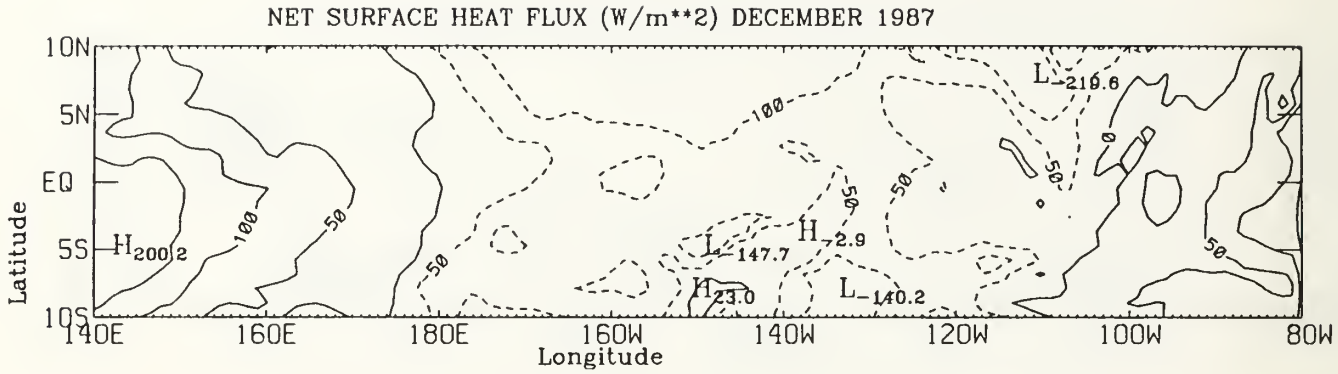
NET SURFACE HEAT FLUX (W/m**2) DECEMBER 1987
10N
5N
EQ
5S
10S
Latitude
140E
160E
180E
160W
140W
120W
100W
80W
Longitude
H200.2
L147.7
H23.0
H2.9
L140.2
L219.6
100
50
0
-50

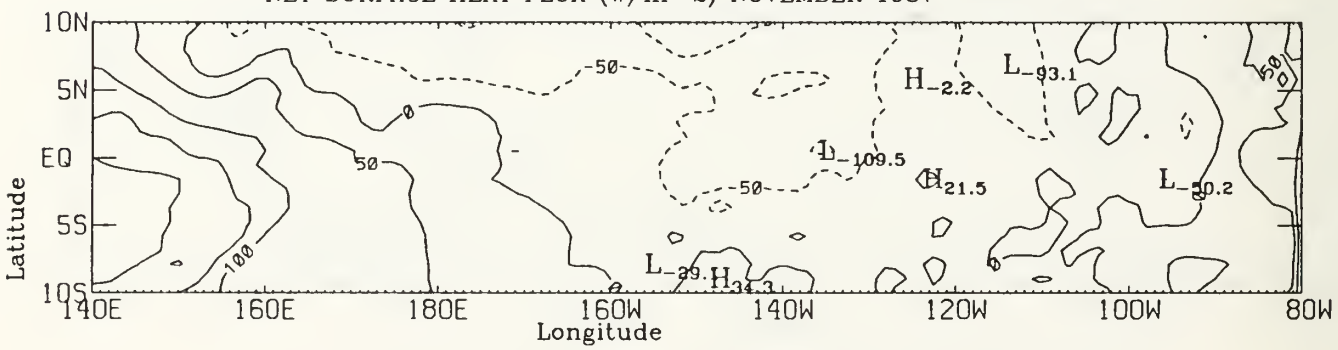
NET SURFACE HEAT FLUX (W/m**2) NOVEMBER 1987
10N
5N
EQ
5S
10S
Latitude
140E
160E
180E
160W
140W
120W
100W
80W
Longitude
H2.2
L93.1
L109.5
H21.5
L50.2
L99.1
H34.3
100
50
0
-50

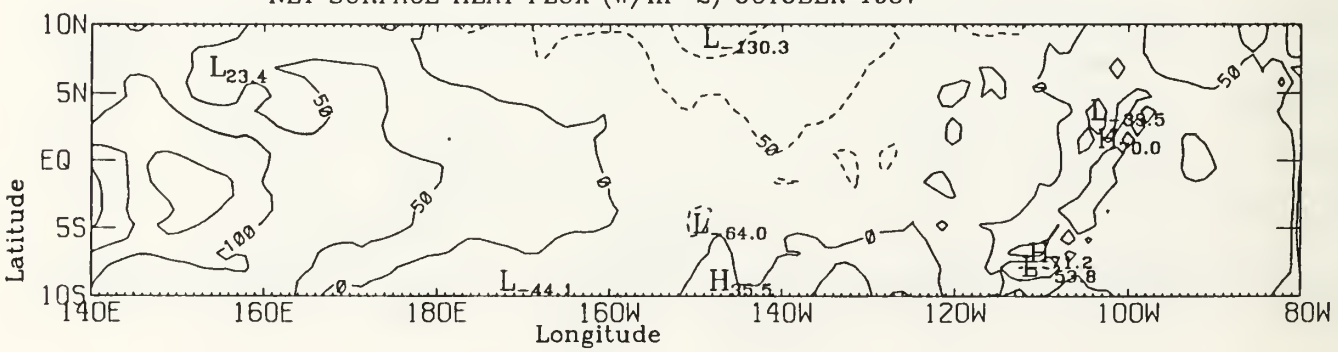
NET SURFACE HEAT FLUX (W/m**2) OCTOBER 1987
10N
5N
EQ
5S
10S
Latitude
140E
160E
180E
160W
140W
120W
100W
80W
Longitude
L23.4
L130.3
L64.0
L44.1
H35.5
100
50
0

APPENDIX B. MONTHLY WATER SURFACE FRICTION VELOCITY FIELDS

WATER SURFACE FRICTION VELOCITY (CM/S) MARCH 1986

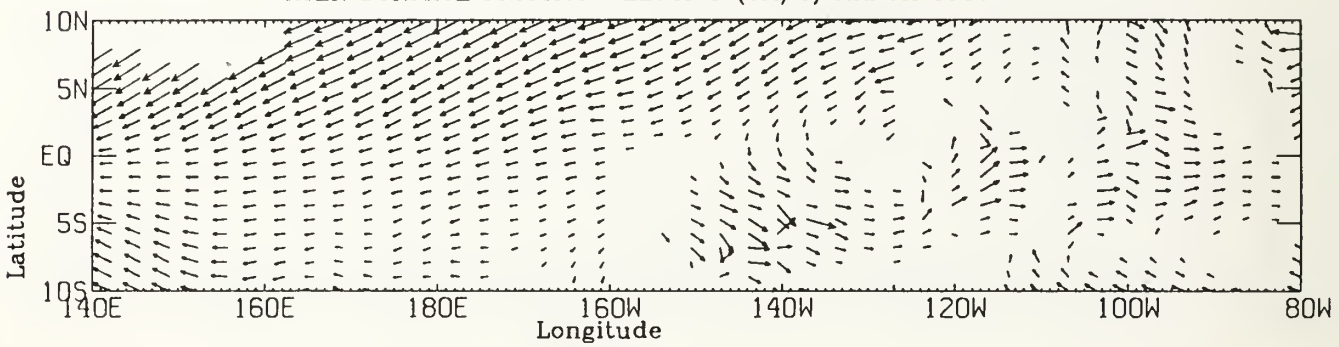

WATER SURFACE FRICTION VELOCITY (CM/S) FEBRUARY 1986

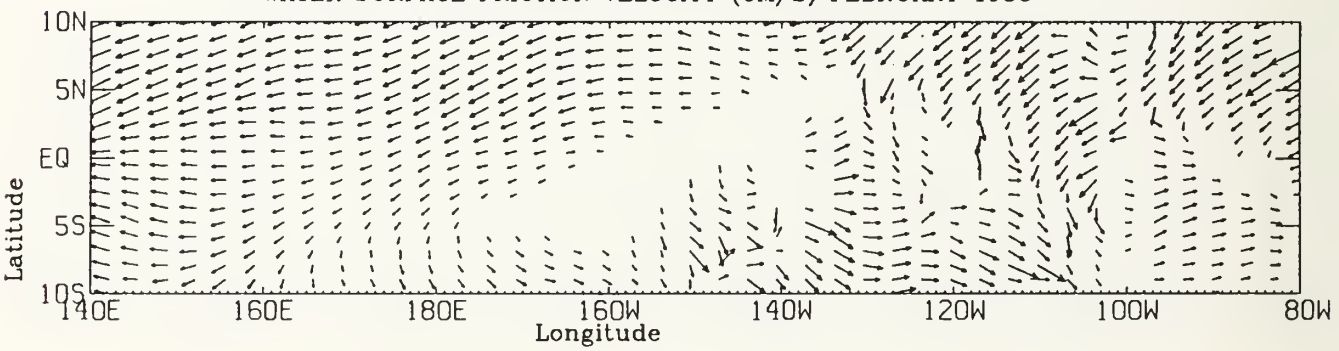

WATER SURFACE FRICTION VELOCITY (CM/S) JANUARY 1986

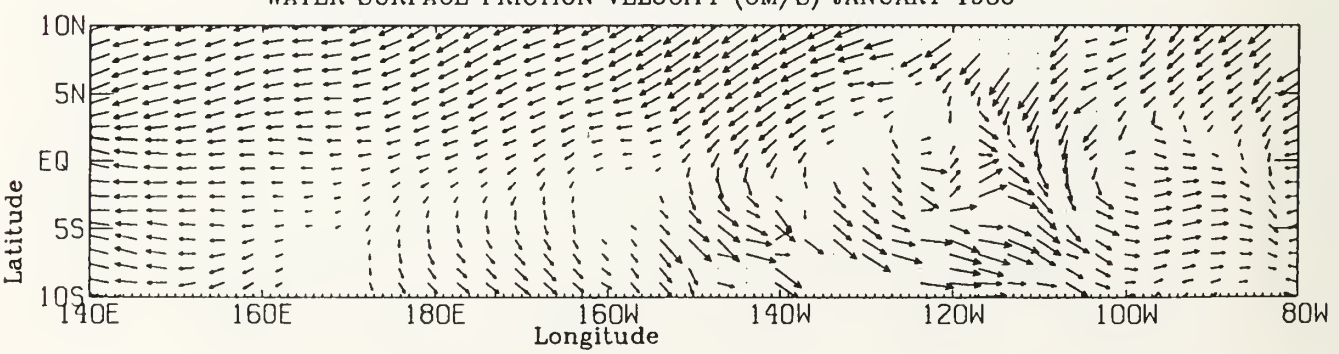

0.300E+00
MAXIMUM VECTOR

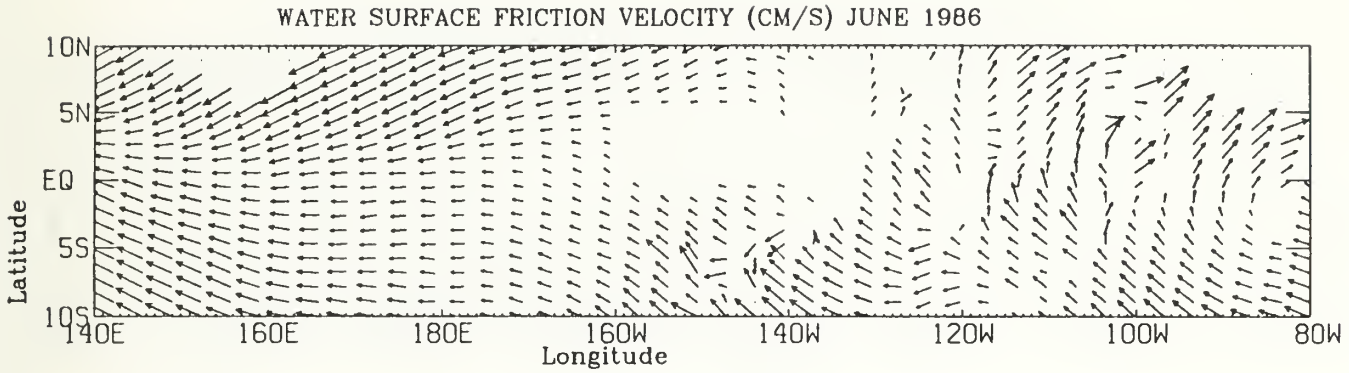
WATER SURFACE FRICTION VELOCITY (CM/S) JUNE 1986
10N
5N
EQ
5S
10S
Latitude
140E
160E
180E
160W
140W
120W
100W
80W
Longitude

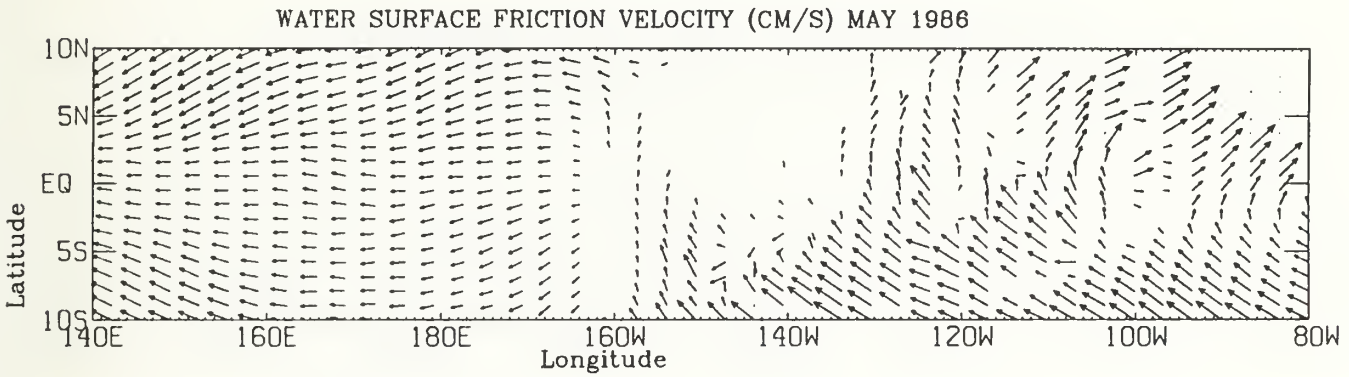
WATER SURFACE FRICTION VELOCITY (CM/S) MAY 1986
10N
5N
EQ
5S
10S
Latitude
140E
160E
180E
160W
140W
120W
100W
80W
Longitude

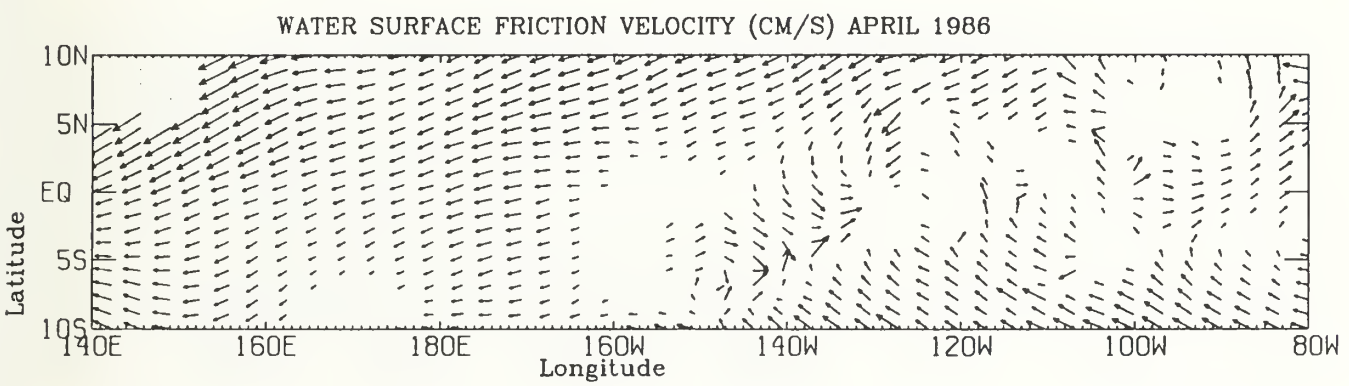
WATER SURFACE FRICTION VELOCITY (CM/S) APRIL 1986
10N
5N
EQ
5S
10S
Latitude
140E
160E
180E
160W
140W
120W
100W
80W
Longitude
0.300E+00
MAXIMUM VECTOR

WATER SURFACE FRICTION VELOCITY (CM/S) SEPTEMBER 1986

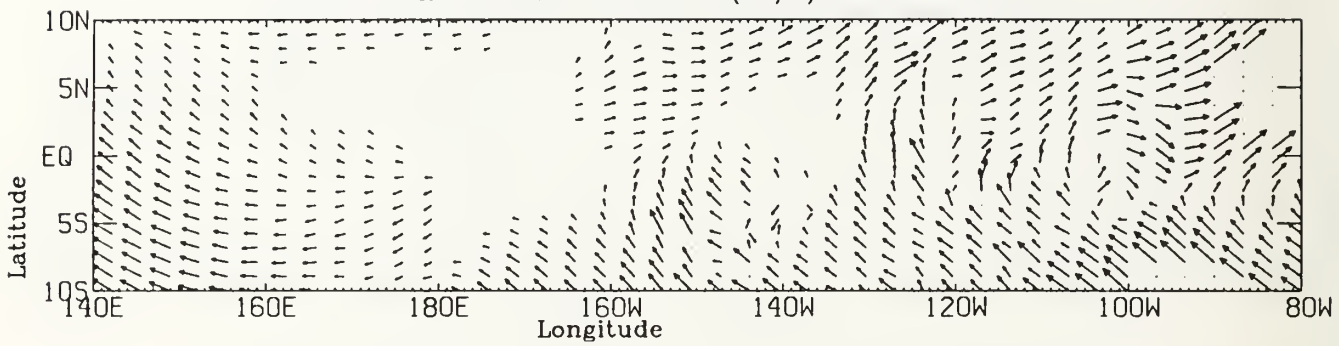

WATER SURFACE FRICTION VELOCITY (CM/S) AUGUST 1986

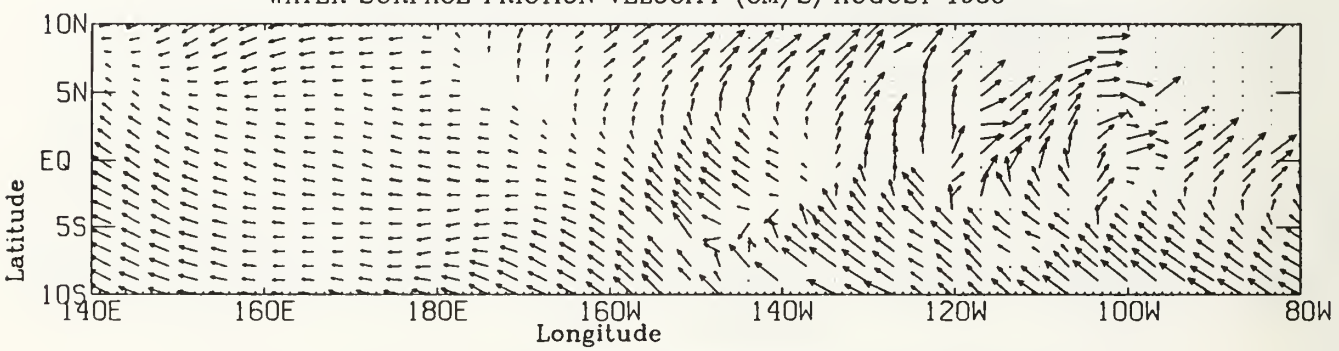

WATER SURFACE FRICTION VELOCITY (CM/S) JULY 1986

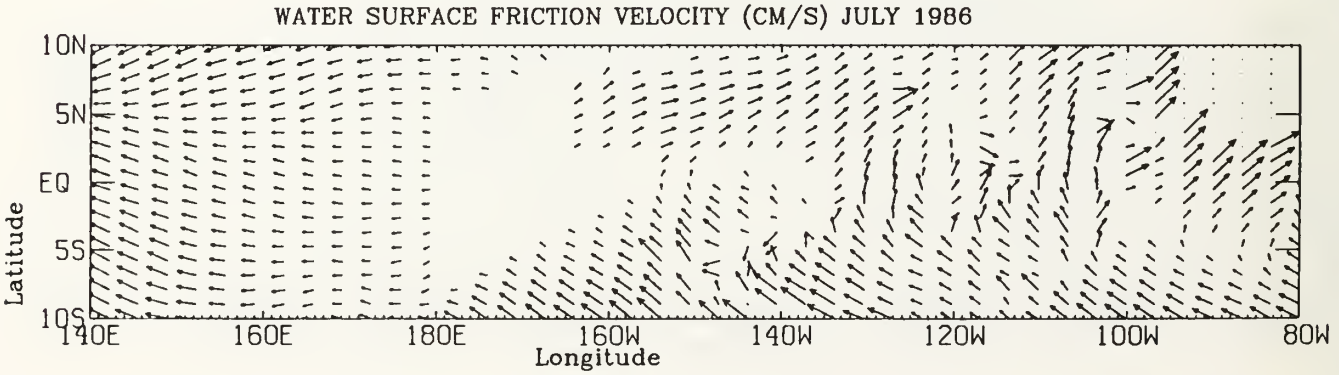

0.300E+00
MAXIMUM VECTOR

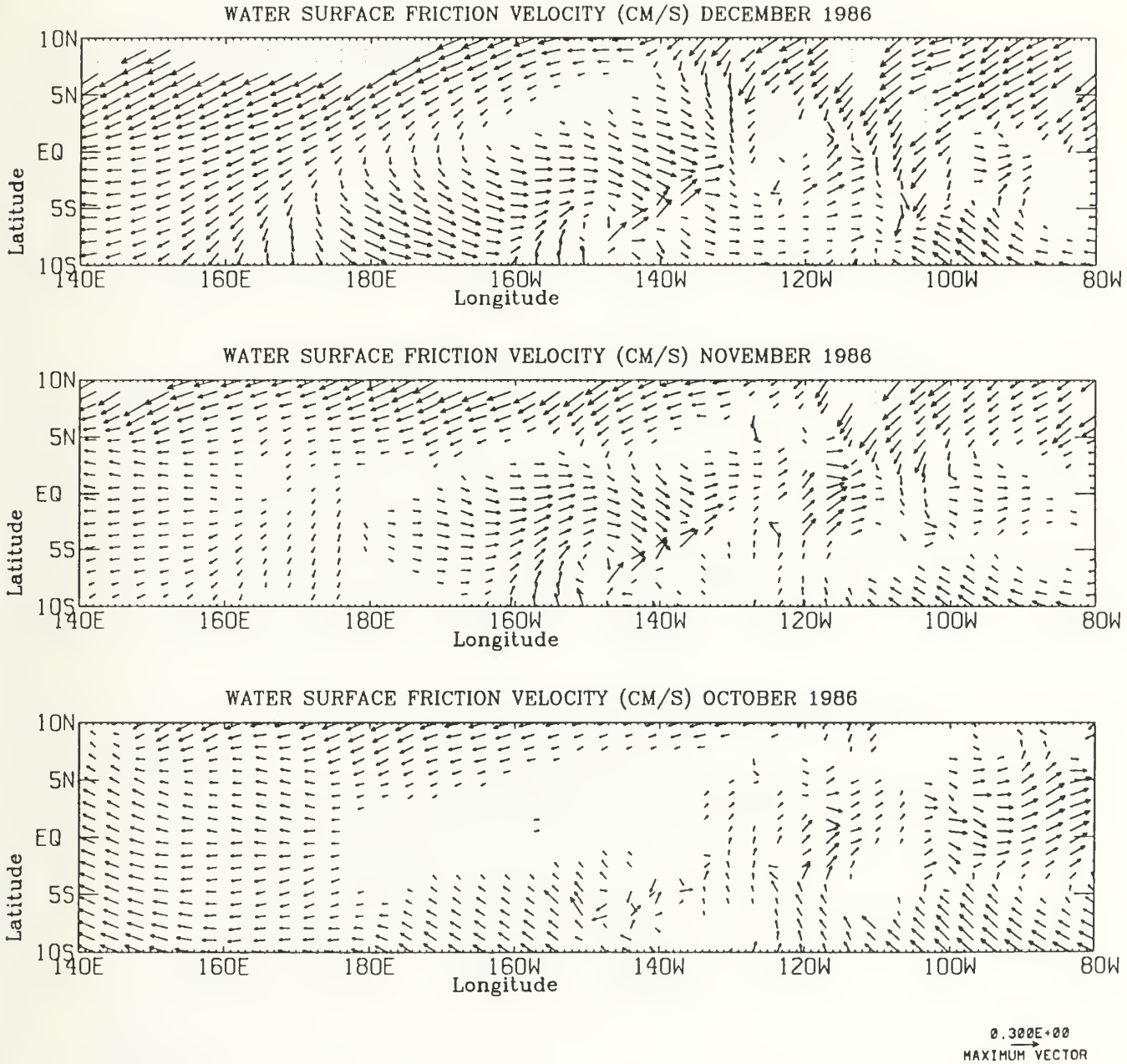
WATER SURFACE FRICTION VELOCITY (CM/S) DECEMBER 1986
10N
5N
EQ
5S
10S
Latitude
140E
160E
180E
160W
140W
120W
100W
80W
Longitude
WATER SURFACE FRICTION VELOCITY (CM/S) NOVEMBER 1986
10N
5N
EQ
5S
10S
Latitude
140E
160E
180E
160W
140W
120W
100W
80W
Longitude
WATER SURFACE FRICTION VELOCITY (CM/S) OCTOBER 1986
10N
5N
EQ
5S
10S
Latitude
140E
160E
180E
160W
140W
120W
100W
80W
Longitude
0.300E+00
MAXIMUM VECTOR

WATER SURFACE FRICTION VELOCITY (CM/S) MARCH 1987

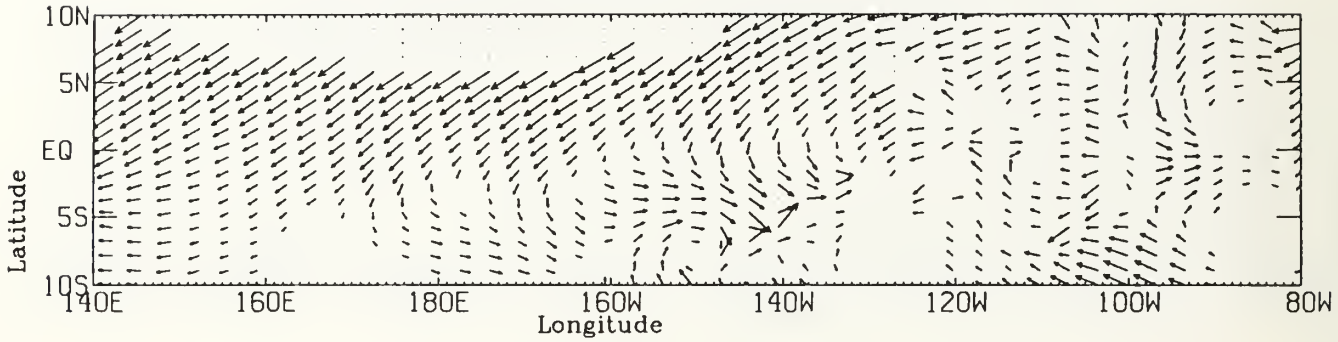

WATER SURFACE FRICTION VELOCITY (CM/S) FEBRUARY 1987

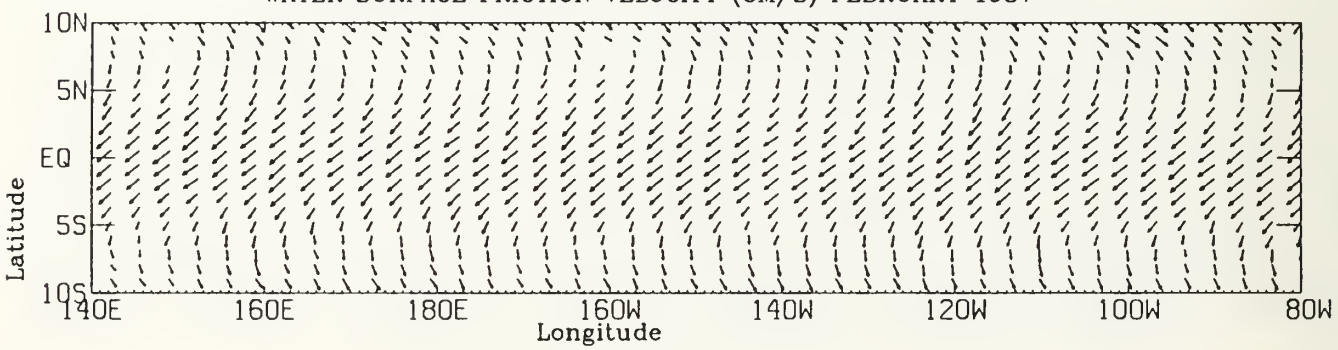

WATER SURFACE FRICTION VELOCITY (CM/S) JANUARY 1987

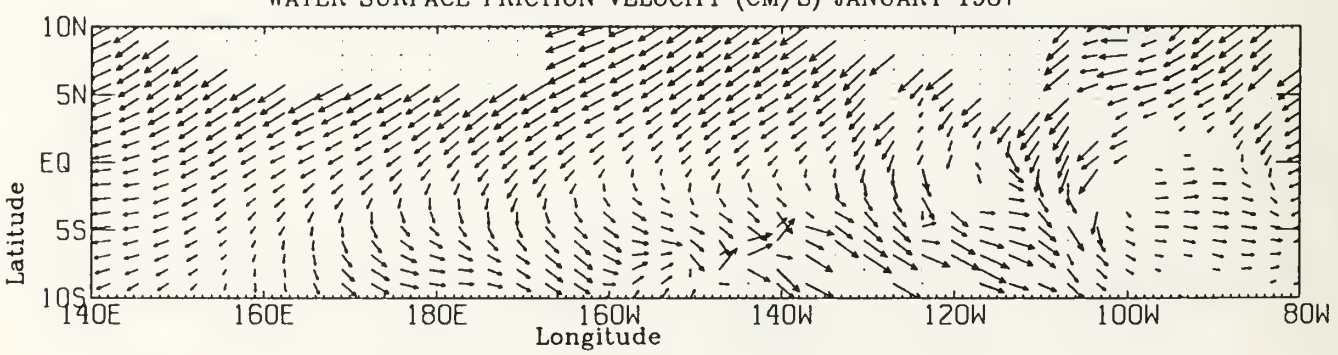

0.300E+00
MAXIMUM VECTOR

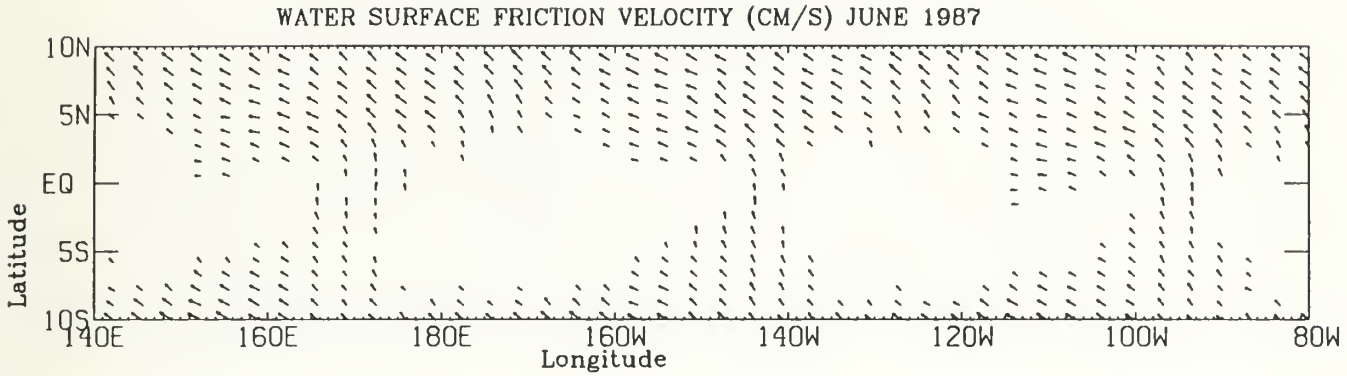
WATER SURFACE FRICTION VELOCITY (CM/S) JUNE 1987
10N
5N
EQ
5S
10S
Latitude
140E
160E
180E
160W
140W
120W
100W
80W
Longitude

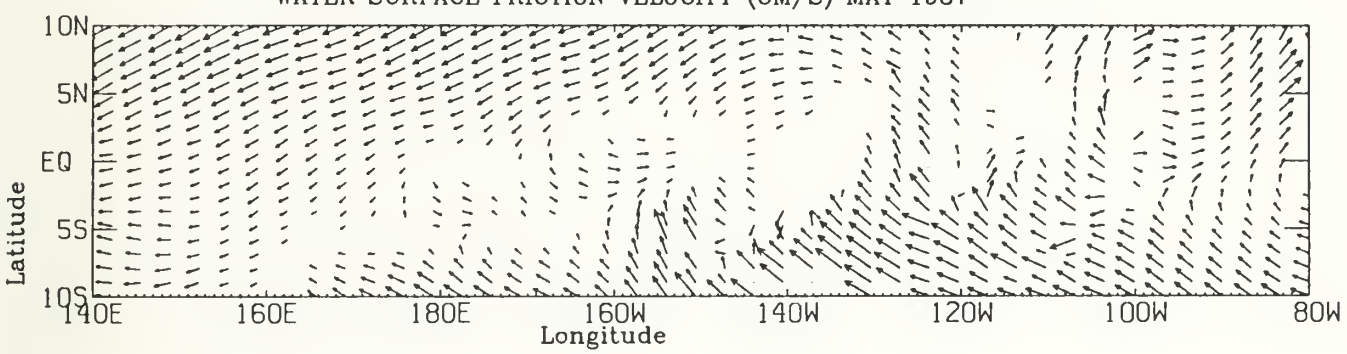
WATER SURFACE FRICTION VELOCITY (CM/S) MAY 1987
10N
5N
EQ
5S
10S
Latitude
140E
160E
180E
160W
140W
120W
100W
80W
Longitude

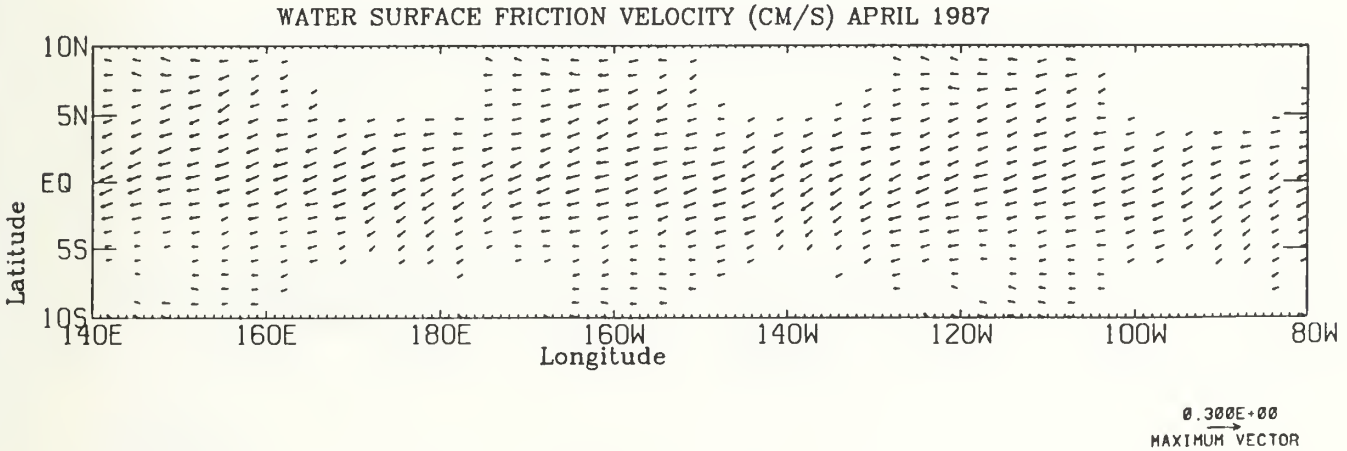
WATER SURFACE FRICTION VELOCITY (CM/S) APRIL 1987
10N
5N
EQ
5S
10S
Latitude
140E
160E
180E
160W
140W
120W
100W
80W
Longitude
0.300E+00
MAXIMUM VECTOR

WATER SURFACE FRICTION VELOCITY (CM/S) SEPTEMBER 1987

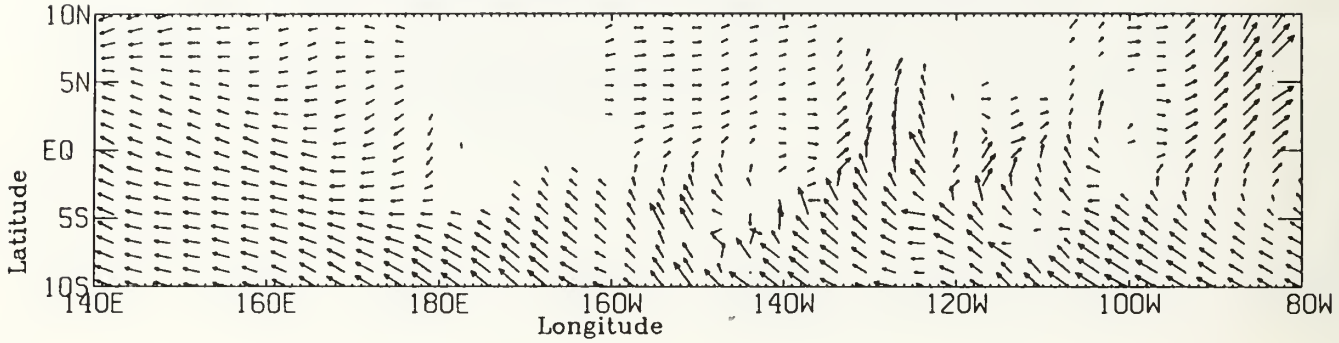

WATER SURFACE FRICTION VELOCITY (CM/S) AUGUST 1987

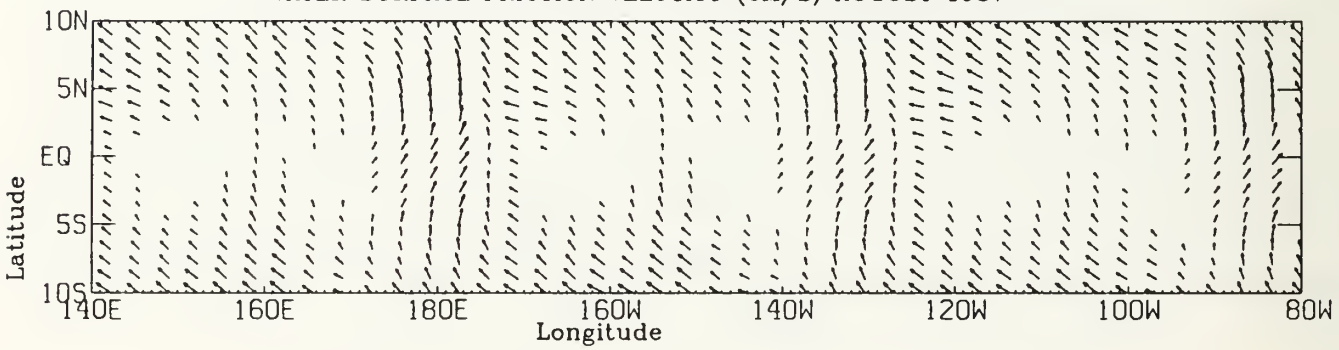

WATER SURFACE FRICTION VELOCITY (CM/S) JULY 1987

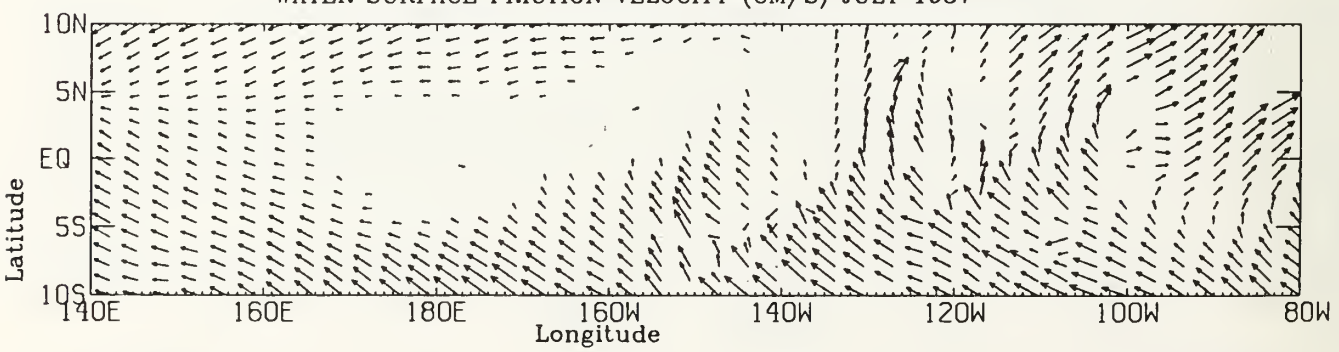

0.300E+00
MAXIMUM VECTOR

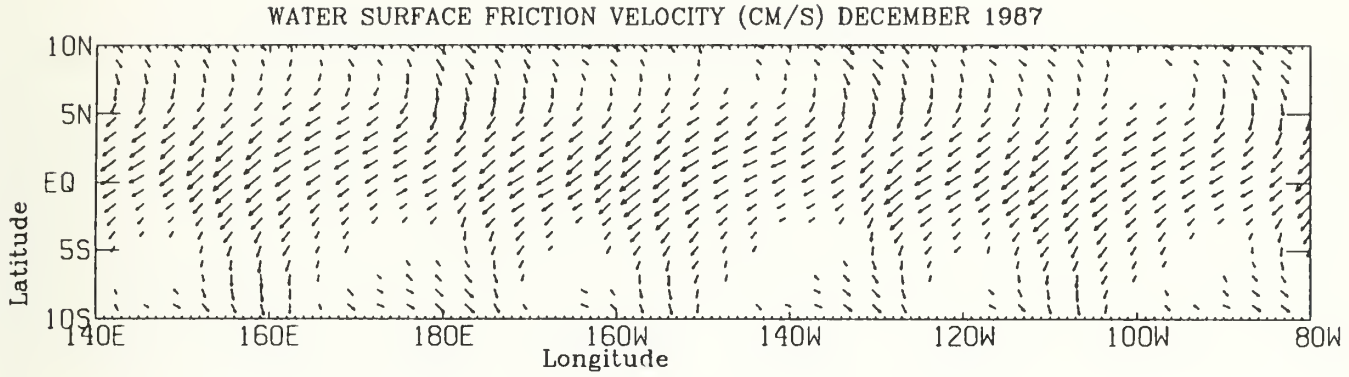
WATER SURFACE FRICTION VELOCITY (CM/S) DECEMBER 1987
10N
5N
EQ
5S
10S
Latitude
140E
160E
180E
160W
140W
120W
100W
80W
Longitude

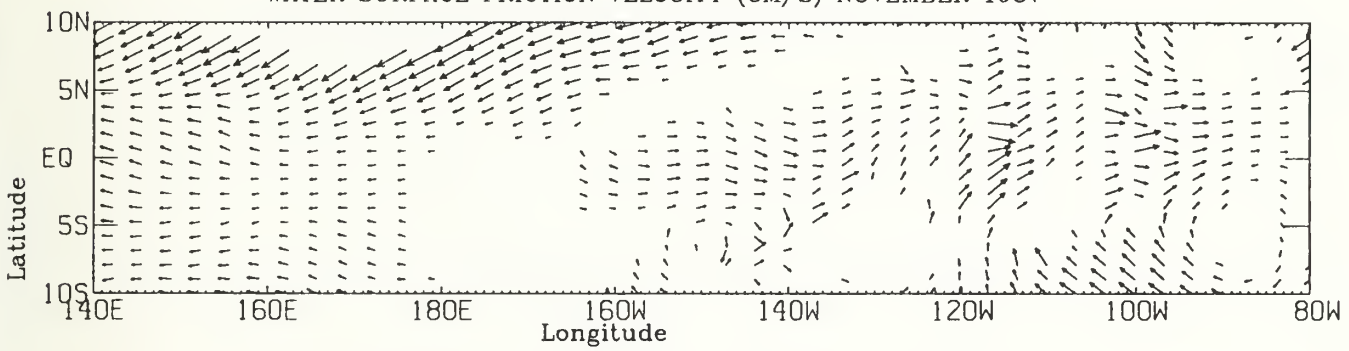
WATER SURFACE FRICTION VELOCITY (CM/S) NOVEMBER 1987
10N
5N
EQ
5S
10S
Latitude
140E
160E
180E
160W
140W
120W
100W
80W
Longitude

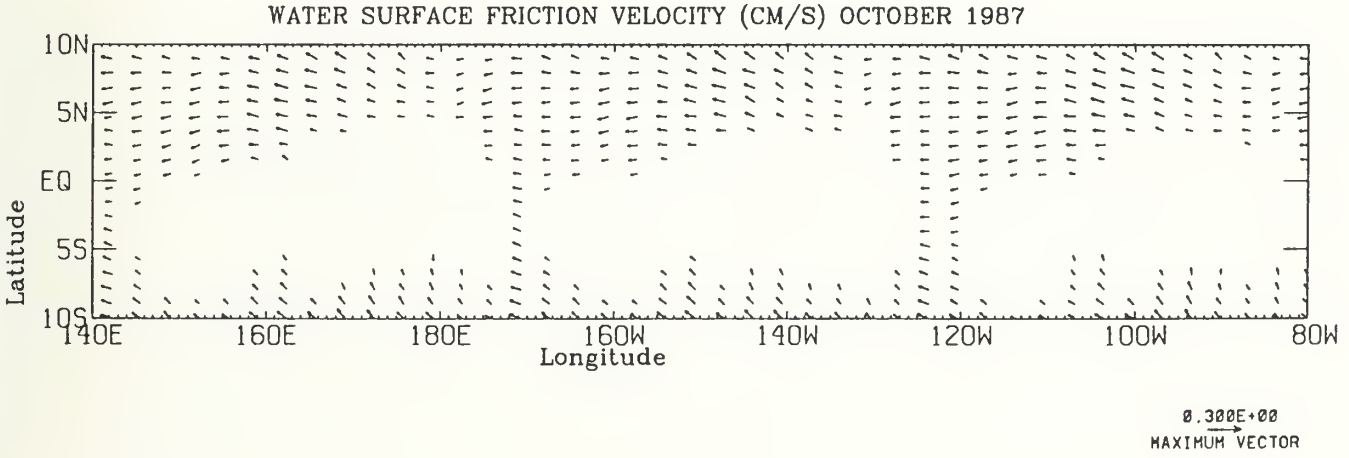
WATER SURFACE FRICTION VELOCITY (CM/S) OCTOBER 1987
10N
5N
EQ
5S
10S
Latitude
140E
160E
180E
160W
140W
120W
100W
80W
Longitude
0.300E+00
MAXIMUM VECTOR

APPENDIX C. MONTHLY SEA SURFACE TEMPERATURE FIELDS

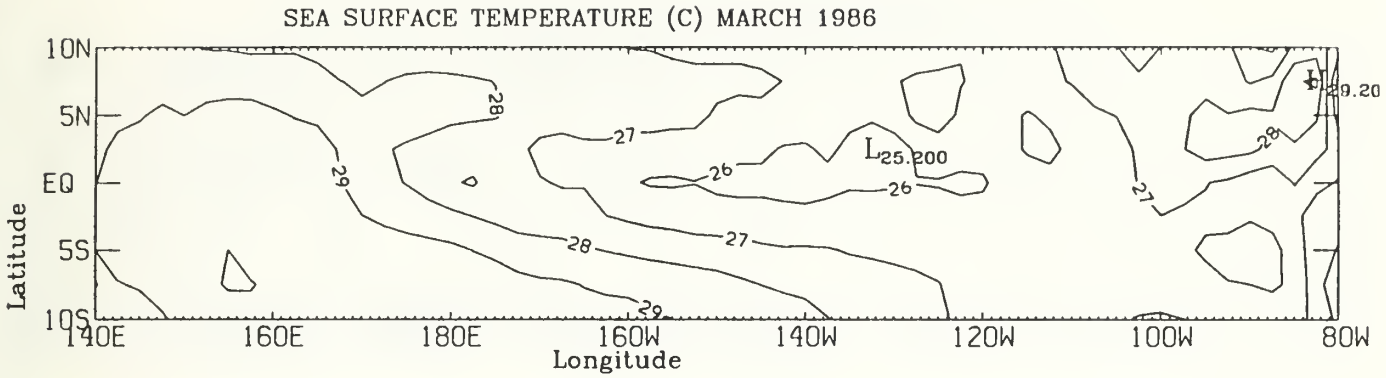
SEA SURFACE TEMPERATURE (C) MARCH 1986
10N
5N
EQ
5S
10S
Latitude
140E
160E
180E
160W
140W
120W
100W
80W
Longitude
L25.200
29
28
27
26

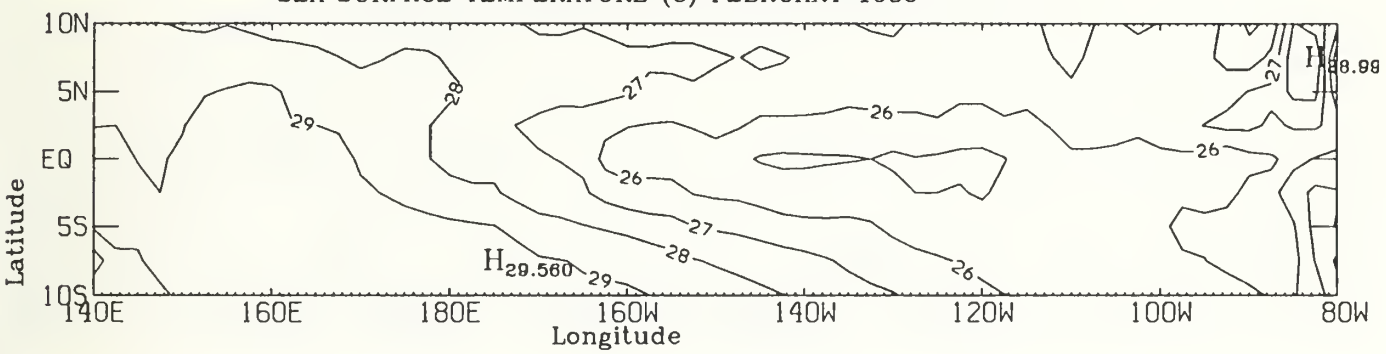
SEA SURFACE TEMPERATURE (C) FEBRUARY 1986
10N
5N
EQ
5S
10S
Latitude
140E
160E
180E
160W
140W
120W
100W
80W
Longitude
H29.560
29
28
27
26

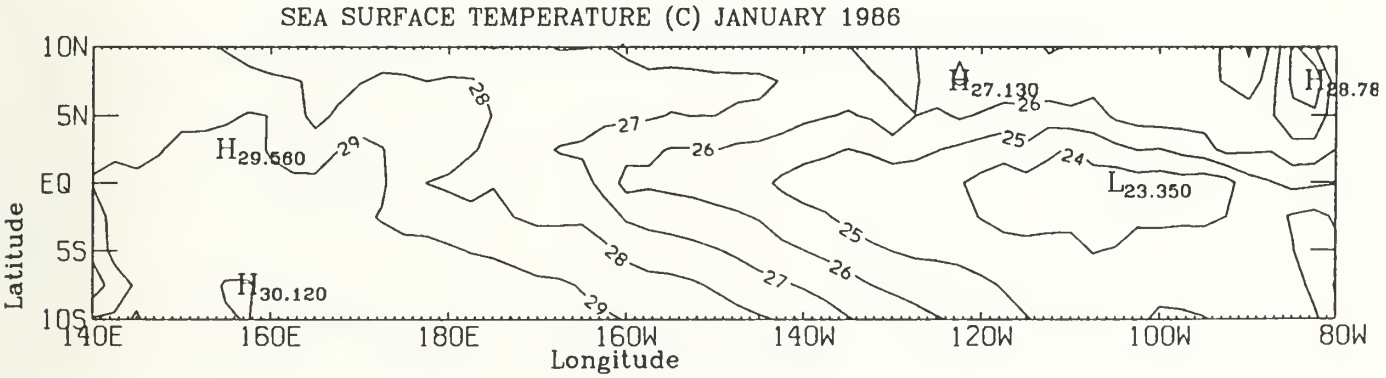
SEA SURFACE TEMPERATURE (C) JANUARY 1986
10N
5N
EQ
5S
10S
Latitude
140E
160E
180E
160W
140W
120W
100W
80W
Longitude
H29.560
H30.120
H27.130
L23.350
29
28
27
26
25
24

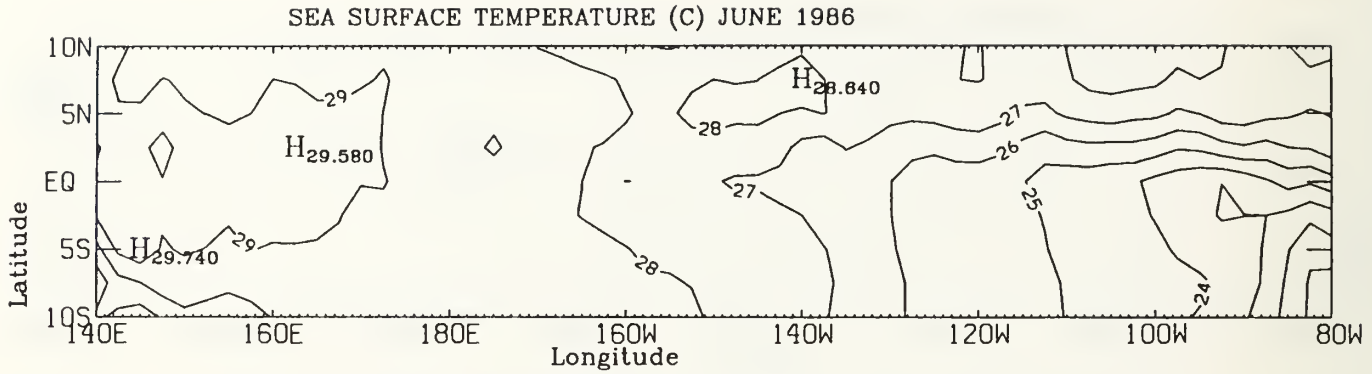
SEA SURFACE TEMPERATURE (C) JUNE 1986
10N
5N
EQ
5S
10S
Latitude
140E
160E
180E
160W
140W
120W
100W
80W
Longitude
H29.580
H29.740
H28.640
29
28
27
26
25
24

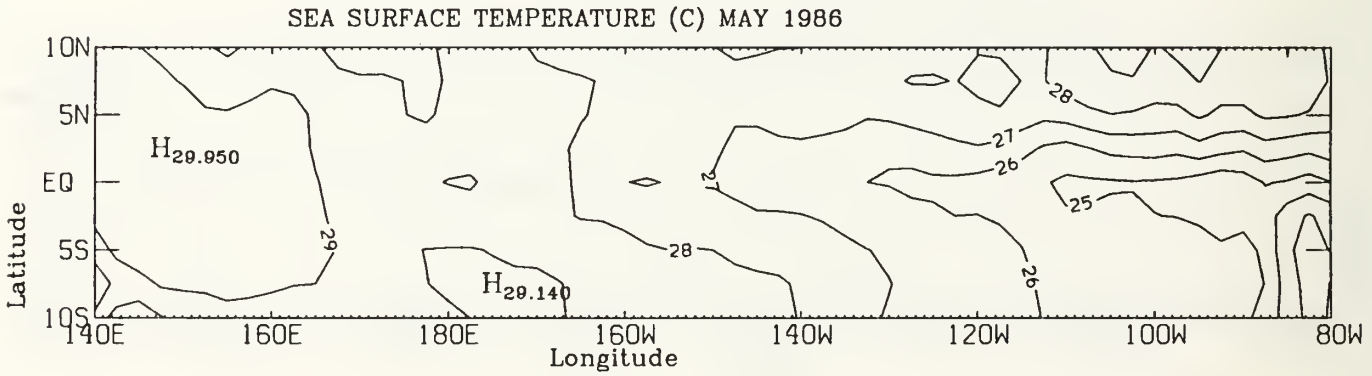
SEA SURFACE TEMPERATURE (C) MAY 1986
10N
5N
EQ
5S
10S
Latitude
140E
160E
180E
160W
140W
120W
100W
80W
Longitude
H29.950
H29.140
28
27
26
25

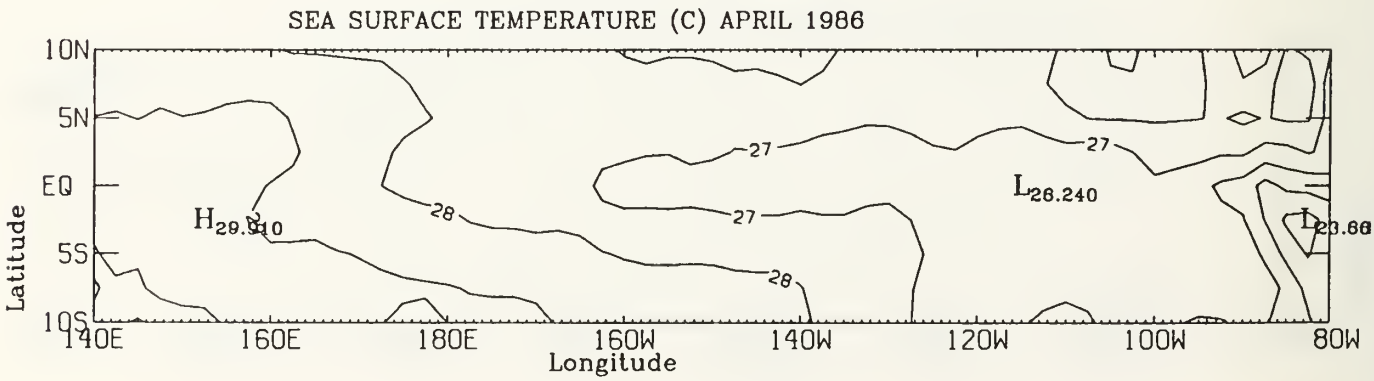
SEA SURFACE TEMPERATURE (C) APRIL 1986
10N
5N
EQ
5S
10S
Latitude
140E
160E
180E
160W
140W
120W
100W
80W
Longitude
H29.810
L26.240
27
28

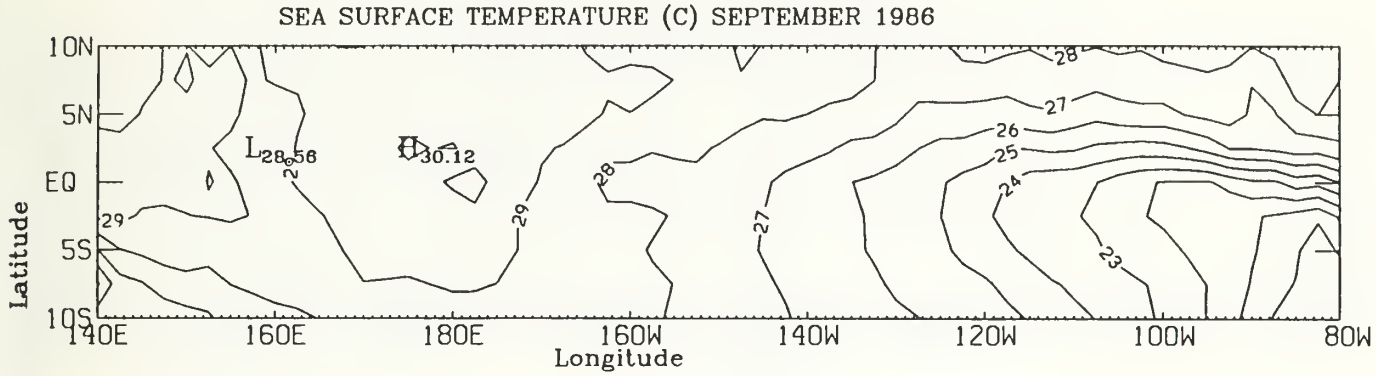
SEA SURFACE TEMPERATURE (C) SEPTEMBER 1986
10N
5N
EQ
5S
10S
Latitude
140E
160E
180E
160W
140W
120W
100W
80W
Longitude
L28.56
H30.12
29
28
27
26
25
24
23

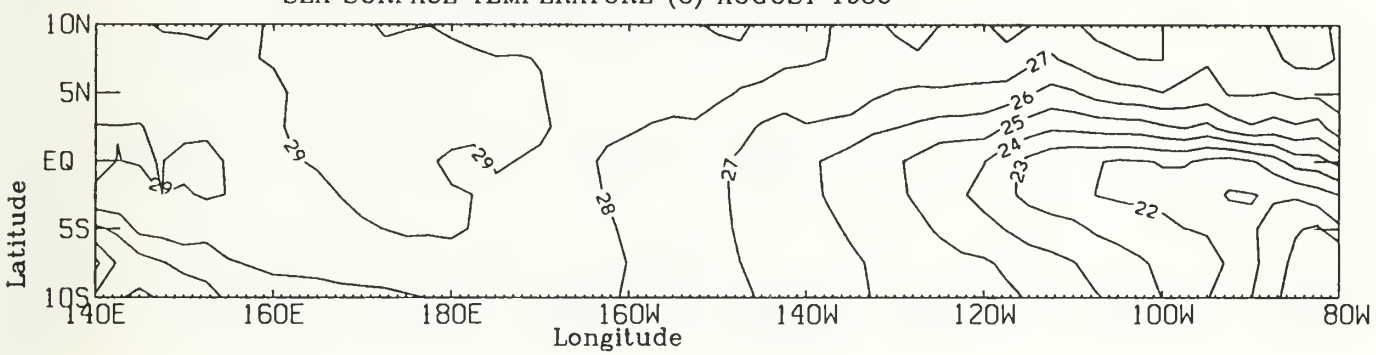
SEA SURFACE TEMPERATURE (C) AUGUST 1986
10N
5N
EQ
5S
10S
Latitude
140E
160E
180E
160W
140W
120W
100W
80W
Longitude
29
28
27
26
25
24
23
22

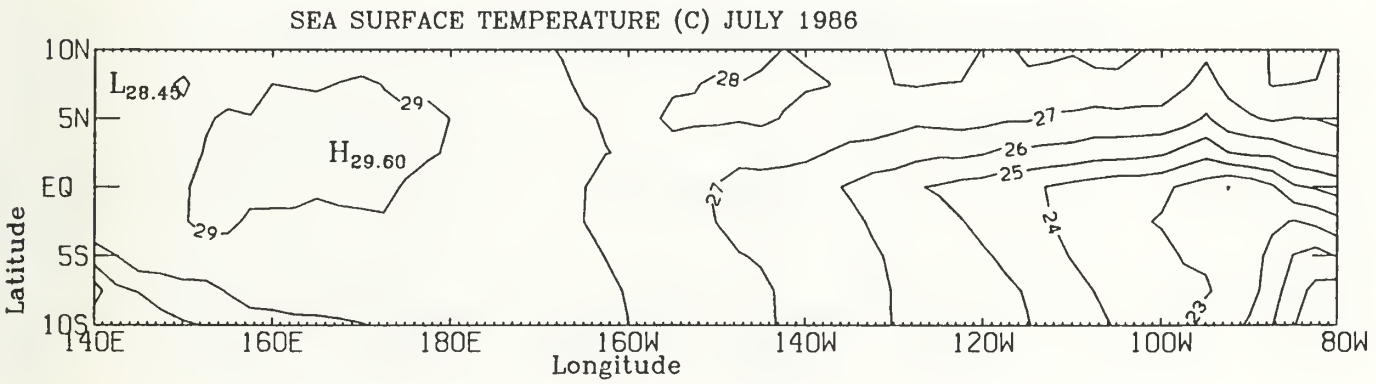
SEA SURFACE TEMPERATURE (C) JULY 1986
10N
5N
EQ
5S
10S
Latitude
140E
160E
180E
160W
140W
120W
100W
80W
Longitude
L28.45
H29.60
29
28
27
26
25
24
23

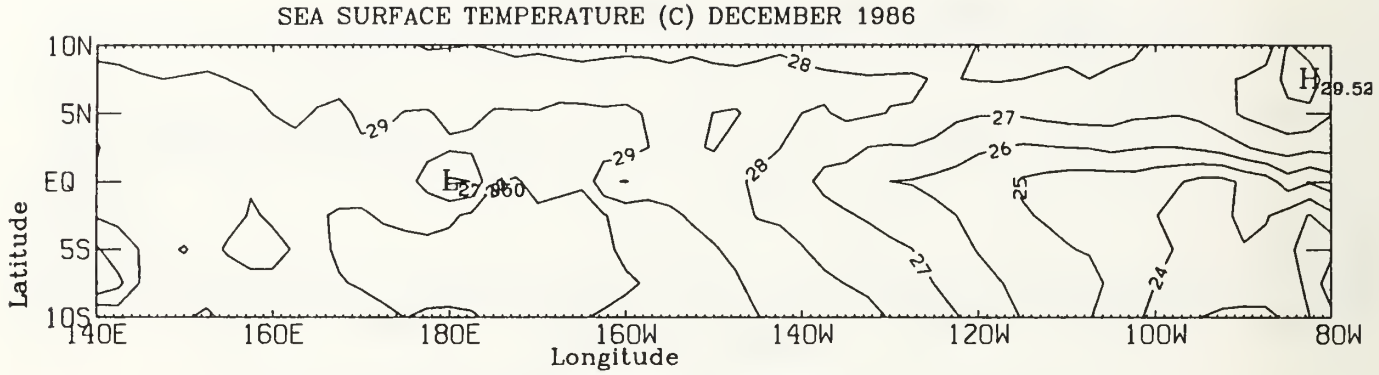
SEA SURFACE TEMPERATURE (C) DECEMBER 1986
10N
5N
EQ
5S
10S
Latitude
140E
160E
180E
160W
140W
120W
100W
80W
Longitude
28
29
29
28
27
26
25
27
24
H29.52
L27.80

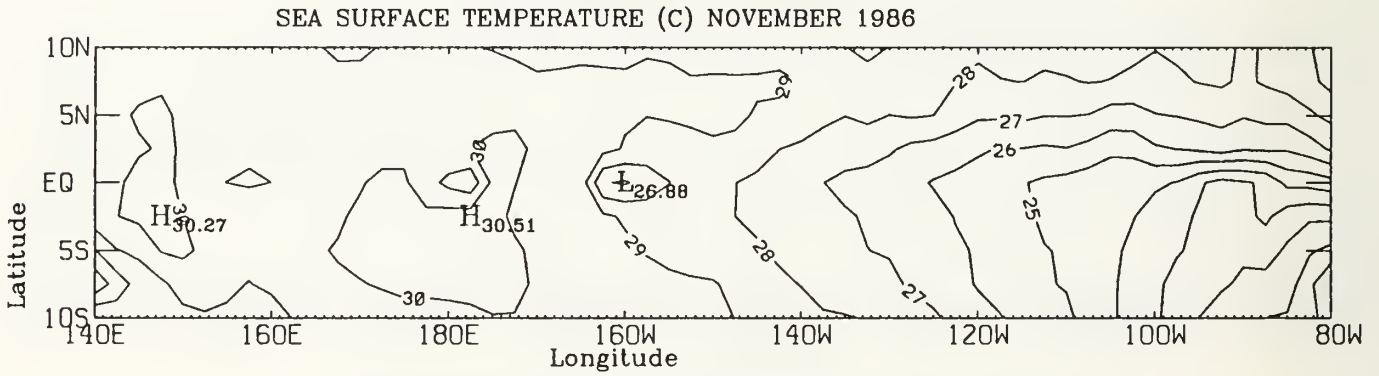
SEA SURFACE TEMPERATURE (C) NOVEMBER 1986
10N
5N
EQ
5S
10S
Latitude
140E
160E
180E
160W
140W
120W
100W
80W
Longitude
29
28
27
26
25
30
30
29
28
27
H30.27
H30.51
L26.88

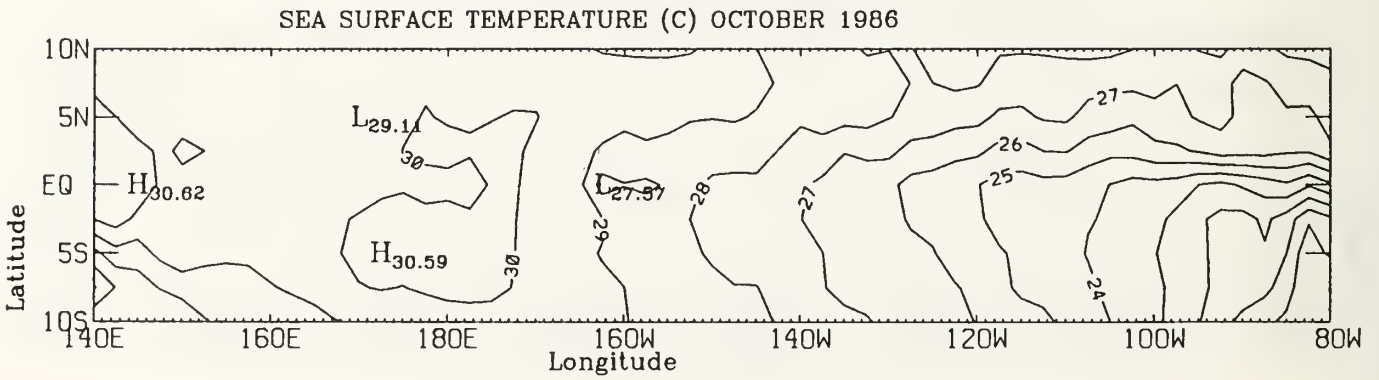
SEA SURFACE TEMPERATURE (C) OCTOBER 1986
10N
5N
EQ
5S
10S
Latitude
140E
160E
180E
160W
140W
120W
100W
80W
Longitude
27
26
25
28
27
29
30
30
24
H30.62
L29.11
H30.59
L27.57

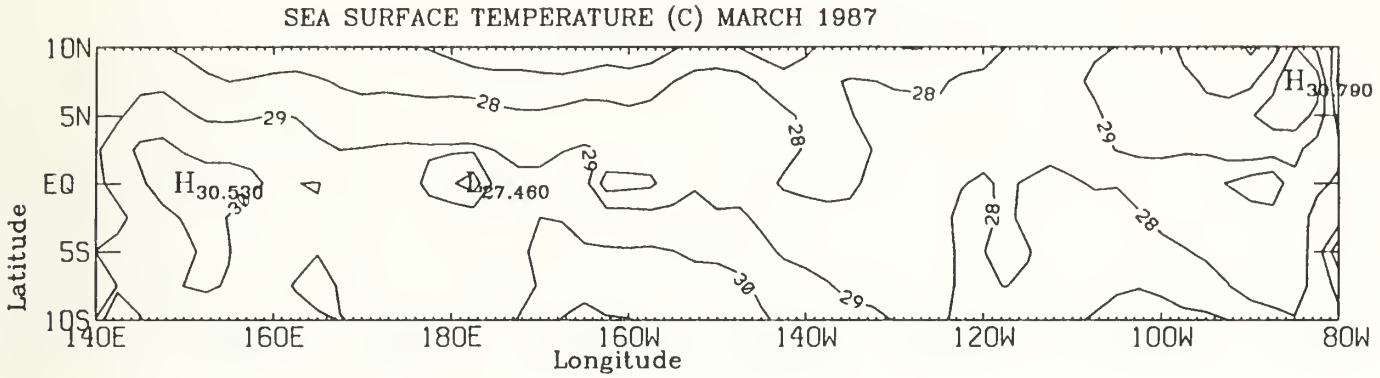
SEA SURFACE TEMPERATURE (C) MARCH 1987
10N
5N
EQ
5S
10S
Latitude
140E
160E
180E
160W
140W
120W
100W
80W
Longitude
H30.530
L27.460
H30.790
28
29
30

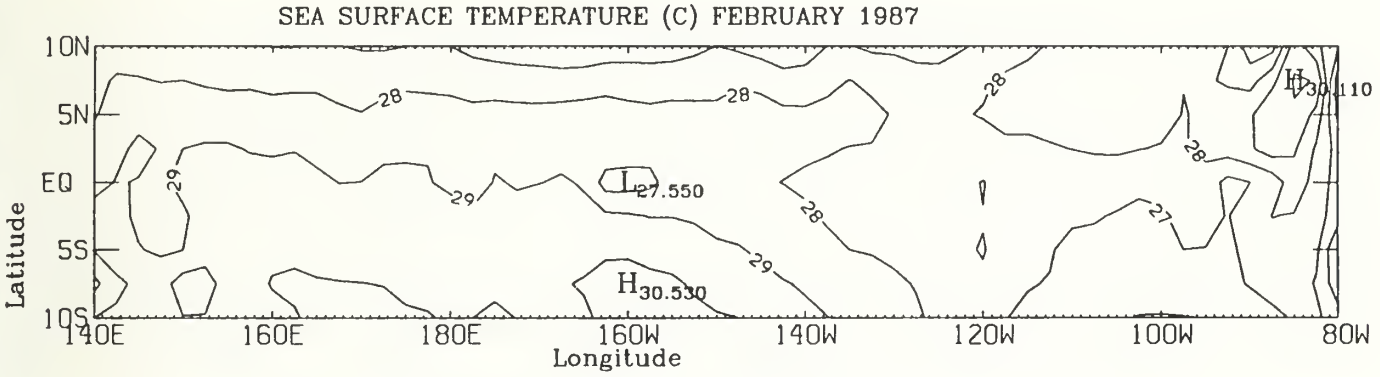
SEA SURFACE TEMPERATURE (C) FEBRUARY 1987
10N
5N
EQ
5S
10S
Latitude
140E
160E
180E
160W
140W
120W
100W
80W
Longitude
L27.550
H30.530
H30.110
28
29
27

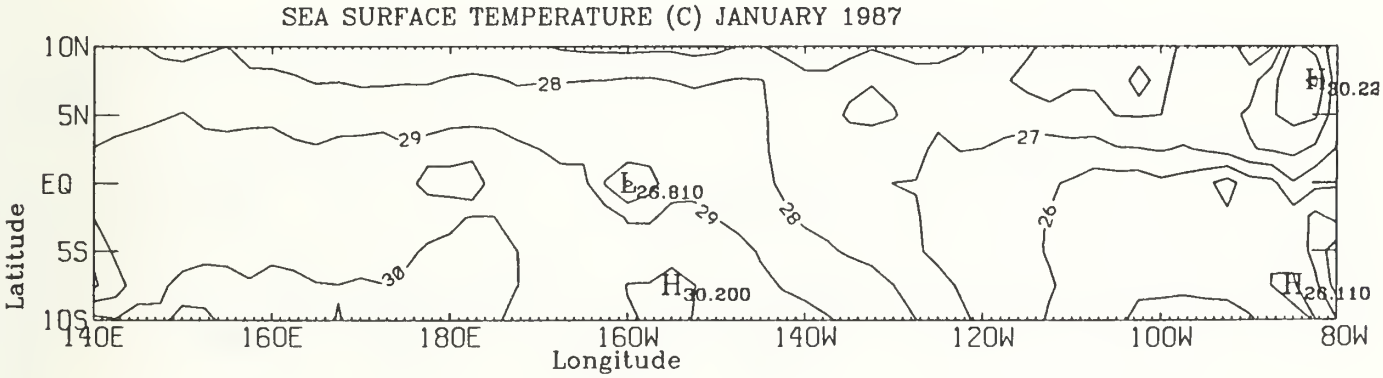
SEA SURFACE TEMPERATURE (C) JANUARY 1987
10N
5N
EQ
5S
10S
Latitude
140E
160E
180E
160W
140W
120W
100W
80W
Longitude
L26.810
H30.200
H28.110
28
29
30
27
26

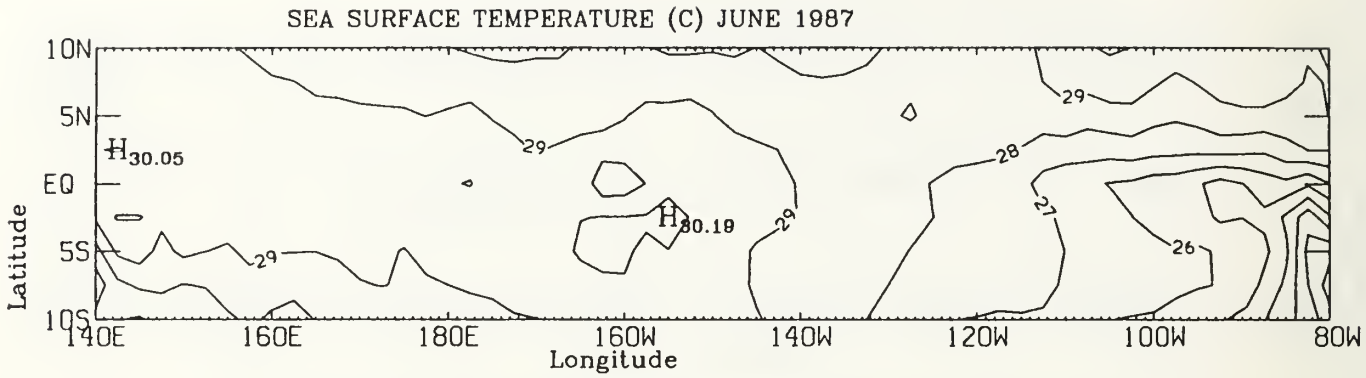
SEA SURFACE TEMPERATURE (C) JUNE 1987
10N
5N
EQ
5S
10S
Latitude
140E
160E
180E
160W
140W
120W
100W
80W
Longitude
H30.05
H30.19
29
28
27
26

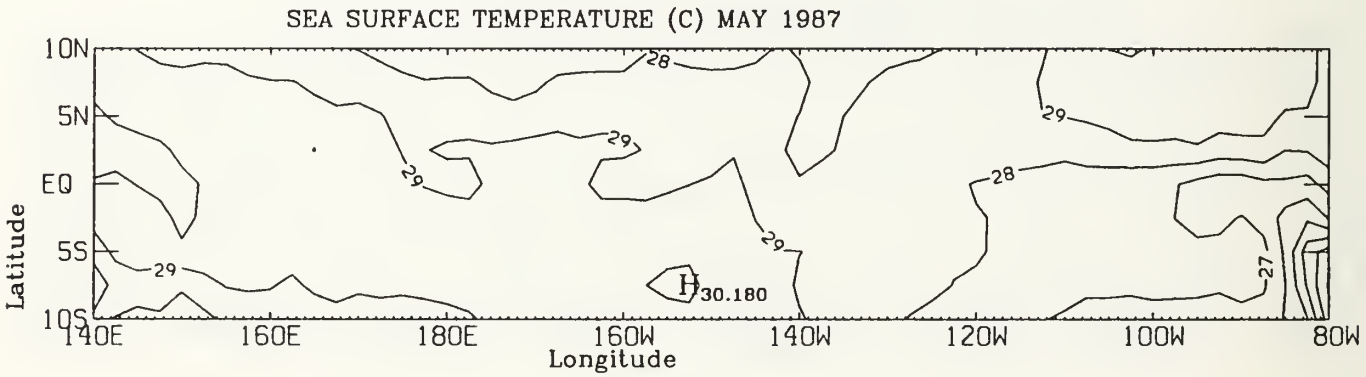
SEA SURFACE TEMPERATURE (C) MAY 1987
10N
5N
EQ
5S
10S
Latitude
140E
160E
180E
160W
140W
120W
100W
80W
Longitude
H30.180
28
29
27

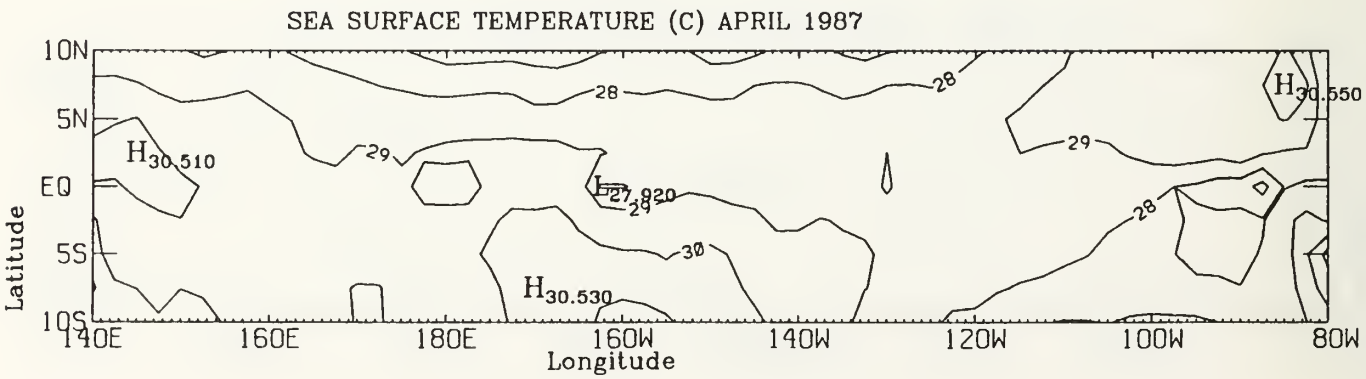
SEA SURFACE TEMPERATURE (C) APRIL 1987
10N
5N
EQ
5S
10S
Latitude
140E
160E
180E
160W
140W
120W
100W
80W
Longitude
H30.510
H30.550
H30.530
28
29
30

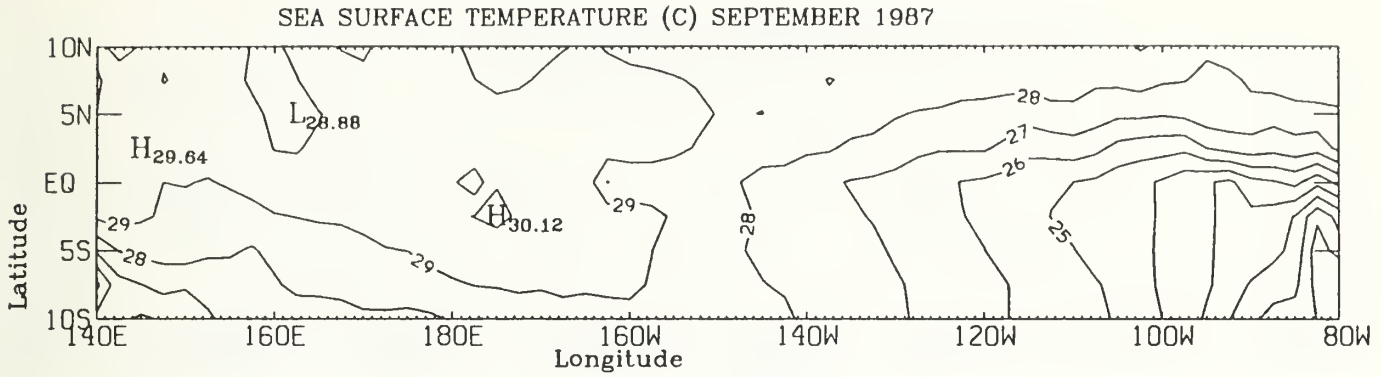
SEA SURFACE TEMPERATURE (C) SEPTEMBER 1987
10N
5N
EQ
5S
10S
Latitude
140E
160E
180E
160W
140W
120W
100W
80W
Longitude
H29.64
L28.88
H30.12
29
28
27
26
25

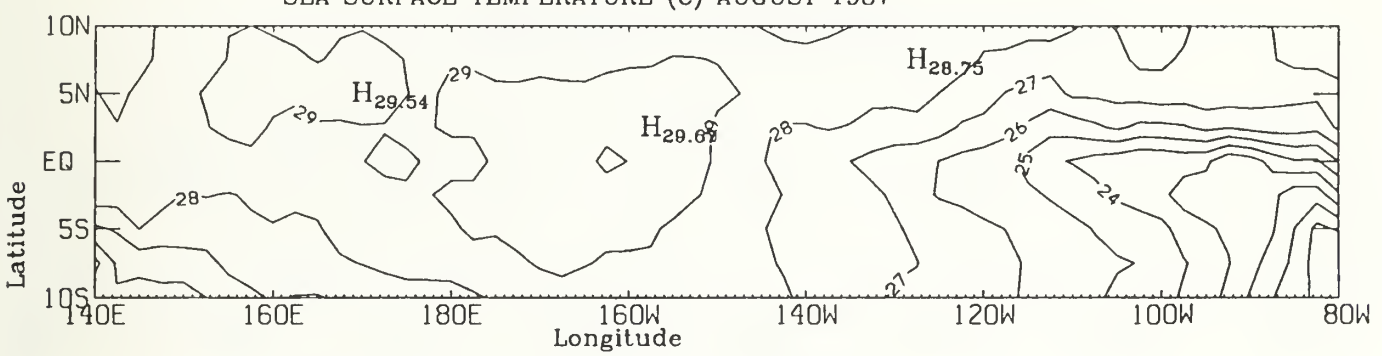
SEA SURFACE TEMPERATURE (C) AUGUST 1987
10N
5N
EQ
5S
10S
Latitude
140E
160E
180E
160W
140W
120W
100W
80W
Longitude
H29.54
H29.62
H28.75
29
28
27
26
25
24

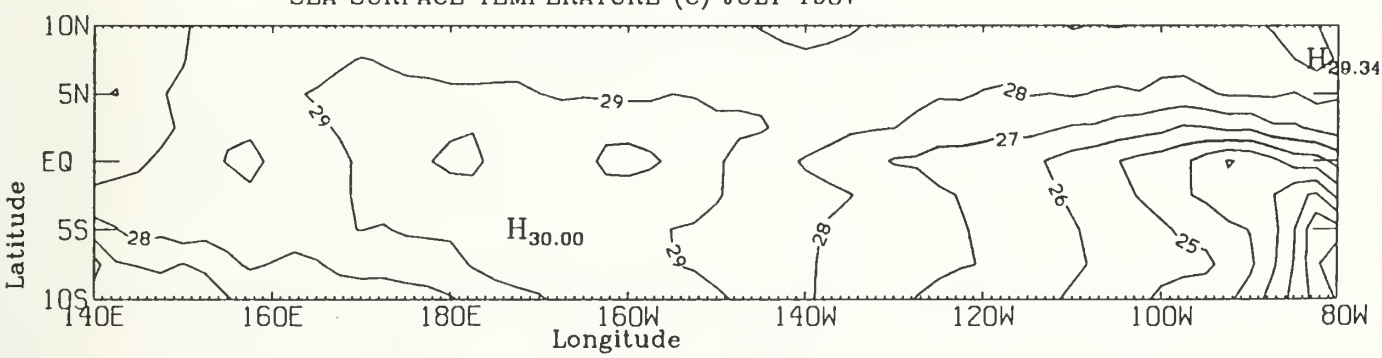
SEA SURFACE TEMPERATURE (C) JULY 1987
10N
5N
EQ
5S
10S
Latitude
140E
160E
180E
160W
140W
120W
100W
80W
Longitude
H30.00
H29.34
29
28
27
26
25

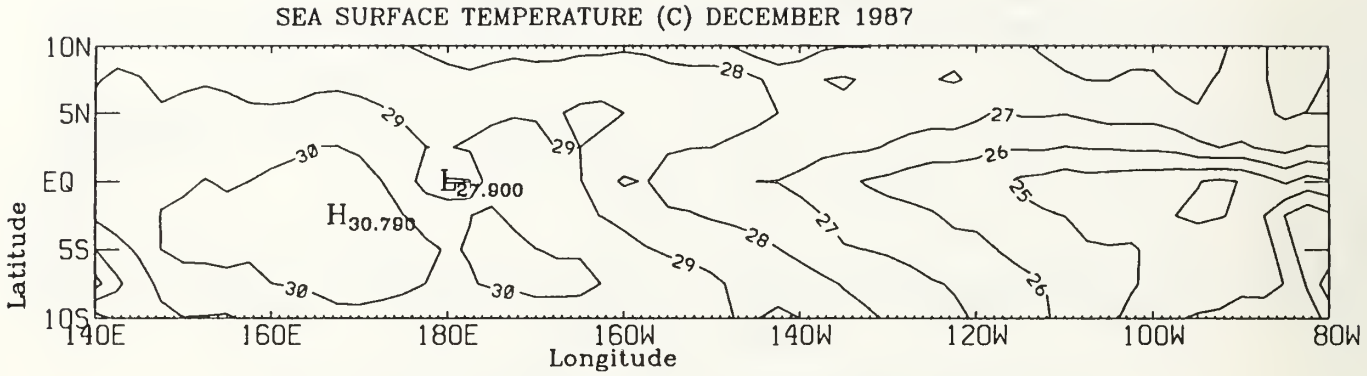
SEA SURFACE TEMPERATURE (C) DECEMBER 1987
10N
5N
EQ
5S
10S
Latitude
140E
160E
180E
160W
140W
120W
100W
80W
Longitude
H30.790
L27.900
28
29
30
27
26
25

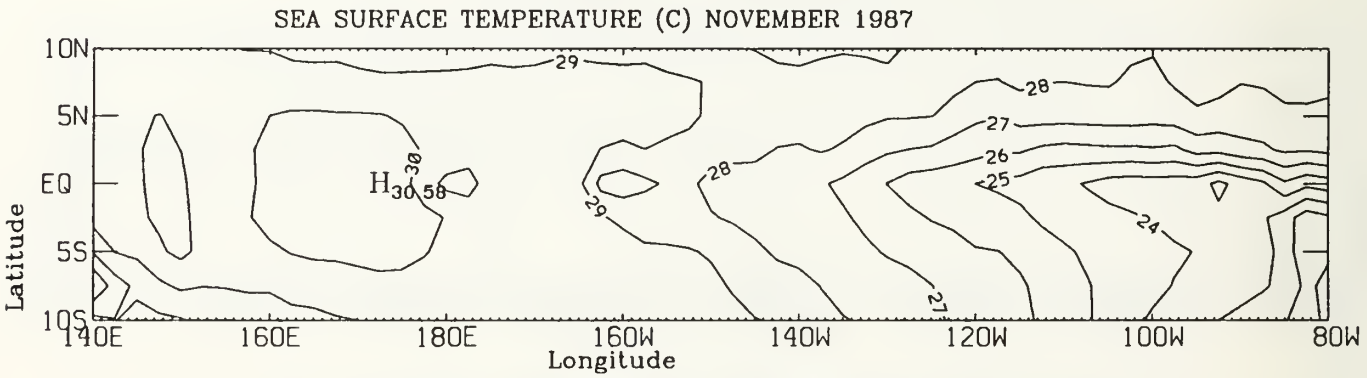
SEA SURFACE TEMPERATURE (C) NOVEMBER 1987
10N
5N
EQ
5S
10S
Latitude
140E
160E
180E
160W
140W
120W
100W
80W
Longitude
H30.58
29
30
28
27
26
25
24

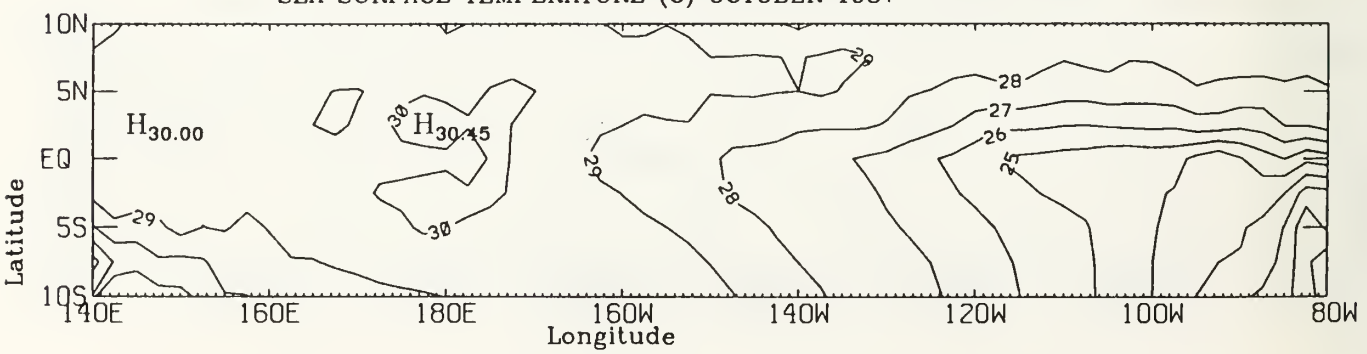
SEA SURFACE TEMPERATURE (C) OCTOBER 1987
10N
5N
EQ
5S
10S
Latitude
140E
160E
180E
160W
140W
120W
100W
80W
Longitude
H30.00
H30.15
29
30
28
27
26
25

APPENDIX D. MONTHLY MIXED LAYER DEPTH FIELDS

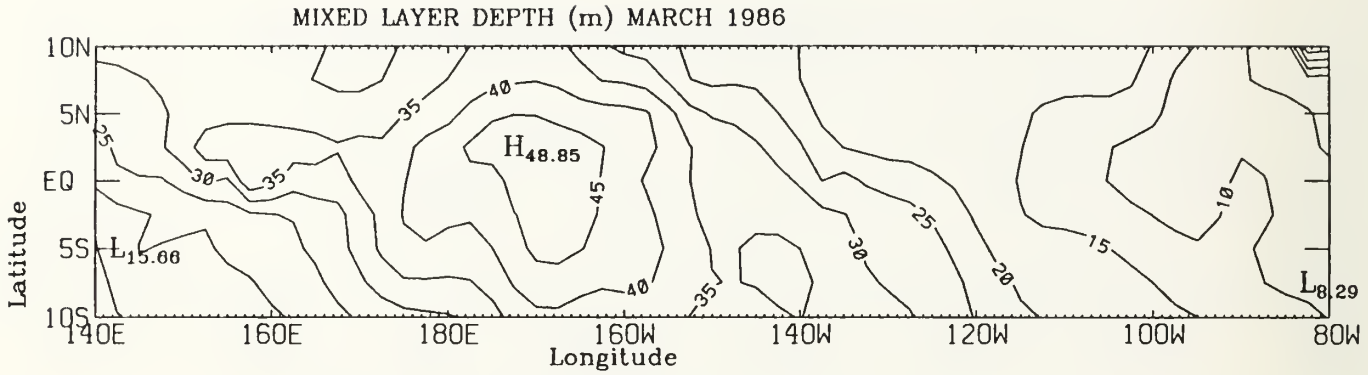
MIXED LAYER DEPTH (m) MARCH 1986
10N
5N
EQ
5S
10S
Latitude
140E
160E
180E
160W
140W
120W
100W
80W
Longitude
H48.85
L15.66
L8.29
25
30
35
40
45
35
30
25
20
15
10

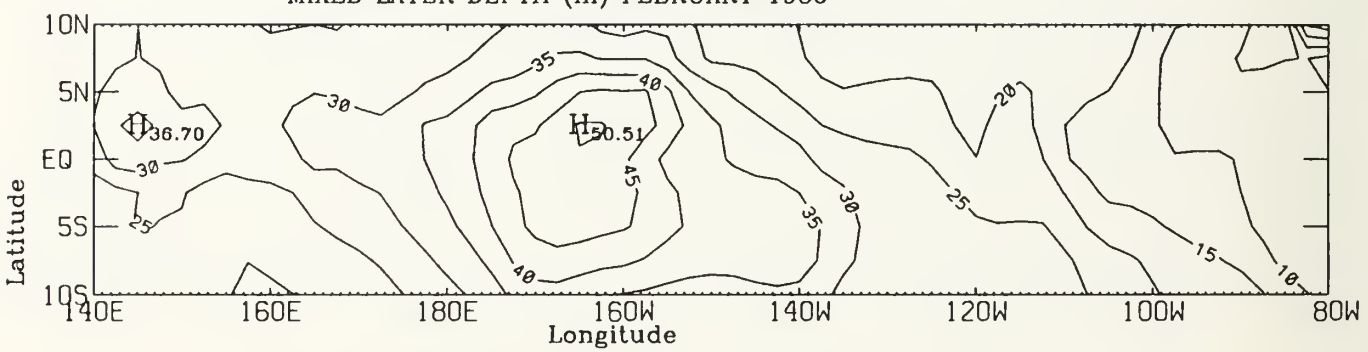
MIXED LAYER DEPTH (m) FEBRUARY 1986
10N
5N
EQ
5S
10S
Latitude
140E
160E
180E
160W
140W
120W
100W
80W
Longitude
H36.70
H50.51
30
25
35
40
45
35
30
25
20
15
10

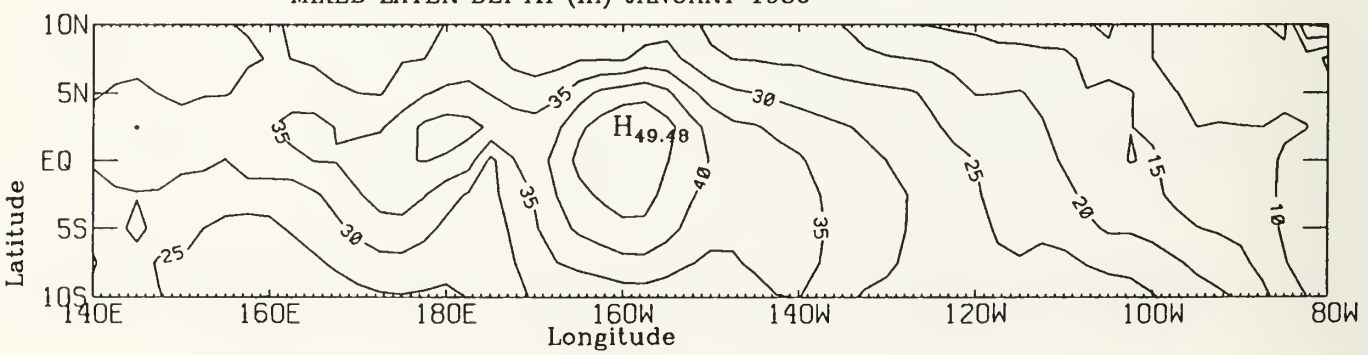
MIXED LAYER DEPTH (m) JANUARY 1986
10N
5N
EQ
5S
10S
Latitude
140E
160E
180E
160W
140W
120W
100W
80W
Longitude
H49.48
25
30
35
40
35
30
25
20
15
10

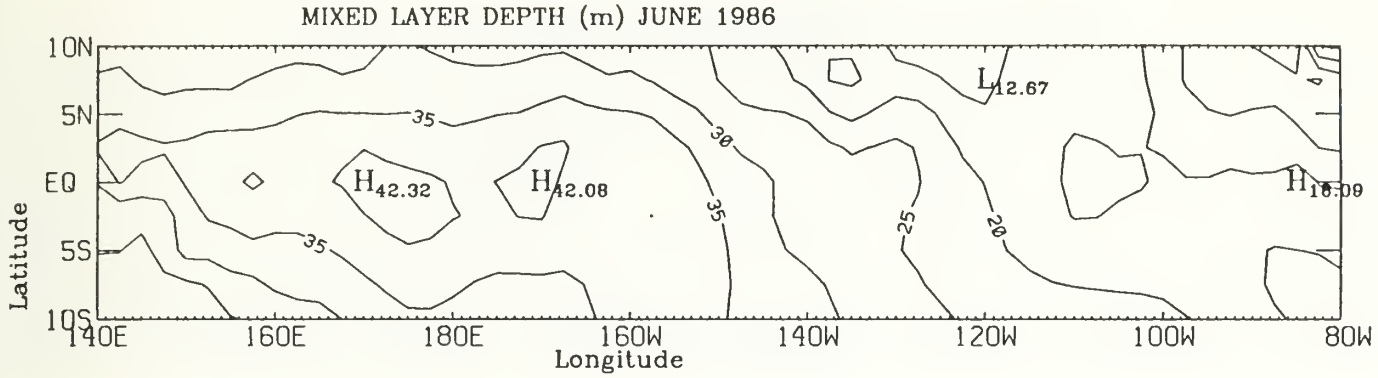
MIXED LAYER DEPTH (m) JUNE 1986
10N
5N
EQ
5S
10S
140E
160E
180E
160W
140W
120W
100W
80W
Latitude
Longitude
H42.32
H42.08
L12.67
35
30
25
20

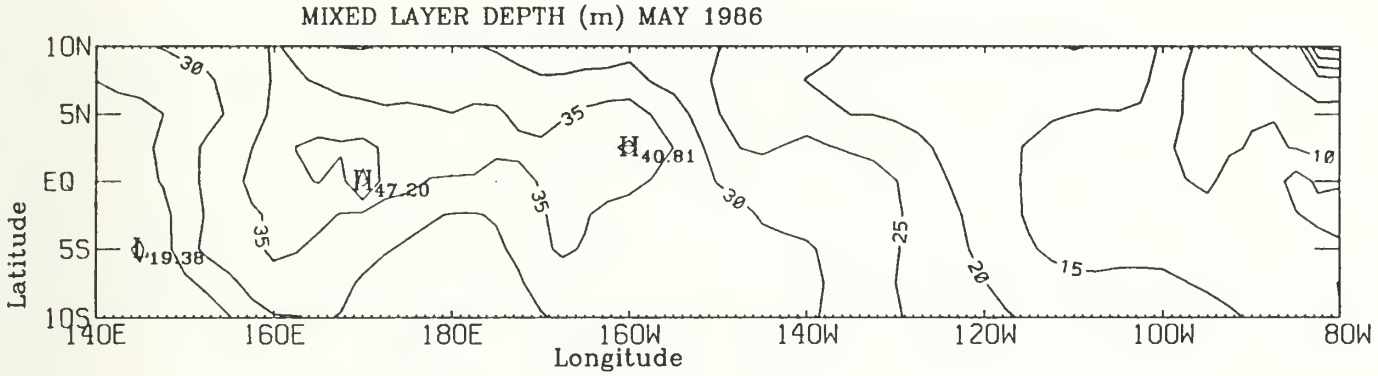
MIXED LAYER DEPTH (m) MAY 1986
10N
5N
EQ
5S
10S
140E
160E
180E
160W
140W
120W
100W
80W
Latitude
Longitude
H40.81
H47.20
L19.38
35
30
25
20
15
10

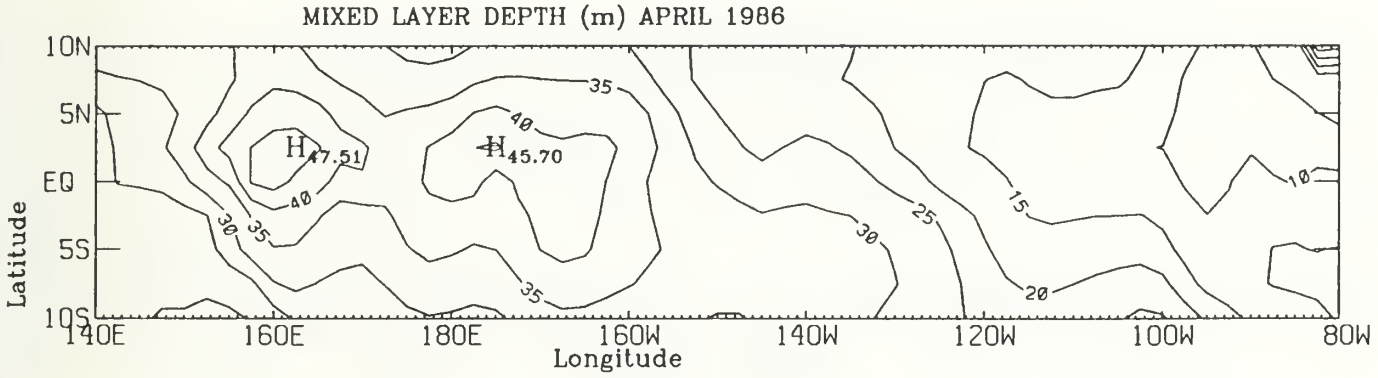
MIXED LAYER DEPTH (m) APRIL 1986
10N
5N
EQ
5S
10S
140E
160E
180E
160W
140W
120W
100W
80W
Latitude
Longitude
H47.51
H45.70
40
35
30
25
20
15
10

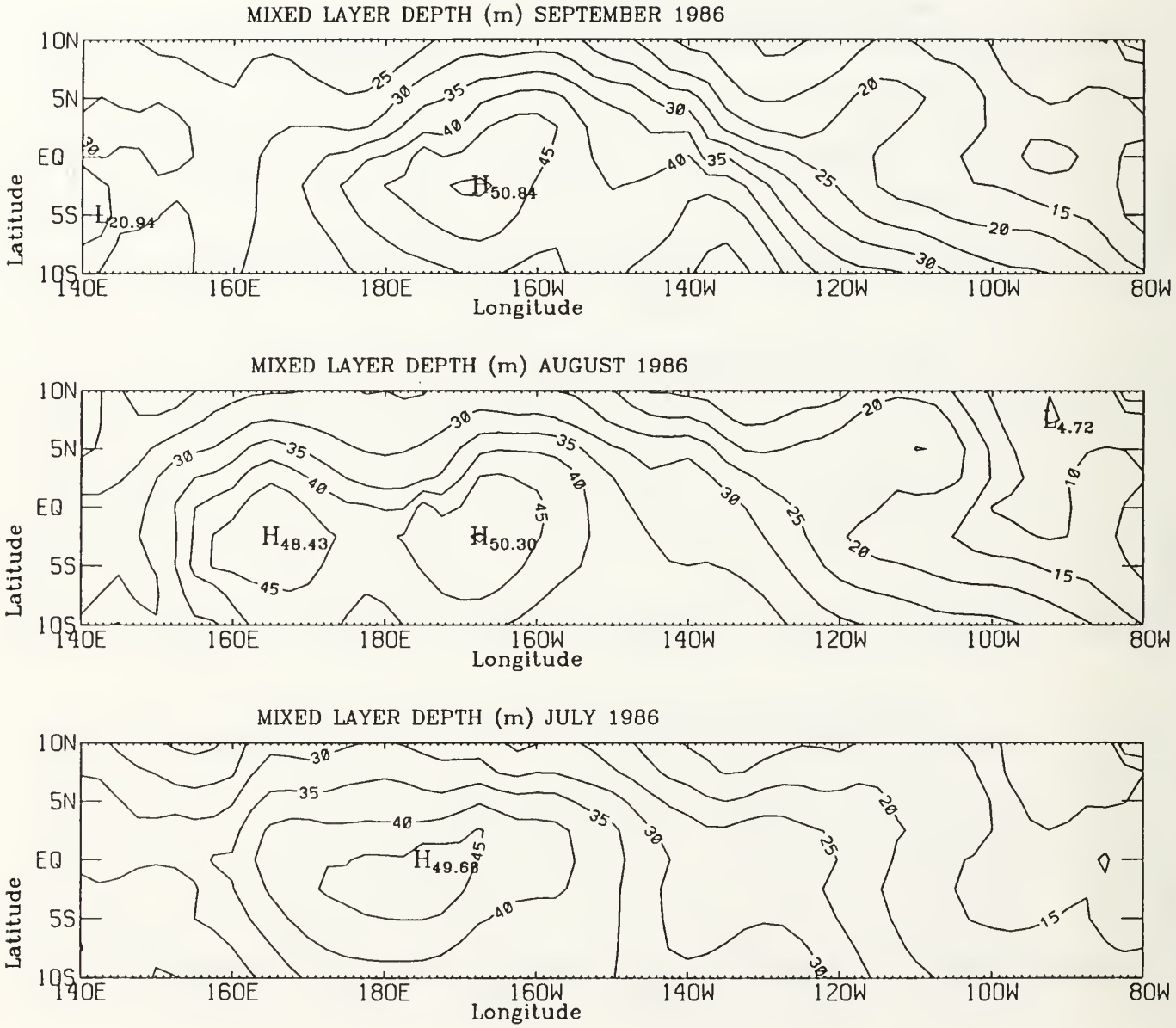
MIXED LAYER DEPTH (m) SEPTEMBER 1986
10N
5N
EQ
5S
10S
Latitude
140E
160E
180E
160W
140W
120W
100W
80W
Longitude
H50.84
L20.94
MIXED LAYER DEPTH (m) AUGUST 1986
H48.43
H50.30
L4.72
MIXED LAYER DEPTH (m) JULY 1986
H49.68

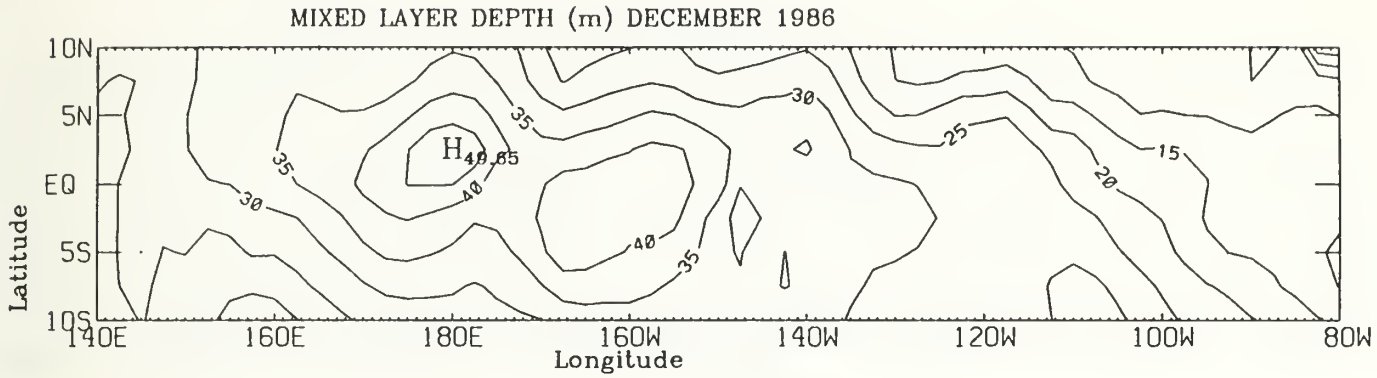
MIXED LAYER DEPTH (m) DECEMBER 1986
10N
5N
EQ
5S
10S
Latitude
140E
160E
180E
160W
140W
120W
100W
80W
Longitude
H49.65
30
35
40
25
20
15

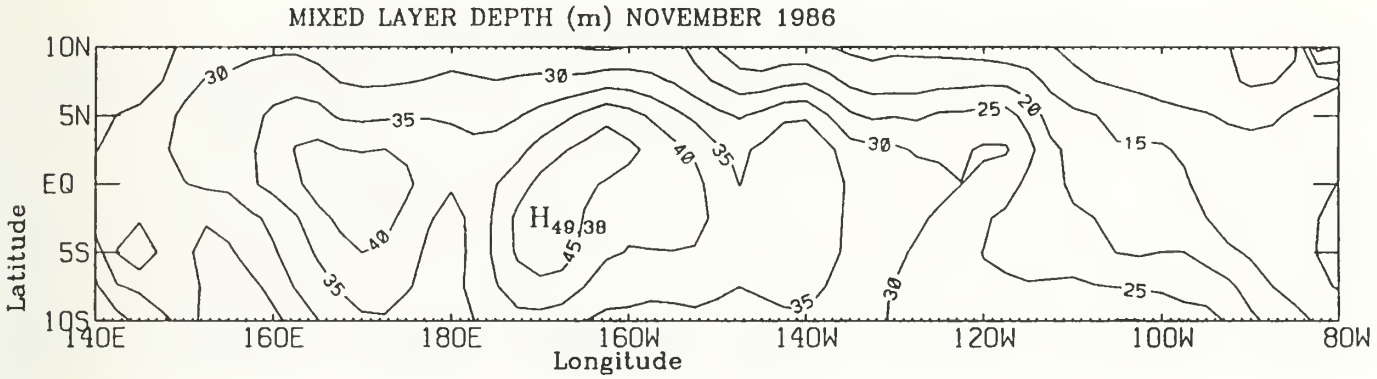
MIXED LAYER DEPTH (m) NOVEMBER 1986
10N
5N
EQ
5S
10S
Latitude
140E
160E
180E
160W
140W
120W
100W
80W
Longitude
H49.38
30
35
40
45
25
20
15

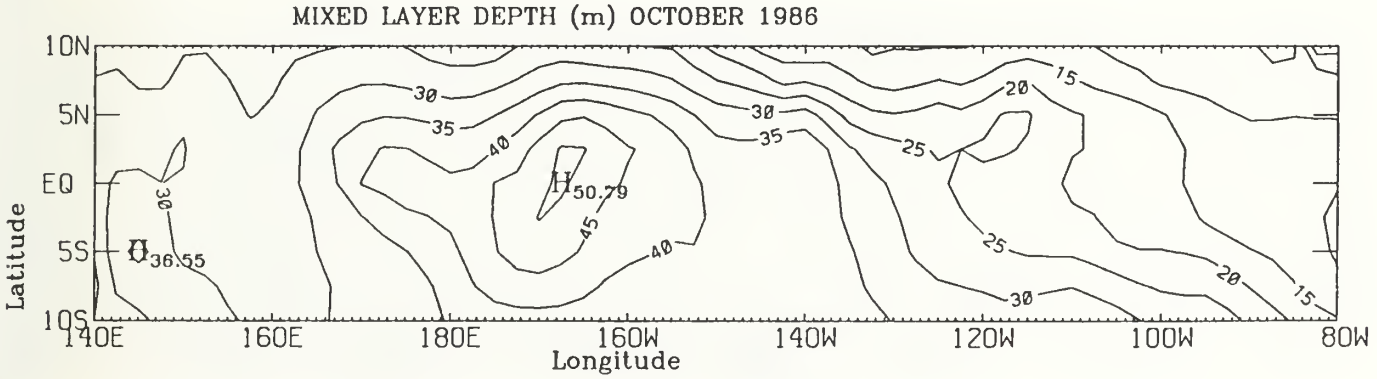
MIXED LAYER DEPTH (m) OCTOBER 1986
10N
5N
EQ
5S
10S
Latitude
140E
160E
180E
160W
140W
120W
100W
80W
Longitude
H50.79
U36.55
30
35
40
45
25
20
15

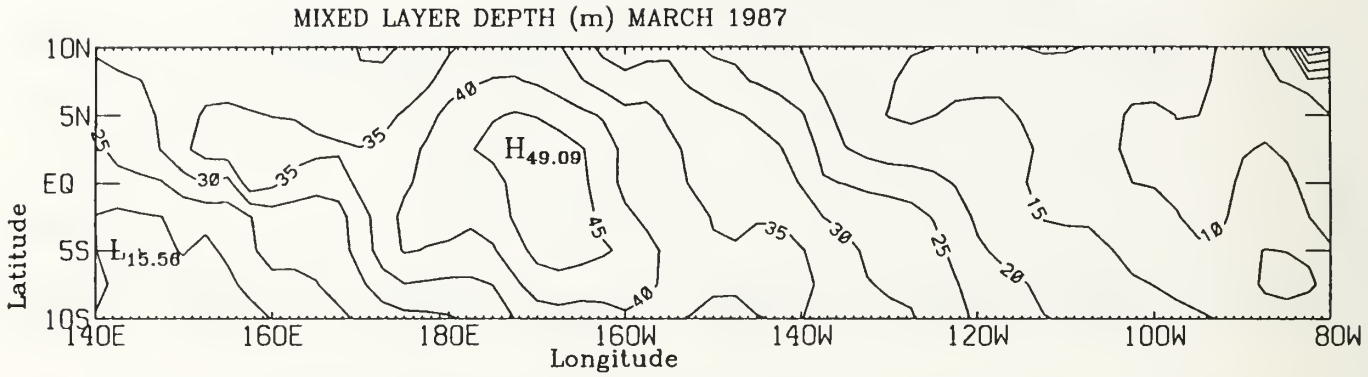
MIXED LAYER DEPTH (m) MARCH 1987
10N
5N
EQ
5S
10S
Latitude
140E
160E
180E
160W
140W
120W
100W
80W
Longitude
H49.09
L15.56

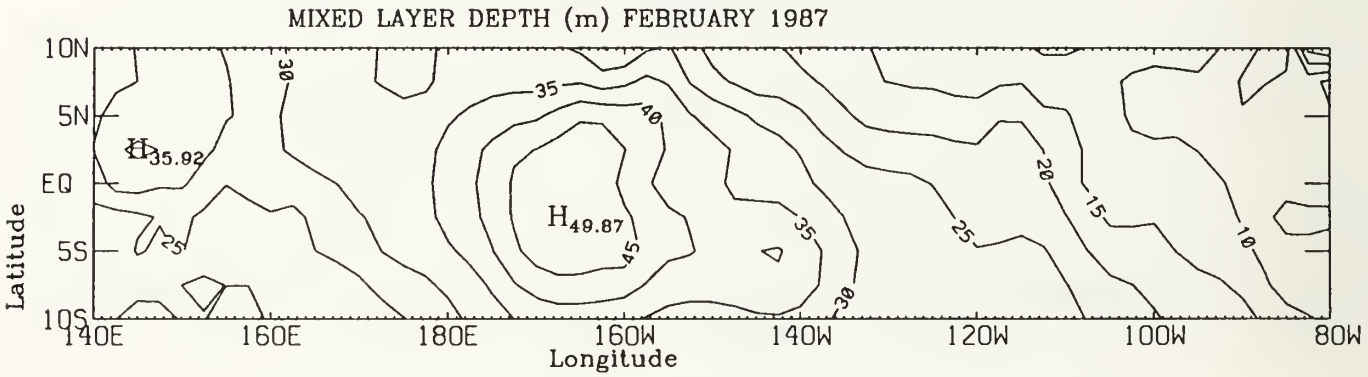
MIXED LAYER DEPTH (m) FEBRUARY 1987
10N
5N
EQ
5S
10S
Latitude
140E
160E
180E
160W
140W
120W
100W
80W
Longitude
H35.92
H49.87

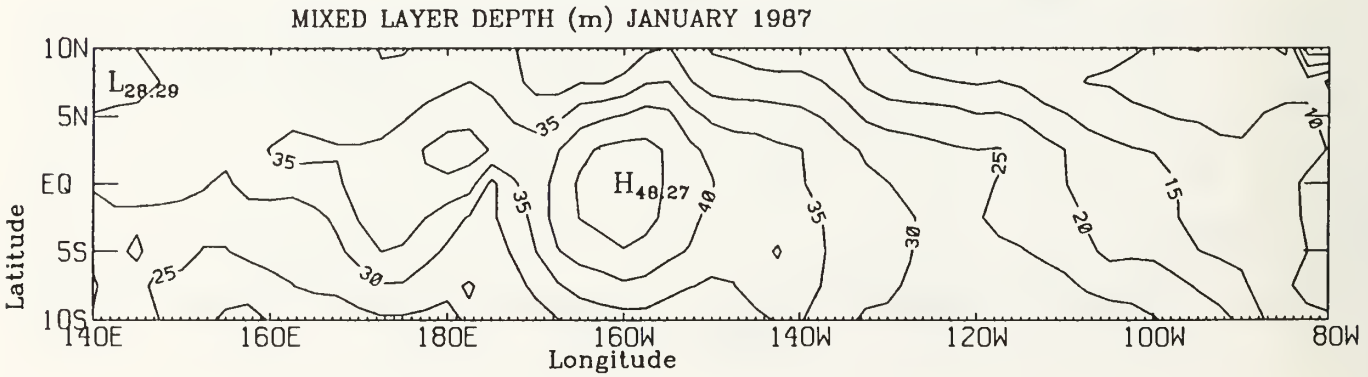
MIXED LAYER DEPTH (m) JANUARY 1987
10N
5N
EQ
5S
10S
Latitude
140E
160E
180E
160W
140W
120W
100W
80W
Longitude
L28.29
H48.27

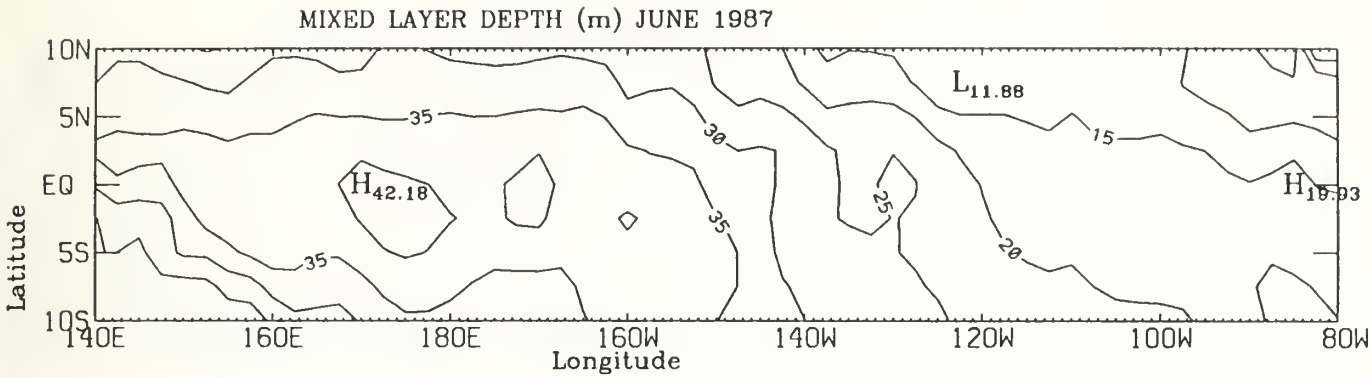
MIXED LAYER DEPTH (m) JUNE 1987
10N
5N
EQ
5S
10S
140E
160E
180E
160W
140W
120W
100W
80W
Latitude
Longitude
35
30
25
20
15
$H_{42.18}$
$L_{11.88}$
$H_{15.93}$

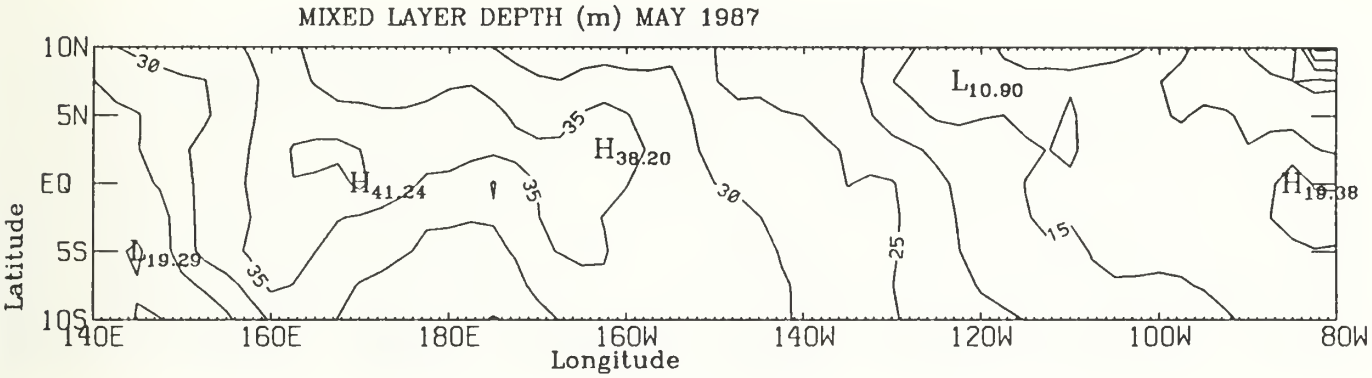
MIXED LAYER DEPTH (m) MAY 1987
10N
5N
EQ
5S
10S
140E
160E
180E
160W
140W
120W
100W
80W
Latitude
Longitude
30
35
25
15
$H_{41.24}$
$H_{38.20}$
$L_{10.90}$
$H_{19.38}$
$L_{19.29}$

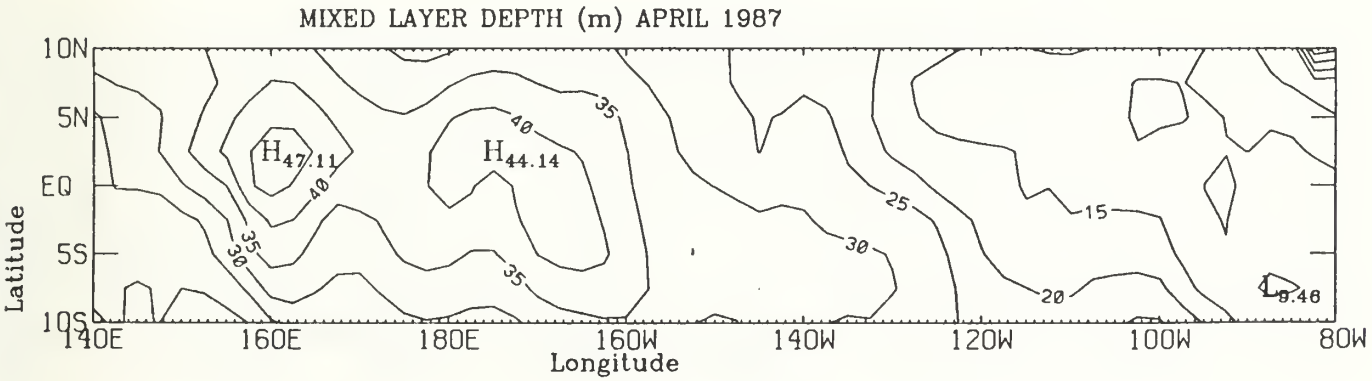
MIXED LAYER DEPTH (m) APRIL 1987
10N
5N
EQ
5S
10S
140E
160E
180E
160W
140W
120W
100W
80W
Latitude
Longitude
40
35
30
25
20
15
$H_{47.11}$
$H_{44.14}$
$L_{9.46}$

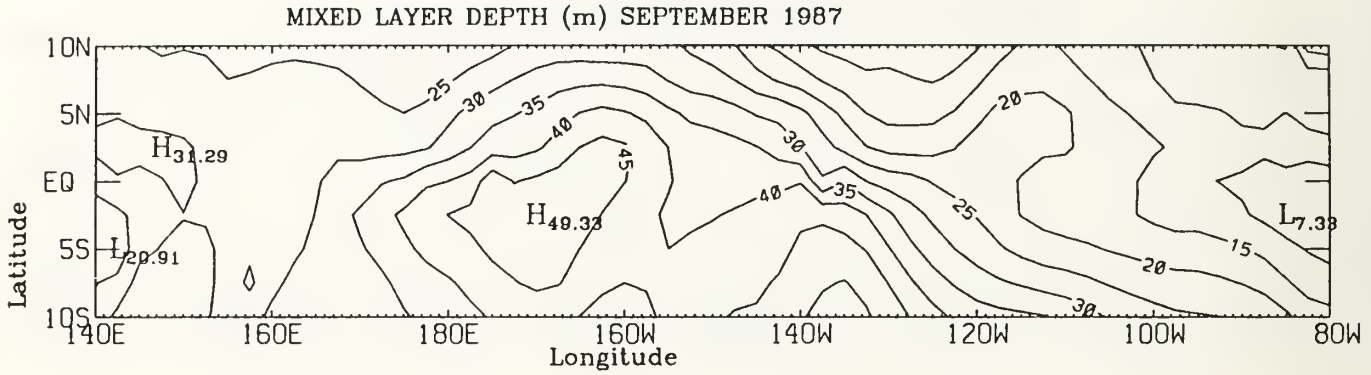
MIXED LAYER DEPTH (m) SEPTEMBER 1987
10N
5N
EQ
5S
10S
Latitude
140E
160E
180E
160W
140W
120W
100W
80W
Longitude
H31.29
H49.33
L20.91
L7.33
25
30
35
40
45
20
15

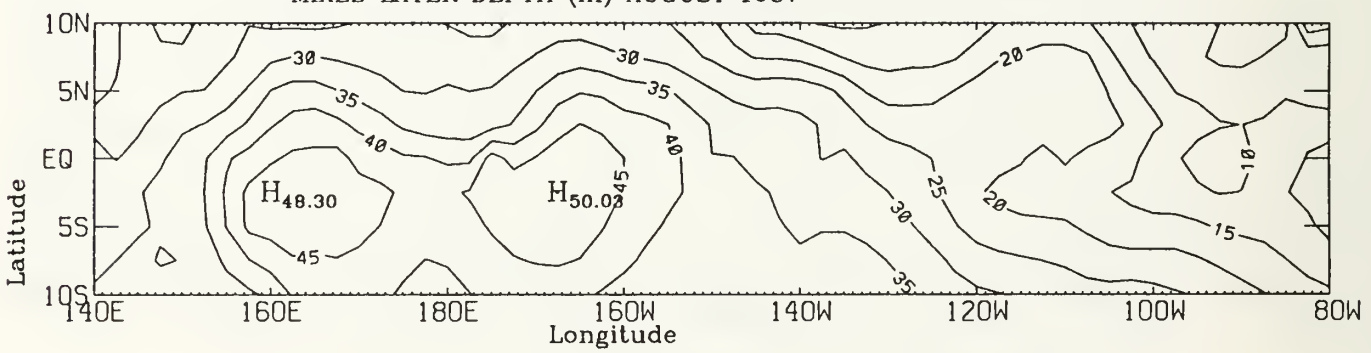
MIXED LAYER DEPTH (m) AUGUST 1987
10N
5N
EQ
5S
10S
Latitude
140E
160E
180E
160W
140W
120W
100W
80W
Longitude
H48.30
H50.03
30
35
40
45
20
25
15
10

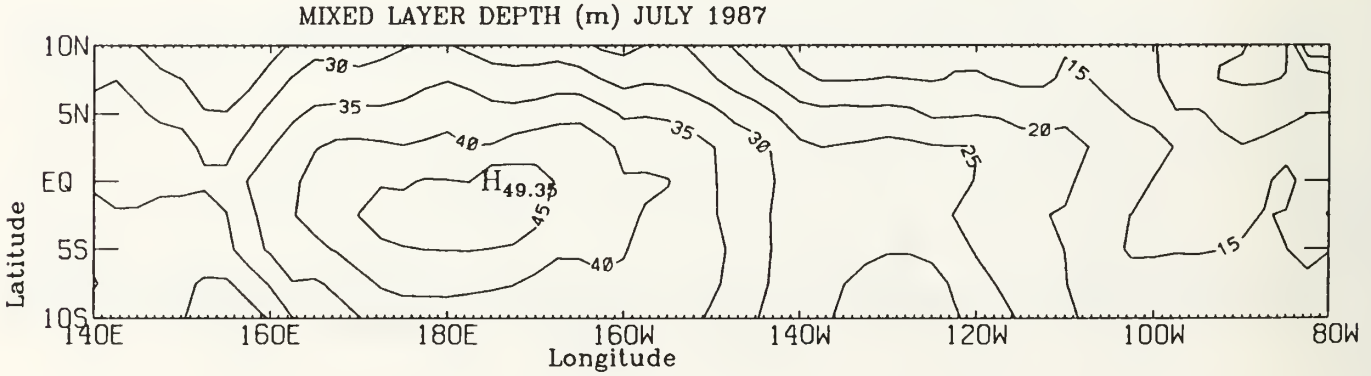
MIXED LAYER DEPTH (m) JULY 1987
10N
5N
EQ
5S
10S
Latitude
140E
160E
180E
160W
140W
120W
100W
80W
Longitude
H49.35
30
35
40
45
20
25
15

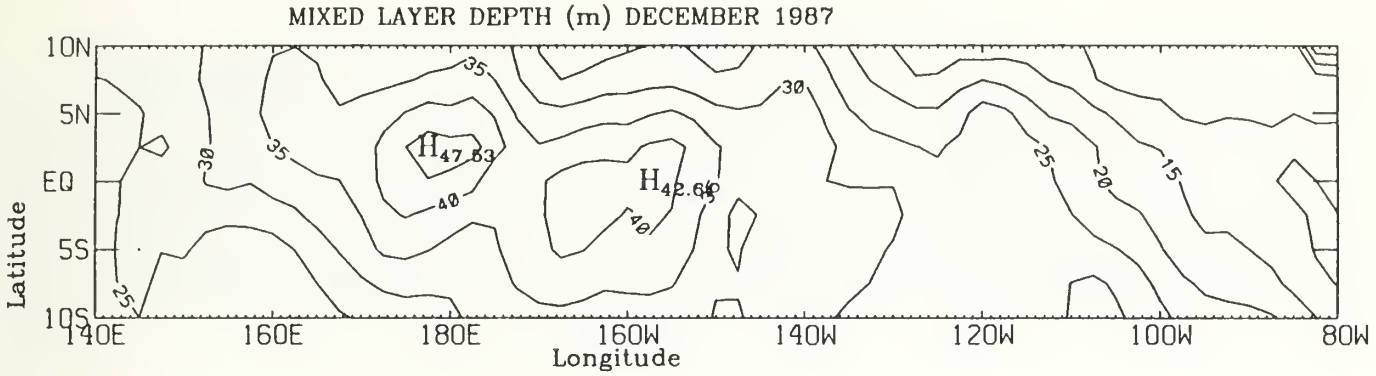
MIXED LAYER DEPTH (m) DECEMBER 1987
10N
5N
EQ
5S
10S
Latitude
140E
160E
180E
160W
140W
120W
100W
80W
Longitude
H47.53
H42.65
35
30
25
20
15
40
45

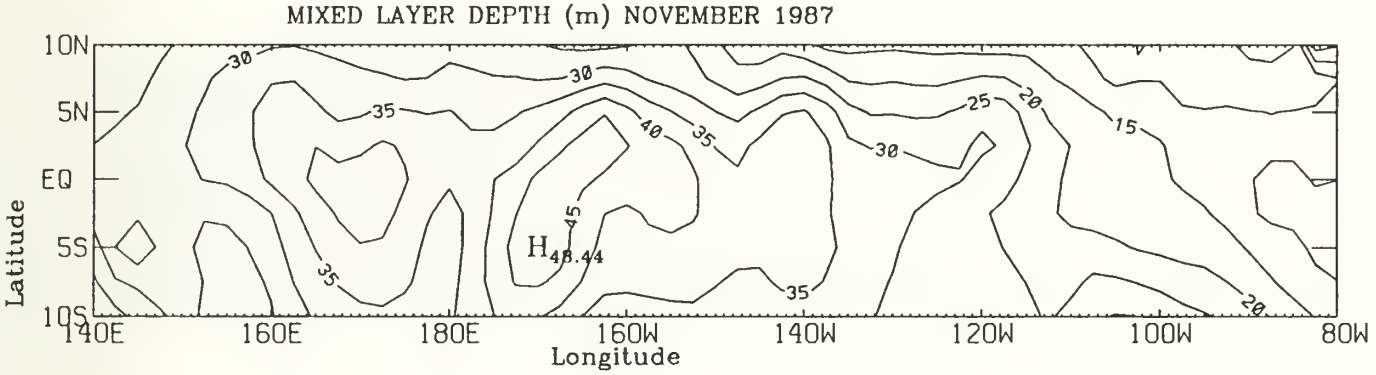
MIXED LAYER DEPTH (m) NOVEMBER 1987
10N
5N
EQ
5S
10S
Latitude
140E
160E
180E
160W
140W
120W
100W
80W
Longitude
H48.44
30
35
40
45
25
20
15

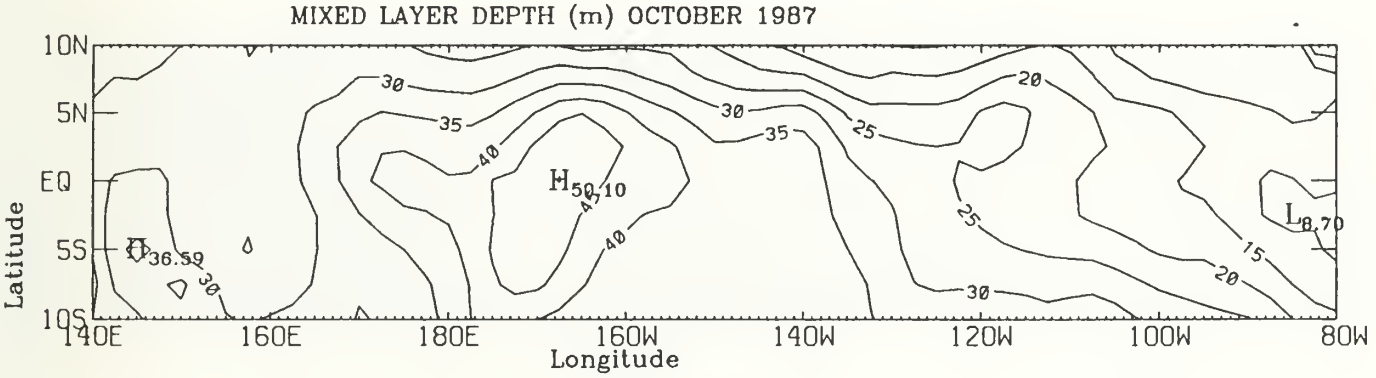
MIXED LAYER DEPTH (m) OCTOBER 1987
10N
5N
EQ
5S
10S
Latitude
140E
160E
180E
160W
140W
120W
100W
80W
Longitude
H50.10
H36.59
L8.70
30
35
40
45
25
20
15

APPENDIX E. MONTHLY P-VALUE FIELDS

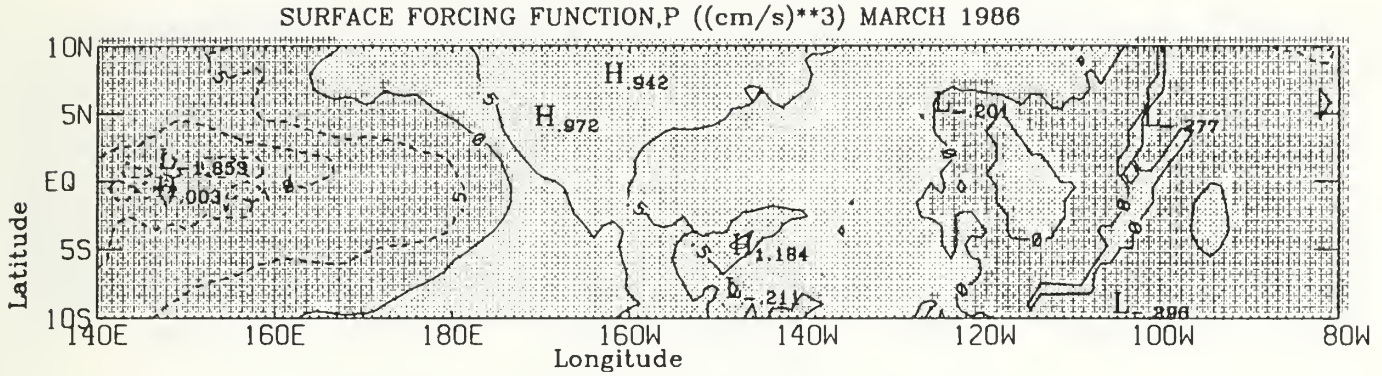
SURFACE FORCING FUNCTION,P ((cm/s)**3) MARCH 1986
10N
5N
EQ
5S
10S
Latitude
140E
160E
180E
160W
140W
120W
100W
80W
Longitude
H .942
H .972
L -.201
L -.377
L -1.853
H .003
H 1.184
L -.211
L -.396

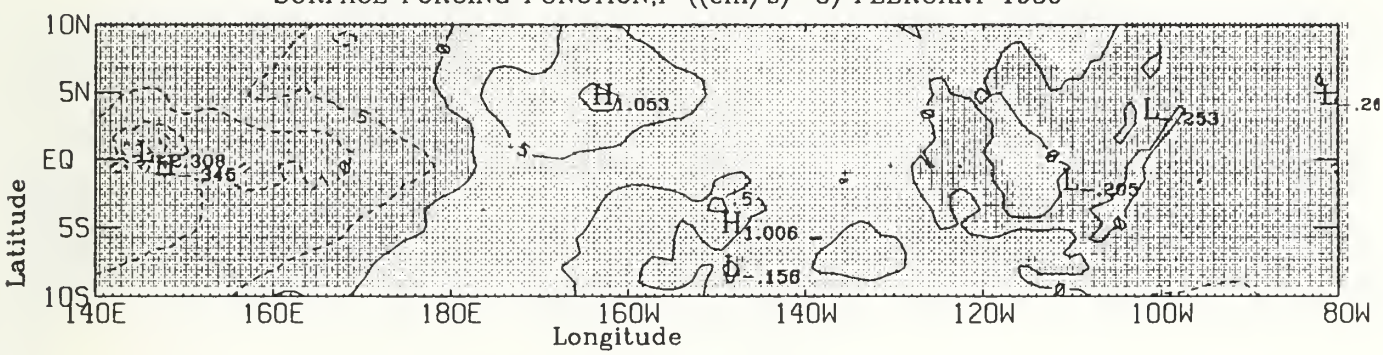
SURFACE FORCING FUNCTION,P ((cm/s)**3) FEBRUARY 1986
10N
5N
EQ
5S
10S
Latitude
140E
160E
180E
160W
140W
120W
100W
80W
Longitude
H 1.053
L -.253
L -.205
H -.308
H -.345
H 1.006
L -.156

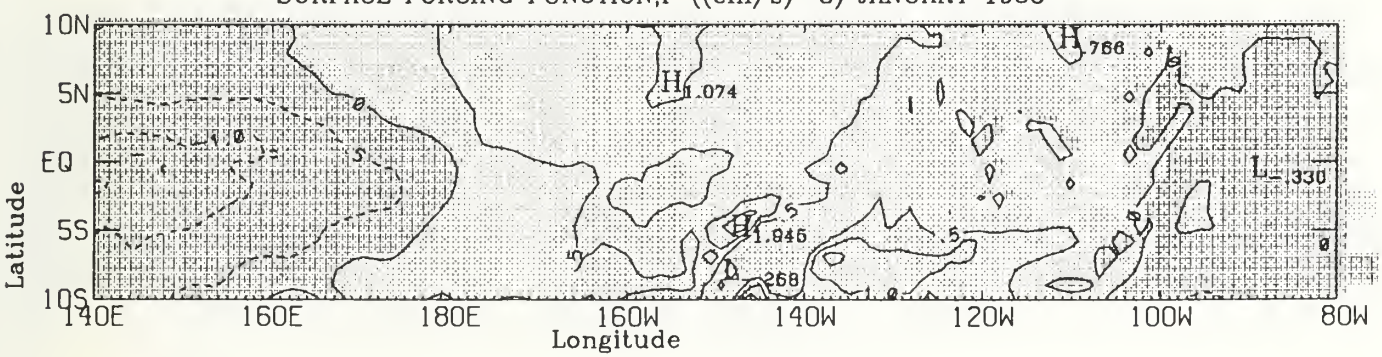
SURFACE FORCING FUNCTION,P ((cm/s)**3) JANUARY 1986
10N
5N
EQ
5S
10S
Latitude
140E
160E
180E
160W
140W
120W
100W
80W
Longitude
H 1.074
H .766
L -.330
H 1.046
L -.268

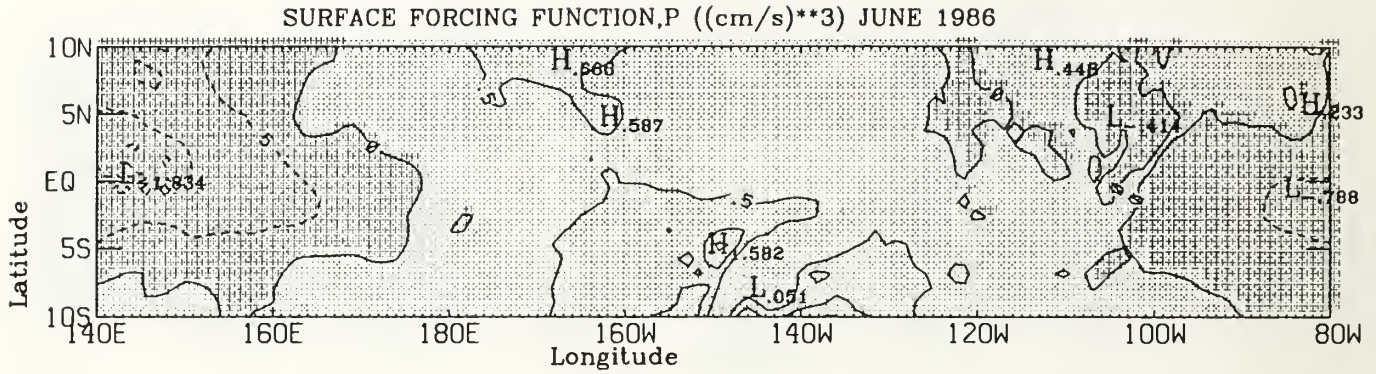
SURFACE FORCING FUNCTION,P ((cm/s)**3) JUNE 1986
10N
5N
EQ
5S
10S
Latitude
140E
160E
180E
160W
140W
120W
100W
80W
Longitude
H .566
H .587
H .448
L -.414
H .233
L -.834
L -.788
H .582
L .051

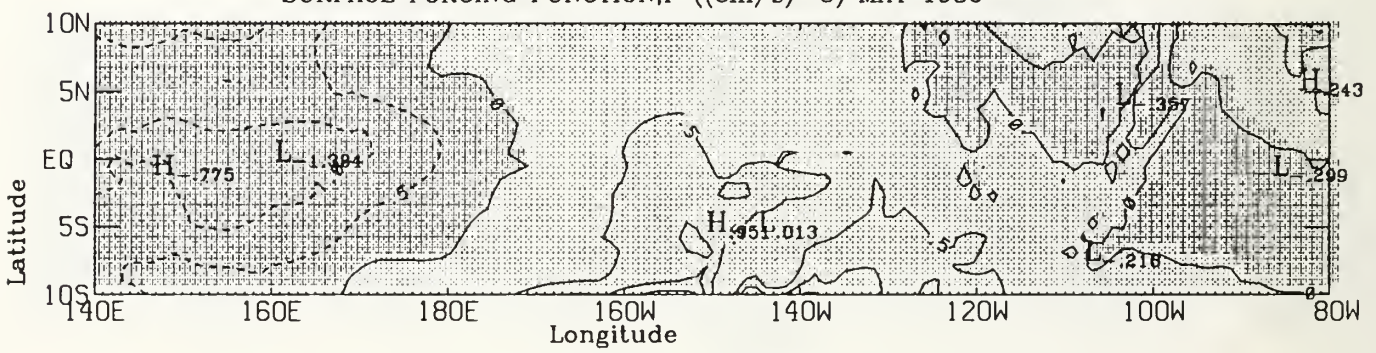
SURFACE FORCING FUNCTION,P ((cm/s)**3) MAY 1986
10N
5N
EQ
5S
10S
Latitude
140E
160E
180E
160W
140W
120W
100W
80W
Longitude
H .243
L -.357
H -.775
L -1.394
L -.299
H .951
H .013
L -.218

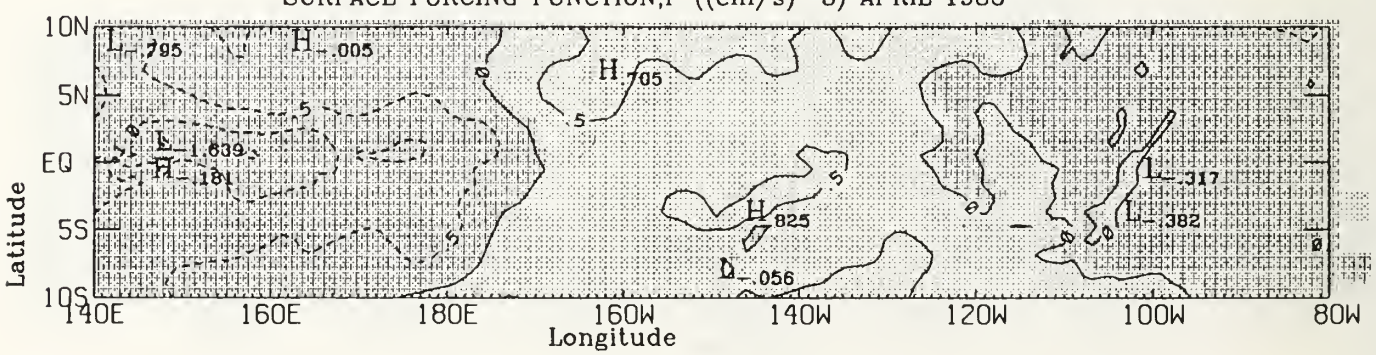
SURFACE FORCING FUNCTION,P ((cm/s)**3) APRIL 1986
10N
5N
EQ
5S
10S
Latitude
140E
160E
180E
160W
140W
120W
100W
80W
Longitude
L -.795
H -.005
H .705
L -1.639
H -.181
L -.317
H .825
L -.382
L -.056

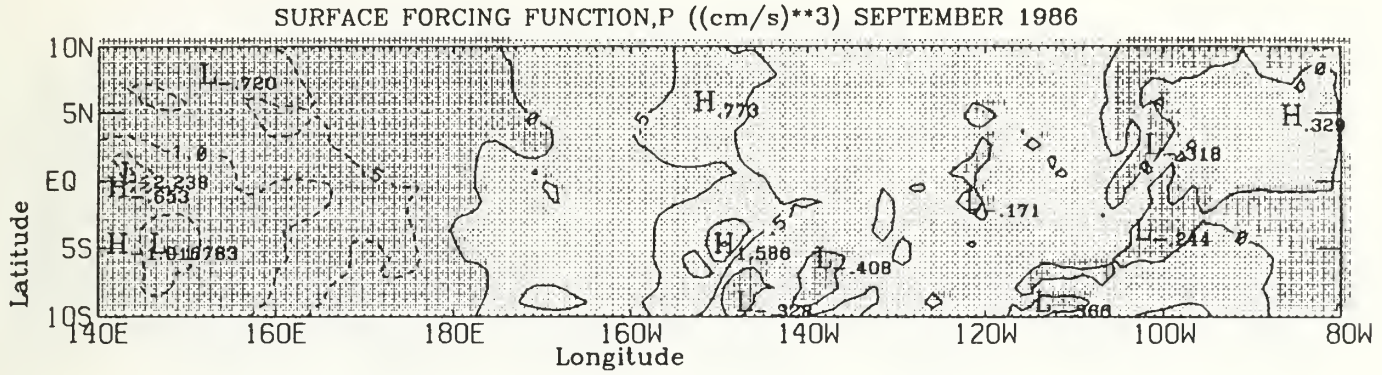
SURFACE FORCING FUNCTION,P ((cm/s)**3) SEPTEMBER 1986
10N
5N
EQ
5S
10S
Latitude
140E
160E
180E
160W
140W
120W
100W
80W
Longitude

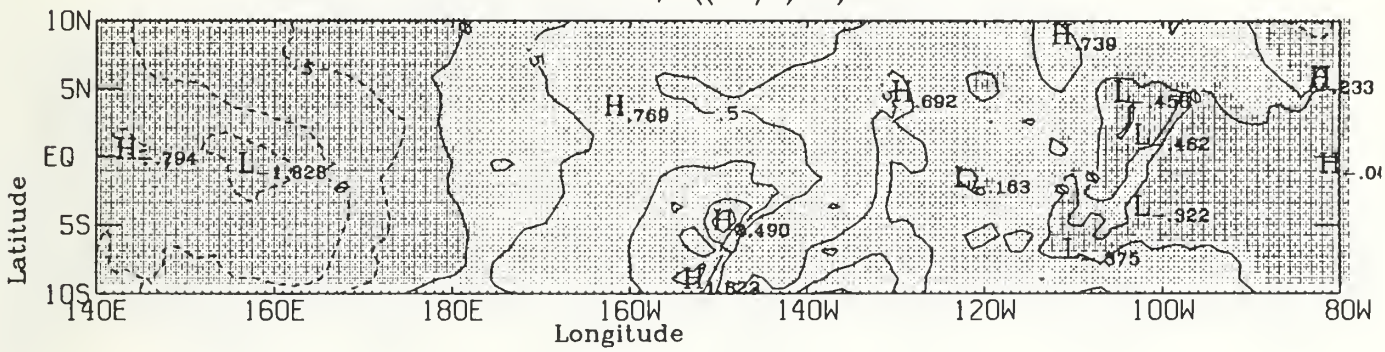
SURFACE FORCING FUNCTION,P ((cm/s)**3) AUGUST 1986
10N
5N
EQ
5S
10S
Latitude
140E
160E
180E
160W
140W
120W
100W
80W
Longitude

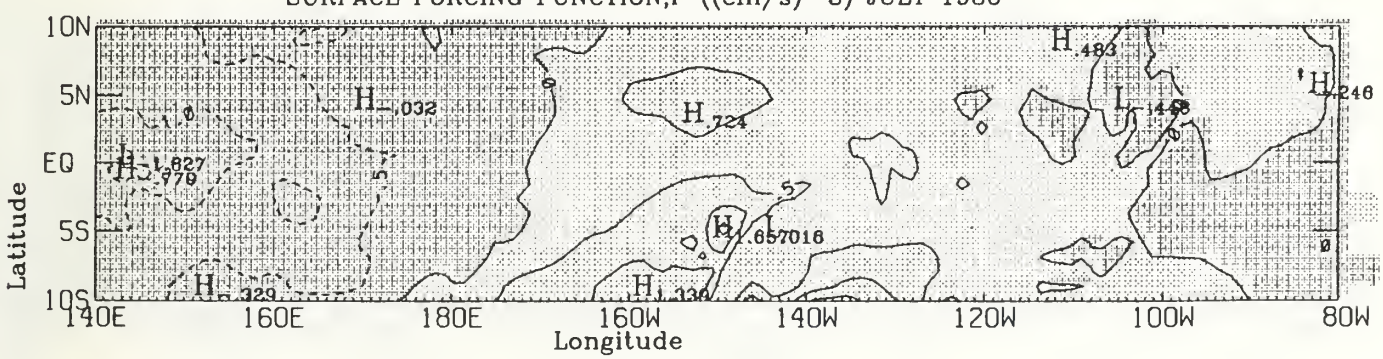
SURFACE FORCING FUNCTION,P ((cm/s)**3) JULY 1986
10N
5N
EQ
5S
10S
Latitude
140E
160E
180E
160W
140W
120W
100W
80W
Longitude

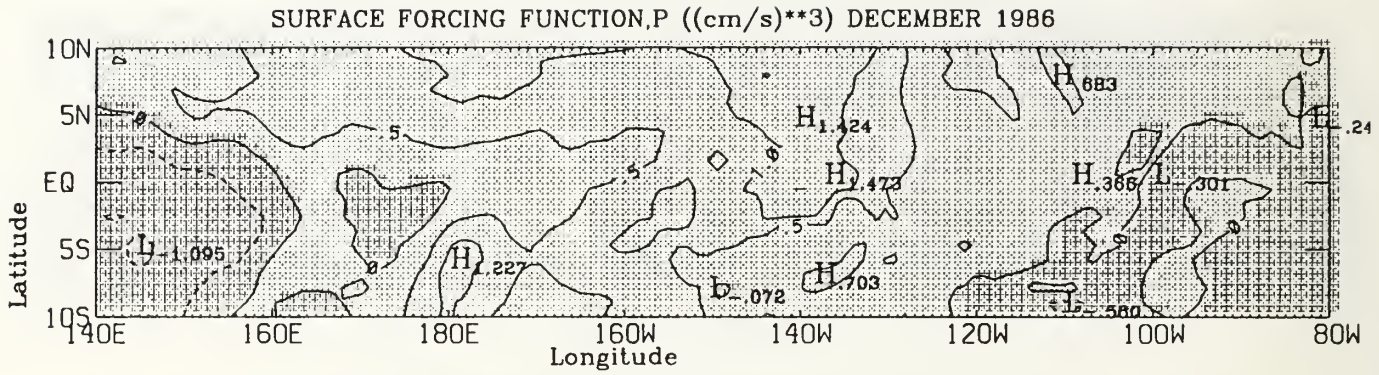
SURFACE FORCING FUNCTION,P ((cm/s)**3) DECEMBER 1986
10N
5N
EQ
5S
10S
140E
160E
180E
160W
140W
120W
100W
80W
Latitude
Longitude
H 683
H 1.424
H 1.473
H .366
L -.301
L -1.095
H 1.227
L -.072
H .703
L -.560

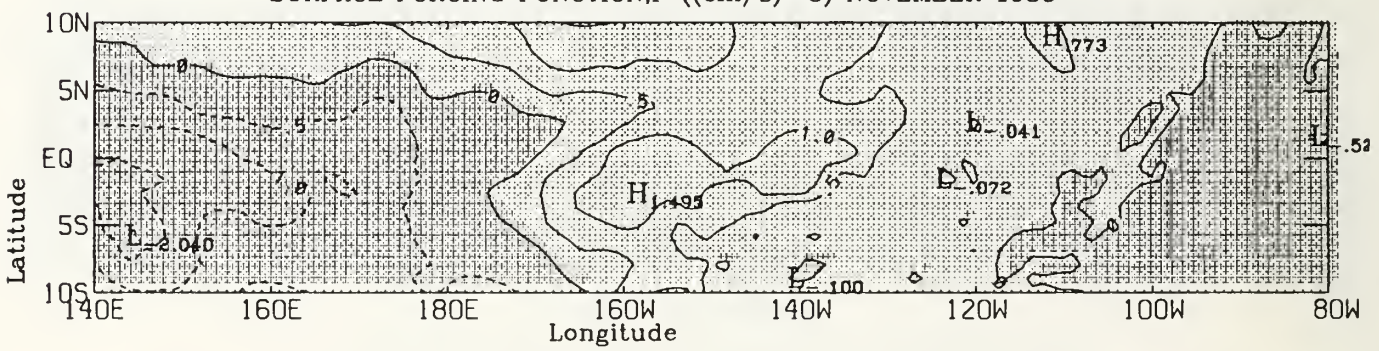
SURFACE FORCING FUNCTION,P ((cm/s)**3) NOVEMBER 1986
10N
5N
EQ
5S
10S
140E
160E
180E
160W
140W
120W
100W
80W
Latitude
Longitude
H .773
L -.041
L -.072
H 1.495
L -2.040
L -.100

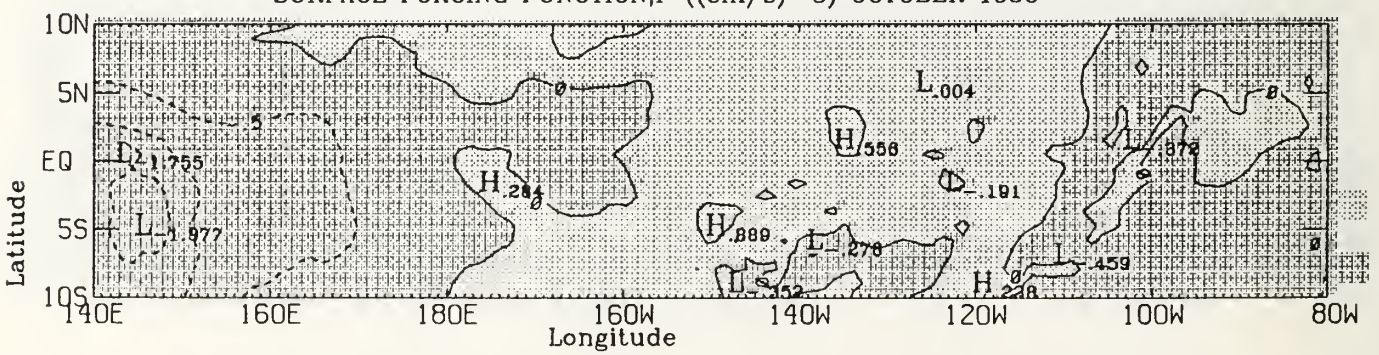
SURFACE FORCING FUNCTION,P ((cm/s)**3) OCTOBER 1986
10N
5N
EQ
5S
10S
140E
160E
180E
160W
140W
120W
100W
80W
Latitude
Longitude
L .004
H .556
L -.872
L -1.755
H .284
L -.191
L -1.977
H .889
L -.278
L -.459
H .228

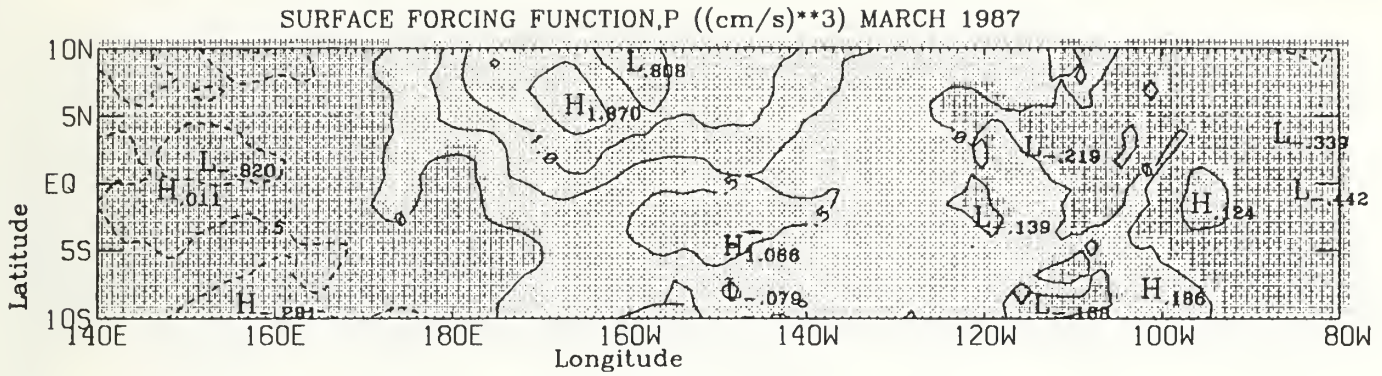
SURFACE FORCING FUNCTION,P ((cm/s)**3) MARCH 1987
10N
5N
EQ
5S
10S
Latitude
140E
160E
180E
160W
140W
120W
100W
80W
Longitude

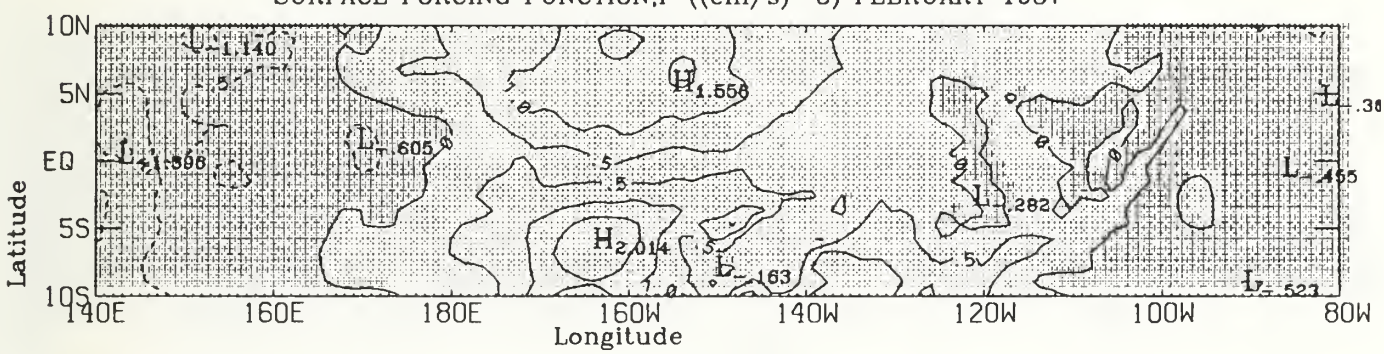
SURFACE FORCING FUNCTION,P ((cm/s)**3) FEBRUARY 1987
10N
5N
EQ
5S
10S
Latitude
140E
160E
180E
160W
140W
120W
100W
80W
Longitude

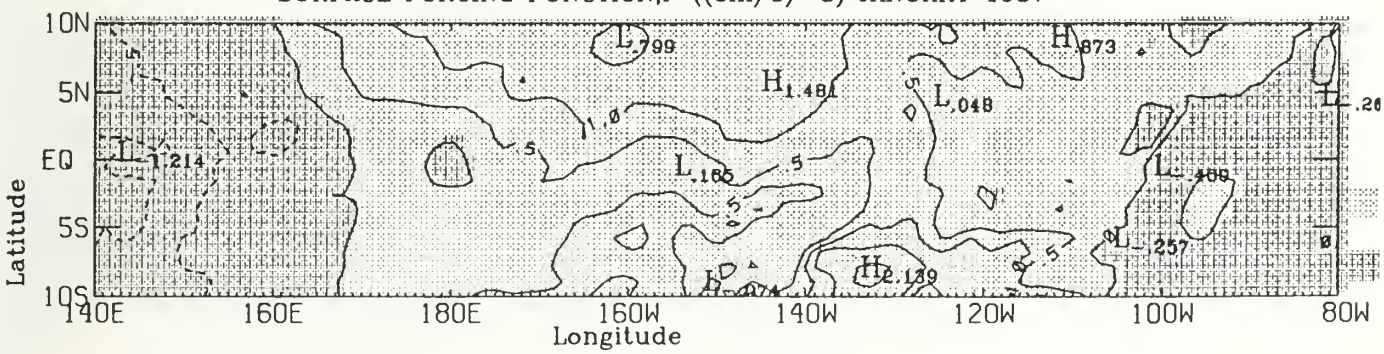
SURFACE FORCING FUNCTION,P ((cm/s)**3) JANUARY 1987
10N
5N
EQ
5S
10S
Latitude
140E
160E
180E
160W
140W
120W
100W
80W
Longitude

SURFACE FORCING FUNCTION,P ((cm/s)**3) JUNE 1987

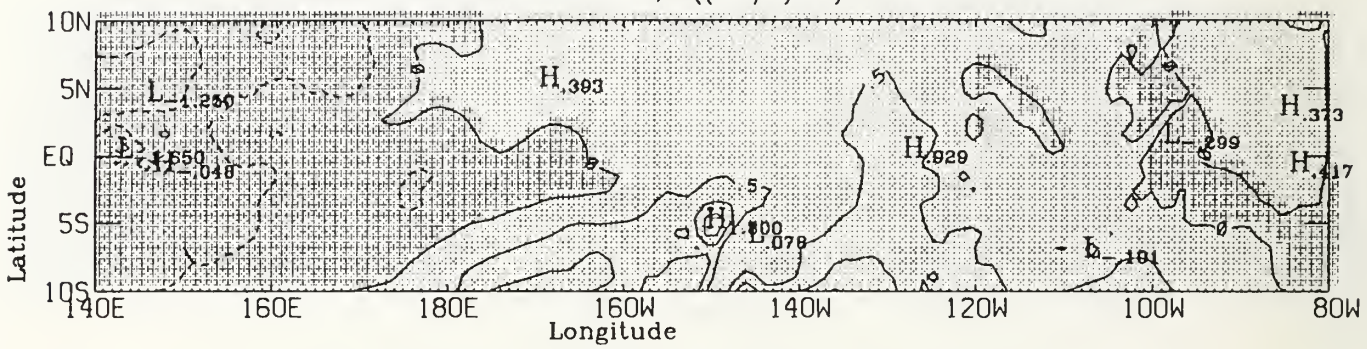

SURFACE FORCING FUNCTION,P ((cm/s)**3) MAY 1987

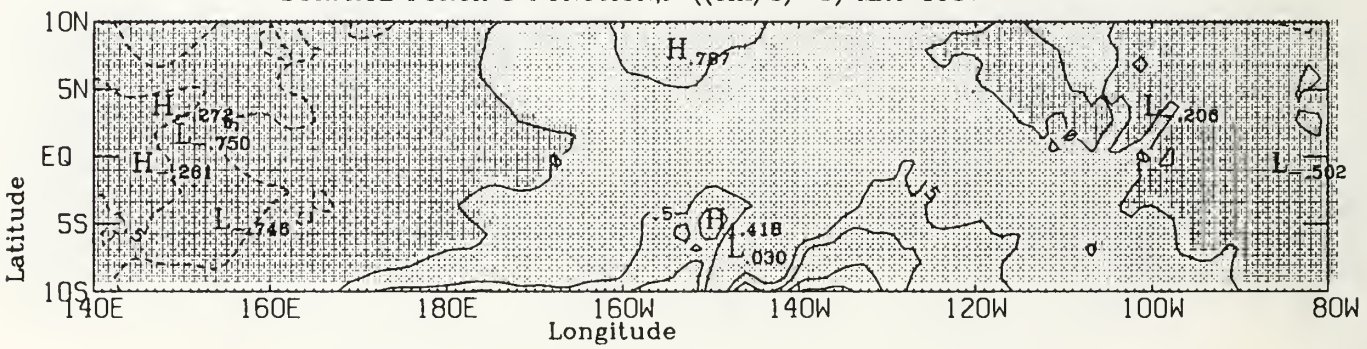

SURFACE FORCING FUNCTION,P ((cm/s)**3) APRIL 1987

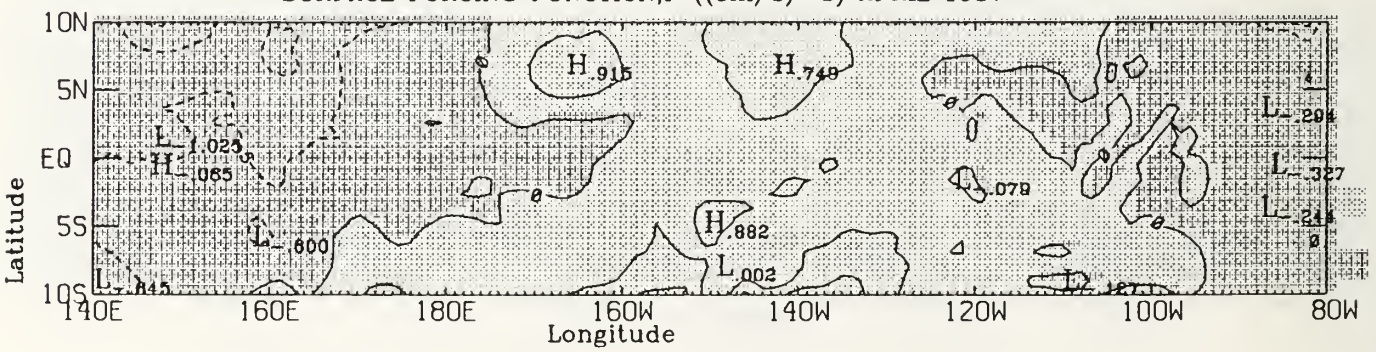

SURFACE FORCING FUNCTION,P ((cm/s)**3) SEPTEMBER 1987

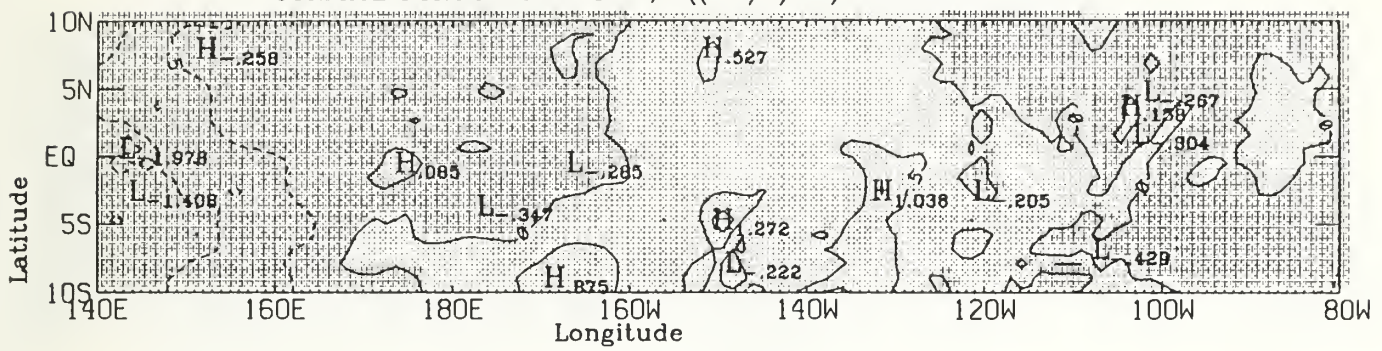

SURFACE FORCING FUNCTION,P ((cm/s)**3) AUGUST 1987

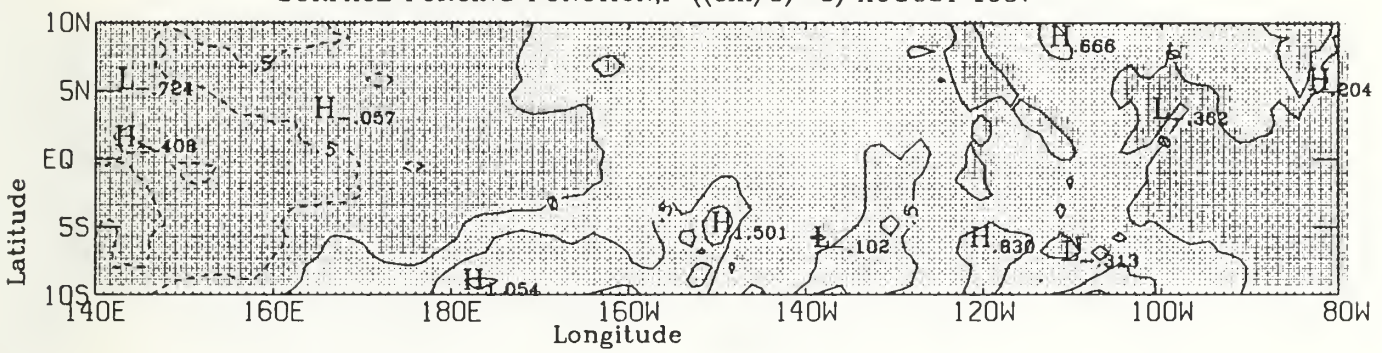

SURFACE FORCING FUNCTION,P ((cm/s)**3) JULY 1987

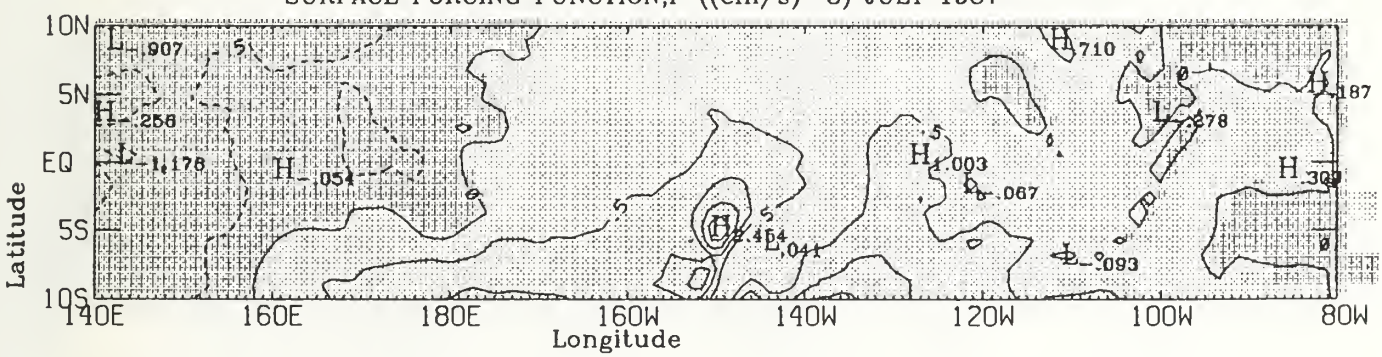

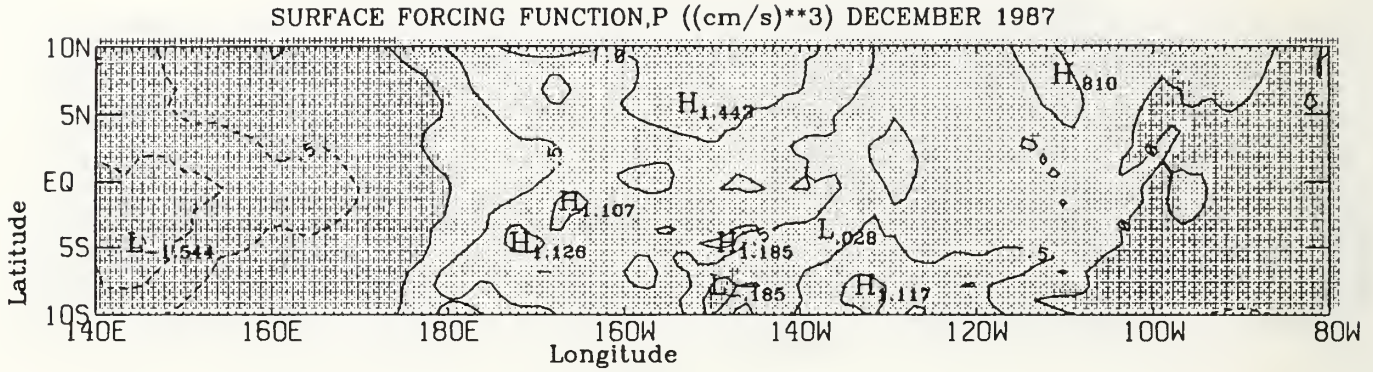
SURFACE FORCING FUNCTION,P ((cm/s)**3) DECEMBER 1987
10N
5N
EQ
5S
10S
Latitude
140E
160E
180E
160W
140W
120W
100W
80W
Longitude
H.810
H1.447
H1.107
H1.126
H1.185
L.028
H1.117
L1.544

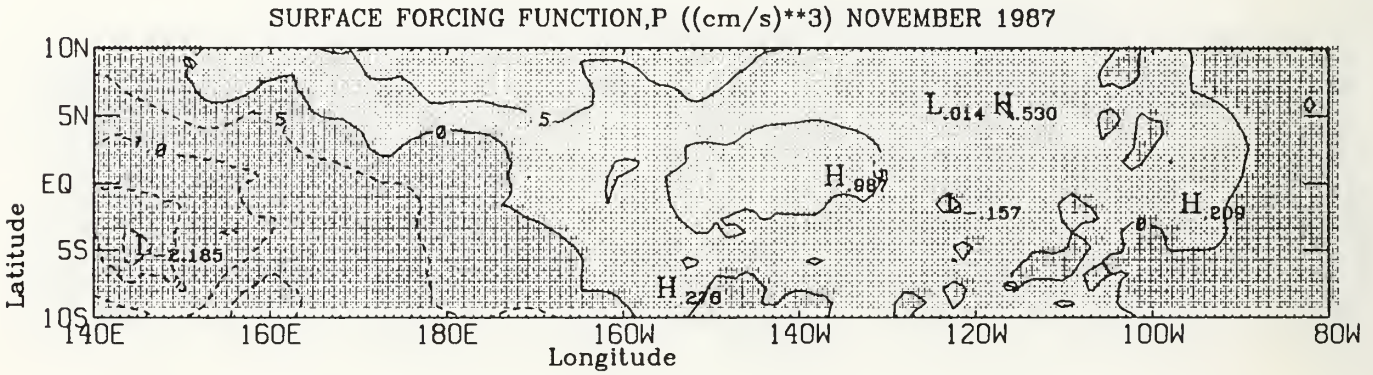
SURFACE FORCING FUNCTION,P ((cm/s)**3) NOVEMBER 1987
10N
5N
EQ
5S
10S
Latitude
140E
160E
180E
160W
140W
120W
100W
80W
Longitude
L.014
H.530
H.887
L.157
H.209
L2.185
H.276

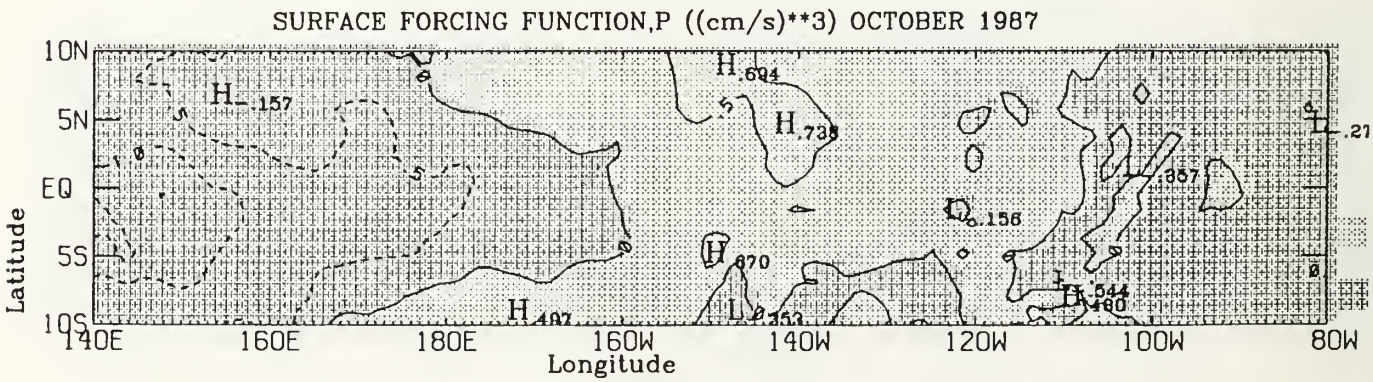
SURFACE FORCING FUNCTION,P ((cm/s)**3) OCTOBER 1987
10N
5N
EQ
5S
10S
Latitude
140E
160E
180E
160W
140W
120W
100W
80W
Longitude
H.694
H.738
H.870
L.156
H.544

APPENDIX F. MONTHLY CORRELATION FIELDS

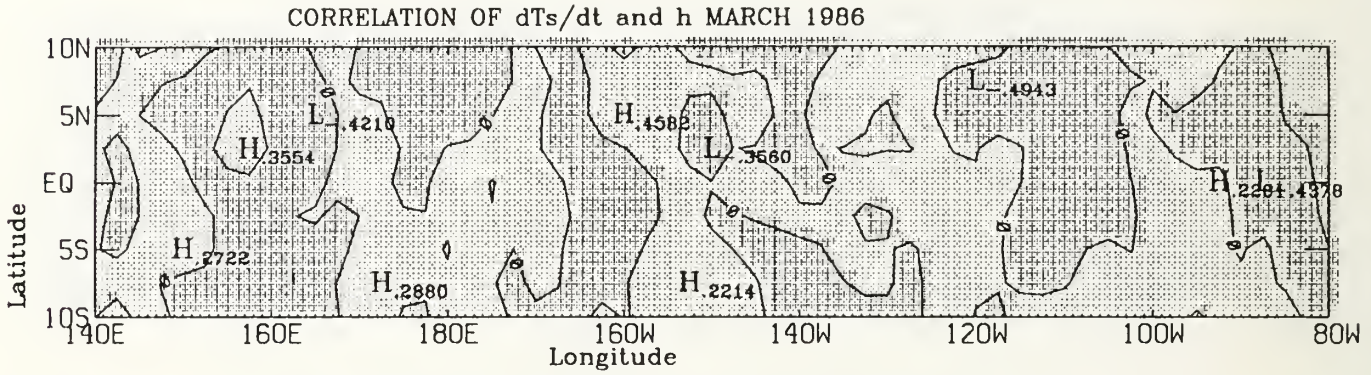
CORRELATION OF dTs/dt and h MARCH 1986
10N
5N
EQ
5S
10S
Latitude
140E
160E
180E
160W
140W
120W
100W
80W
Longitude
L -.4210
H .3554
H .4582
L -.3560
L -.4943
H .2722
H .2880
H .2214
H .2284 .4378

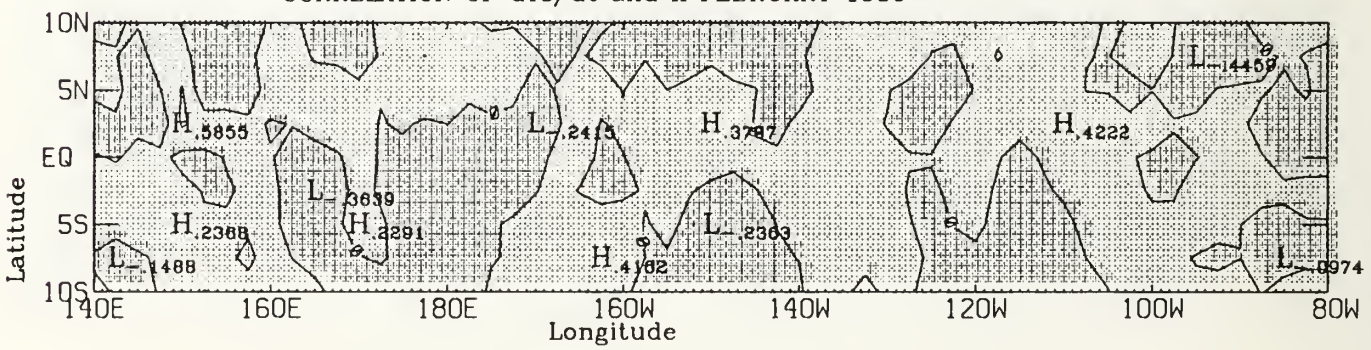
CORRELATION OF dTs/dt and h FEBRUARY 1986
10N
5N
EQ
5S
10S
Latitude
140E
160E
180E
160W
140W
120W
100W
80W
Longitude
H .5855
L -.2413
H .3797
L -.4459
H .4222
L -.3639
H .2368
H .2291
L -.2363
L -.1488
H .4162
L -.0974

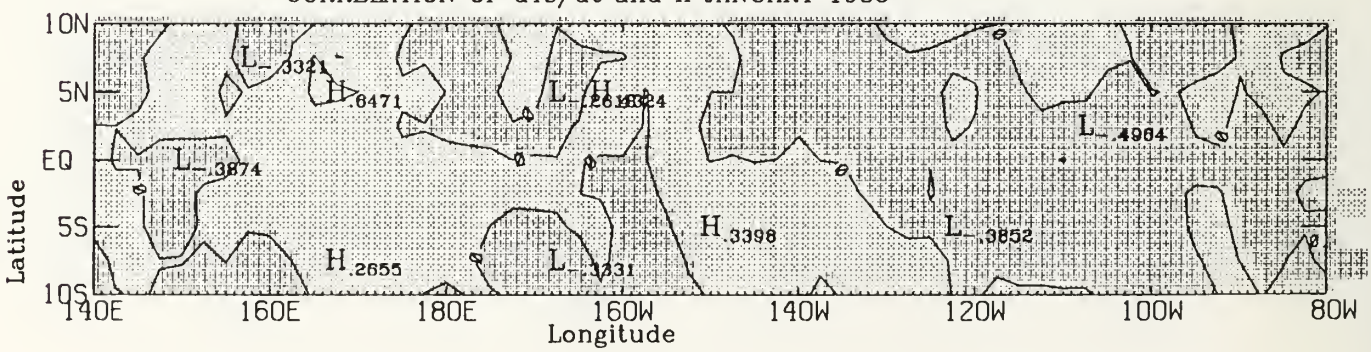
CORRELATION OF dTs/dt and h JANUARY 1986
10N
5N
EQ
5S
10S
Latitude
140E
160E
180E
160W
140W
120W
100W
80W
Longitude
L -.3321
H .6471
L -.3874
L -.4964
H .3398
L -.3852
H .2655
L -.3331

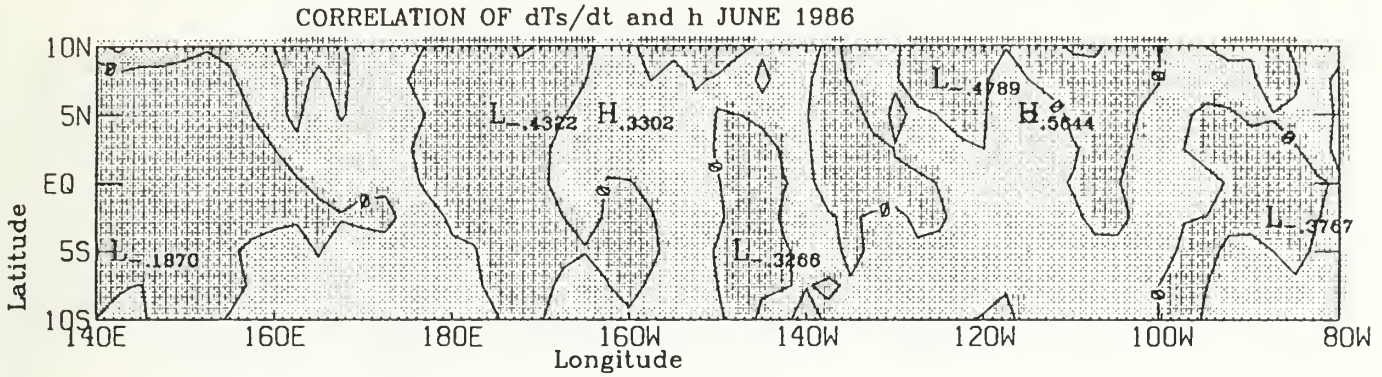
CORRELATION OF dTs/dt and h JUNE 1986
10N
5N
EQ
5S
10S
Latitude
140E
160E
180E
160W
140W
120W
100W
80W
Longitude
L -.4322
H .3302
L -.4789
H .5644
L -.3767
L -.1870
L -.3266

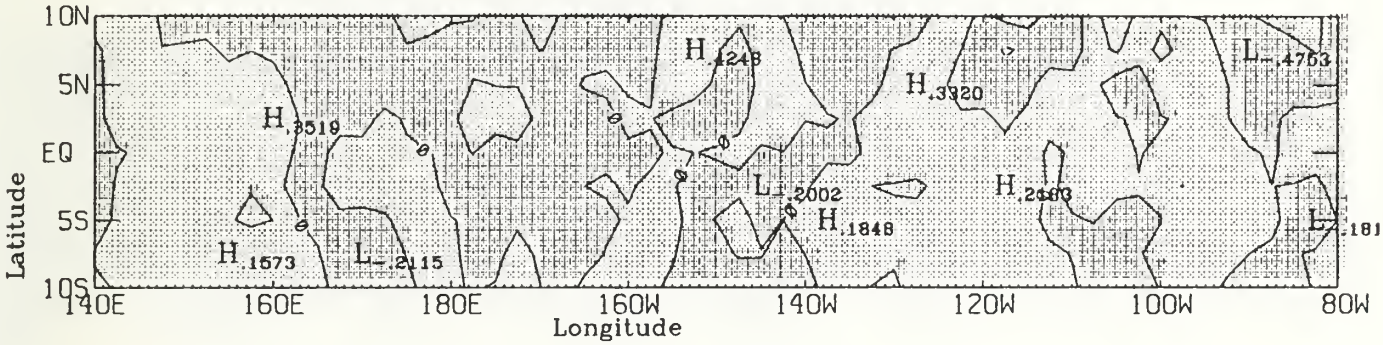
CORRELATION OF dTs/dt and h MAY 1986
10N
5N
EQ
5S
10S
Latitude
140E
160E
180E
160W
140W
120W
100W
80W
Longitude
H .4248
H .3320
L -.4753
H .3519
L -.2002
H .2483
H .1848
H .1573
L -.2115

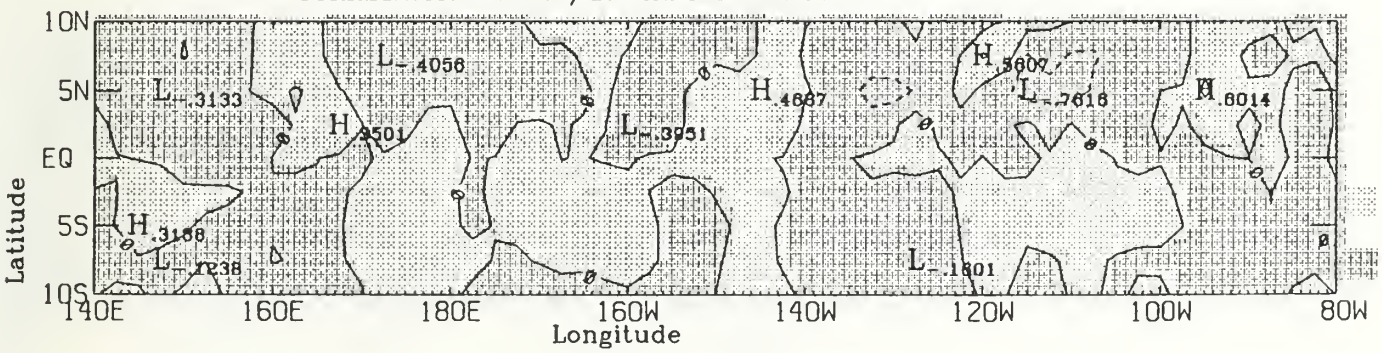
CORRELATION OF dTs/dt and h APRIL 1986
10N
5N
EQ
5S
10S
Latitude
140E
160E
180E
160W
140W
120W
100W
80W
Longitude
L -.4056
L -.3133
H .4687
H .3609
L -.7616
H .6014
H .3501
L -.3951
H .3168
L -.1238
L -.1801

CORRELATION OF dTs/dt and h SEPTEMBER 1986

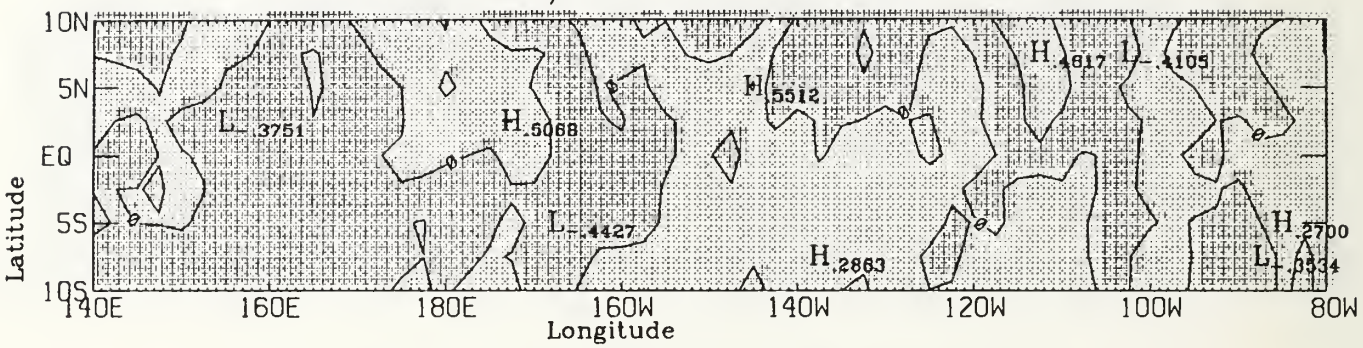

CORRELATION OF dTs/dt and h AUGUST 1986

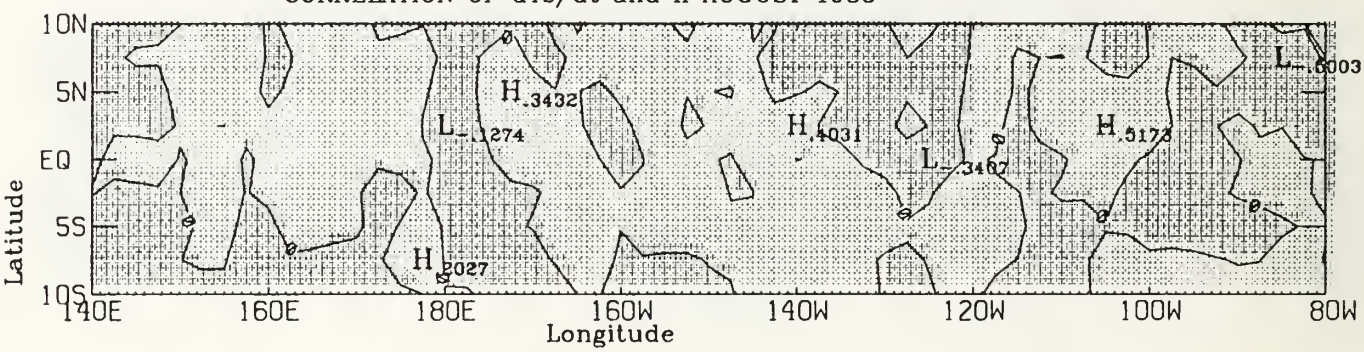

CORRELATION OF dTs/dt and h JULY 1986

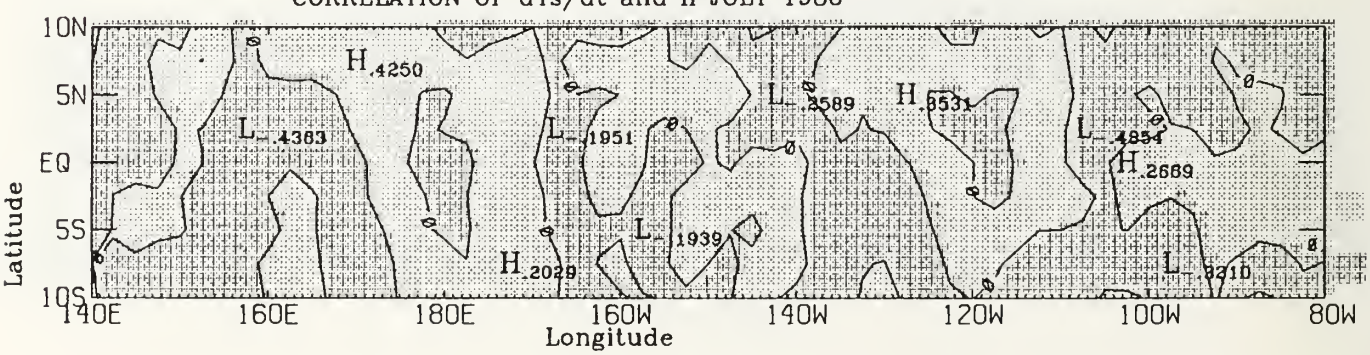

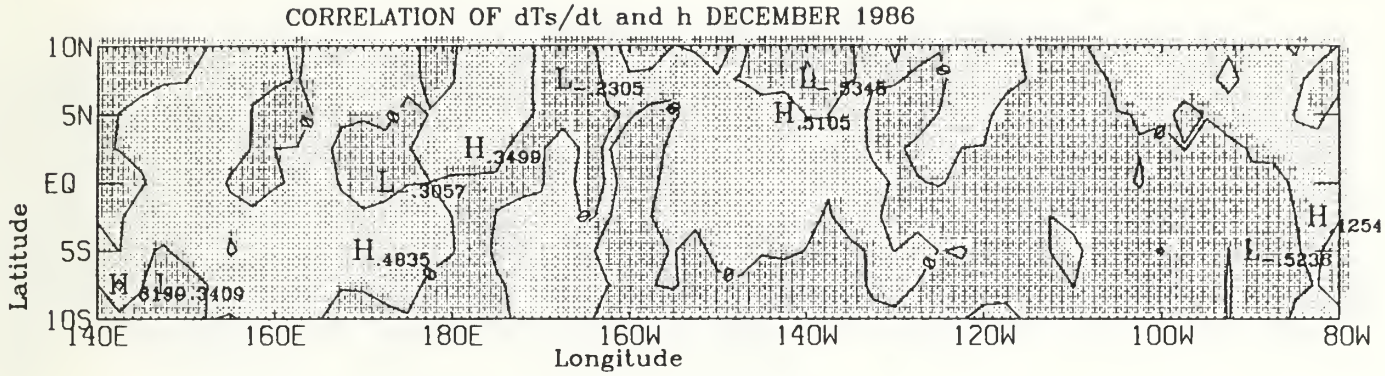
CORRELATION OF dTs/dt and h DECEMBER 1986
10N
5N
EQ
5S
10S
Latitude
140E
160E
180E
160W
140W
120W
100W
80W
Longitude
L -.2305
L -.3345
H .3105
H .3499
L -.3057
H .4835
H .6190 .3409
H .1254
L -.1523

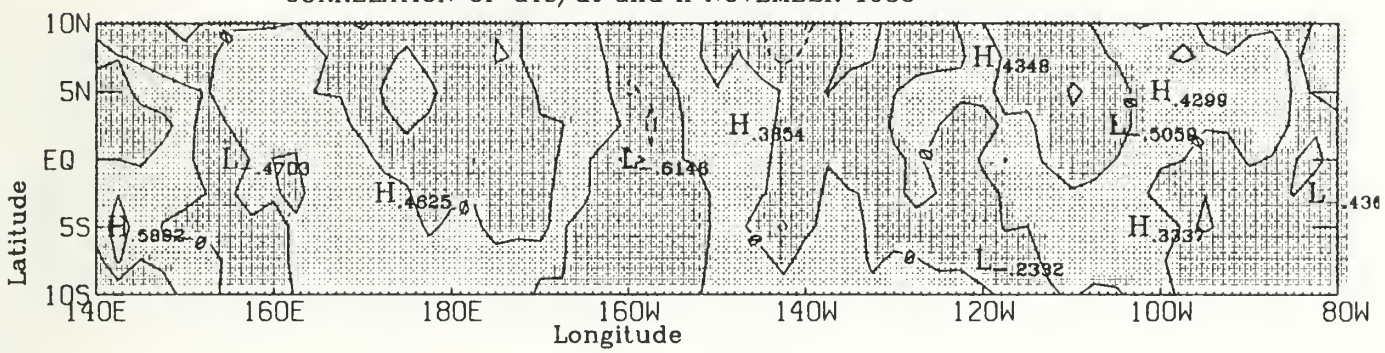
CORRELATION OF dTs/dt and h NOVEMBER 1986
10N
5N
EQ
5S
10S
Latitude
140E
160E
180E
160W
140W
120W
100W
80W
Longitude
H .4348
H .4299
H .3854
L -.5059
L -.4700
L -.6146
H .4625
H .5882
L -.2392
H .3337

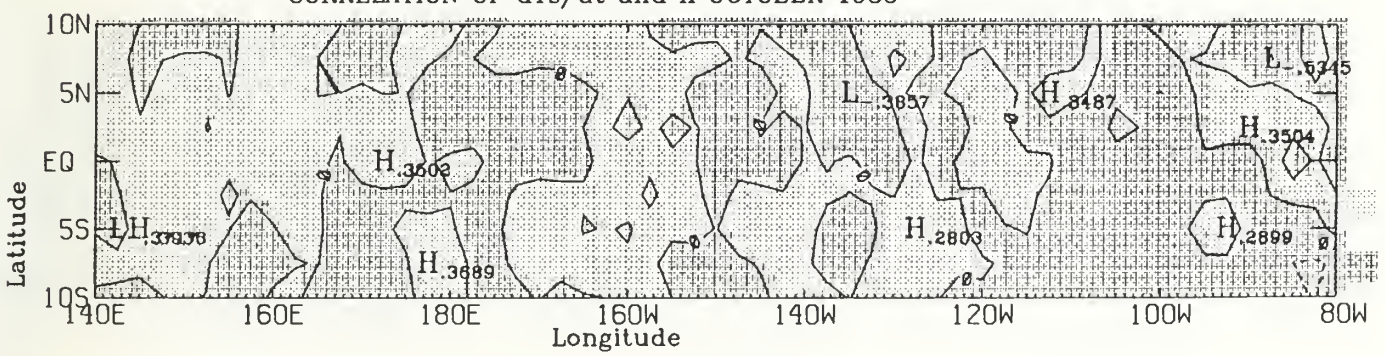
CORRELATION OF dTs/dt and h OCTOBER 1986
10N
5N
EQ
5S
10S
Latitude
140E
160E
180E
160W
140W
120W
100W
80W
Longitude
L -.5345
L -.3857
H .3487
H .3504
H .3502
H .3936
H .2803
H .2899
H .3689

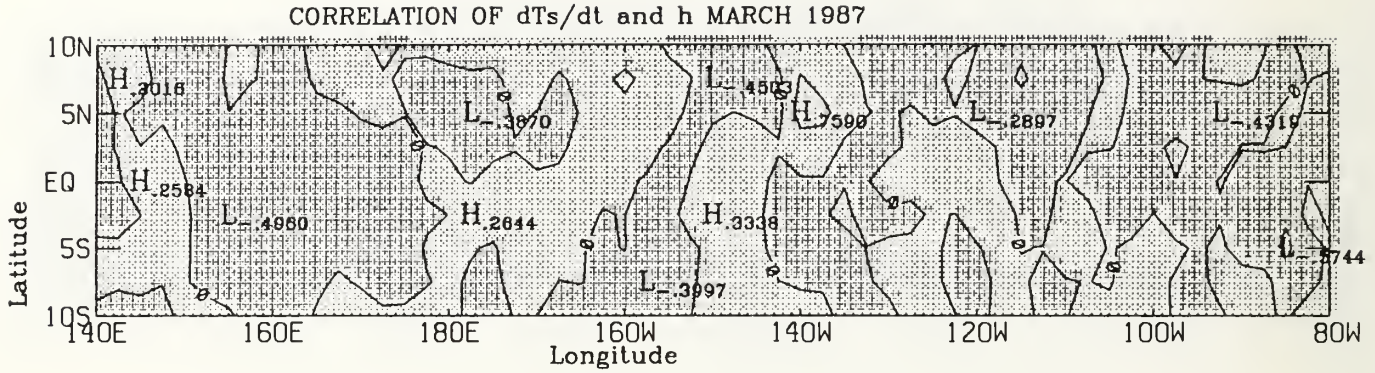
CORRELATION OF dTs/dt and h MARCH 1987
10N
5N
EQ
5S
10S
Latitude
140E
160E
180E
160W
140W
120W
100W
80W
Longitude
H .3016
L -.3870
L -.4503
H .7590
L -.2897
L -.4310
H .2584
L -.4980
H .2644
H .3338
L -.3997
L -.3744

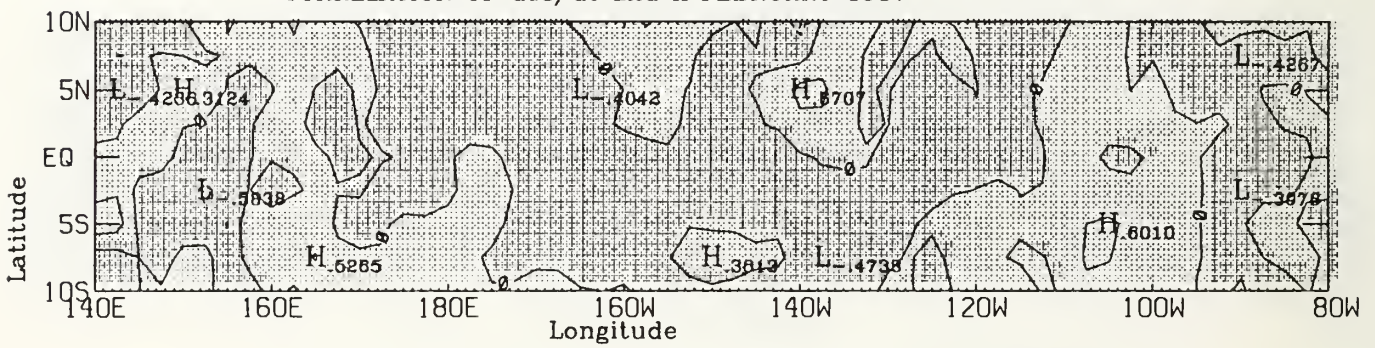
CORRELATION OF dTs/dt and h FEBRUARY 1987
10N
5N
EQ
5S
10S
Latitude
140E
160E
180E
160W
140W
120W
100W
80W
Longitude
L -.4267
L -.4042
H .5707
H .3124
L -.5838
L -.3678
H .6010
H .5265
H .3813
L -.4738

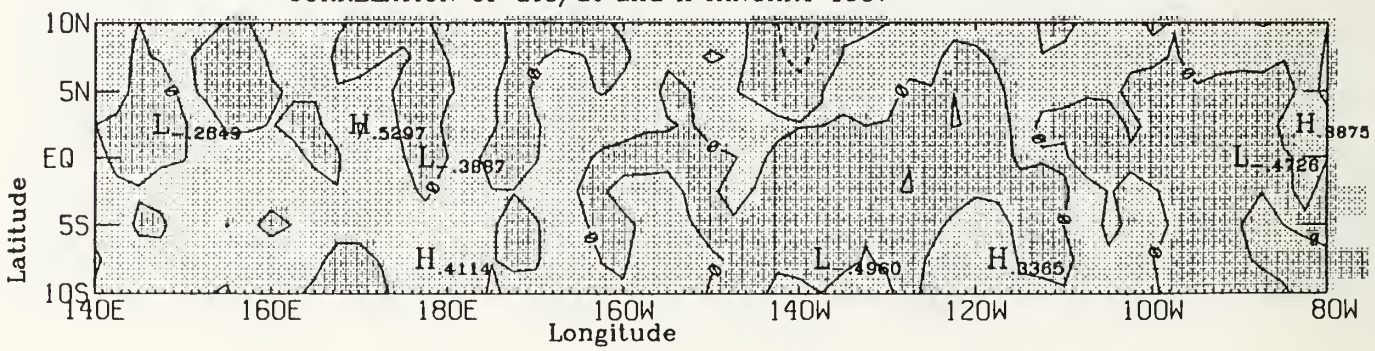
CORRELATION OF dTs/dt and h JANUARY 1987
10N
5N
EQ
5S
10S
Latitude
140E
160E
180E
160W
140W
120W
100W
80W
Longitude
L -.2849
H .5297
L -.3887
H .3875
L -.4726
H .4114
L -.4960
H .3365

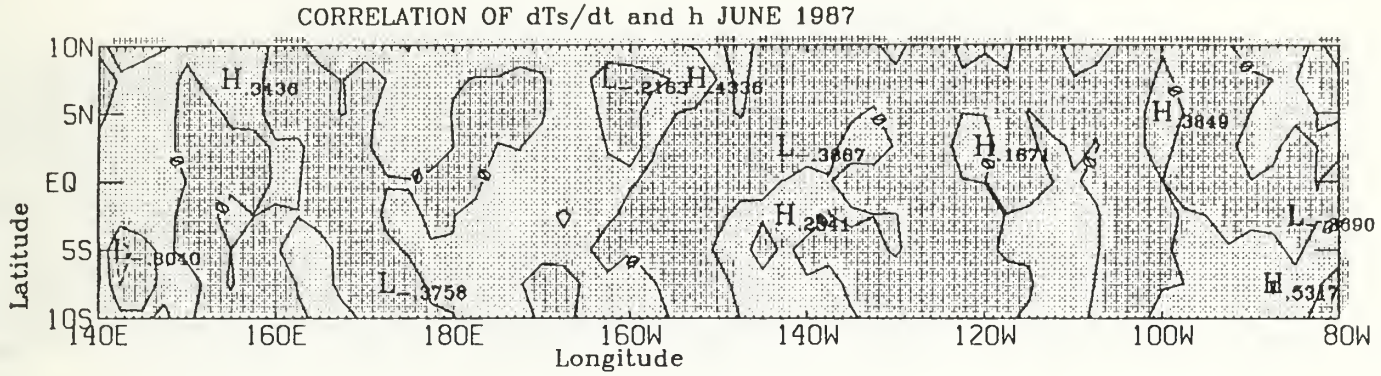
CORRELATION OF dTs/dt and h JUNE 1987
10N
5N
EQ
5S
10S
Latitude
140E
160E
180E
160W
140W
120W
100W
80W
Longitude
H .3436
L -.2163
H .4336
L -.3667
H .1671
H .3849
L -.3758
H .5317

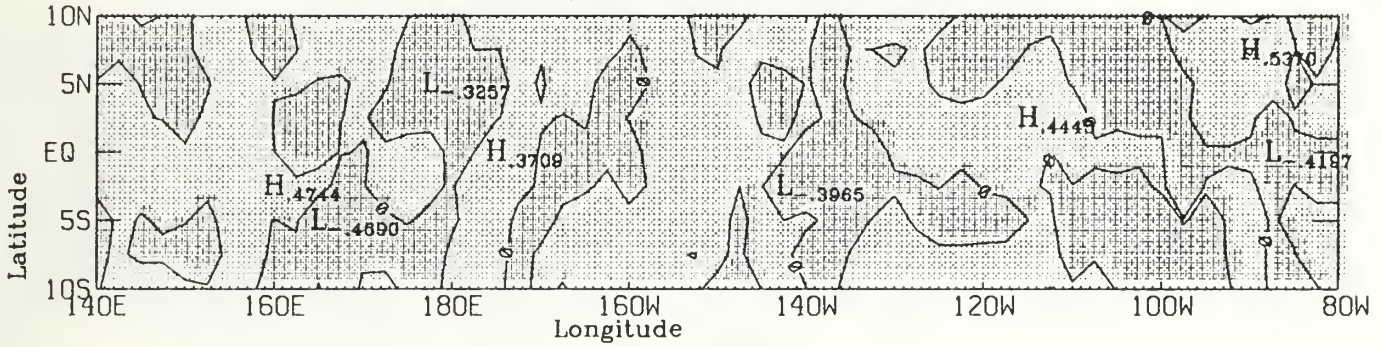
CORRELATION OF dTs/dt and h MAY 1987
10N
5N
EQ
5S
10S
Latitude
140E
160E
180E
160W
140W
120W
100W
80W
Longitude
L -.3257
H .3709
H .4744
L -.4690
L -.3965
H .4449
H .5370
L -.4197

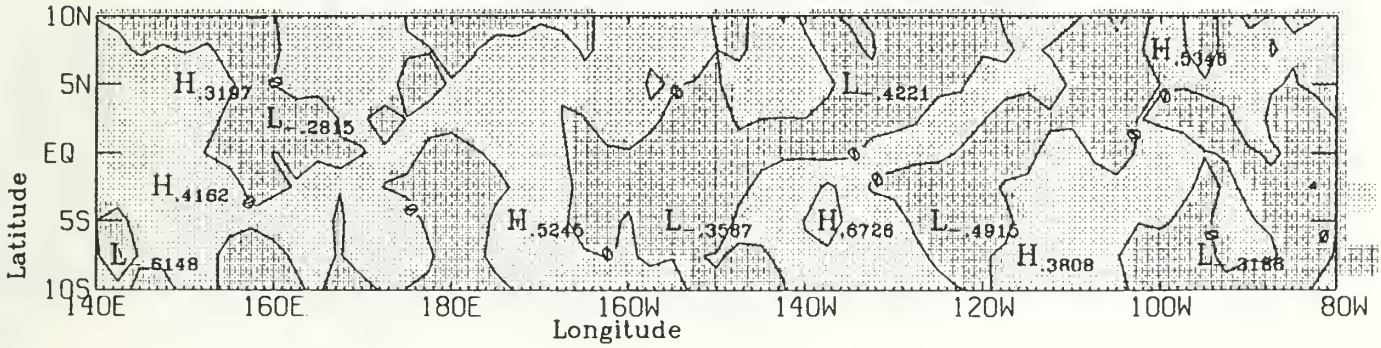
CORRELATION OF dTs/dt and h APRIL 1987
10N
5N
EQ
5S
10S
Latitude
140E
160E
180E
160W
140W
120W
100W
80W
Longitude
H .3197
L -.2815
H .4162
L -.6148
H .5246
L -.3587
L -.4221
H .6726
L -.4916
H .3808
H .5146
L -.3186

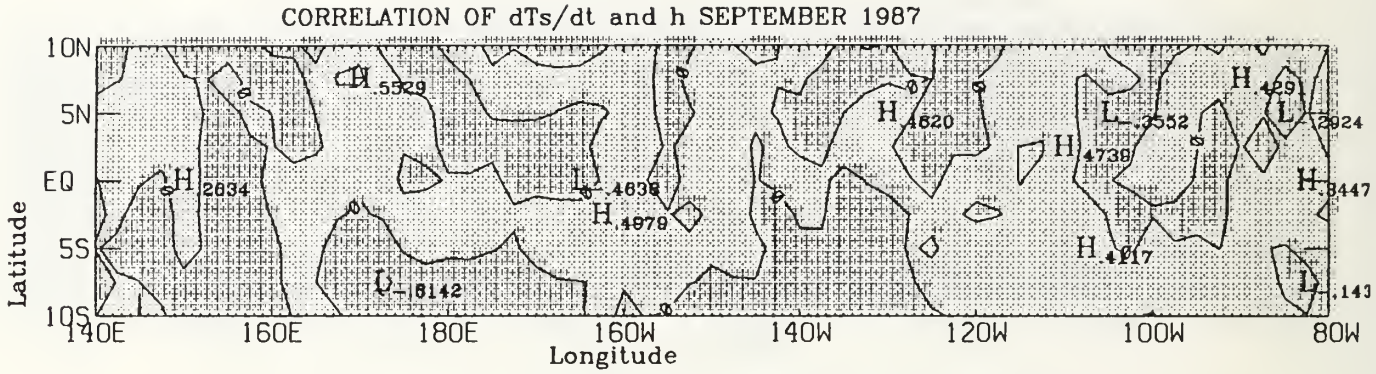
CORRELATION OF dTs/dt and h SEPTEMBER 1987
10N
5N
EQ
5S
10S
Latitude
140E
160E
180E
160W
140W
120W
100W
80W
Longitude
H .5329
H .4620
L -.3552
H .4739
H .4917
H .2834
L -.4638
H .4979
L -.6142
L -.143

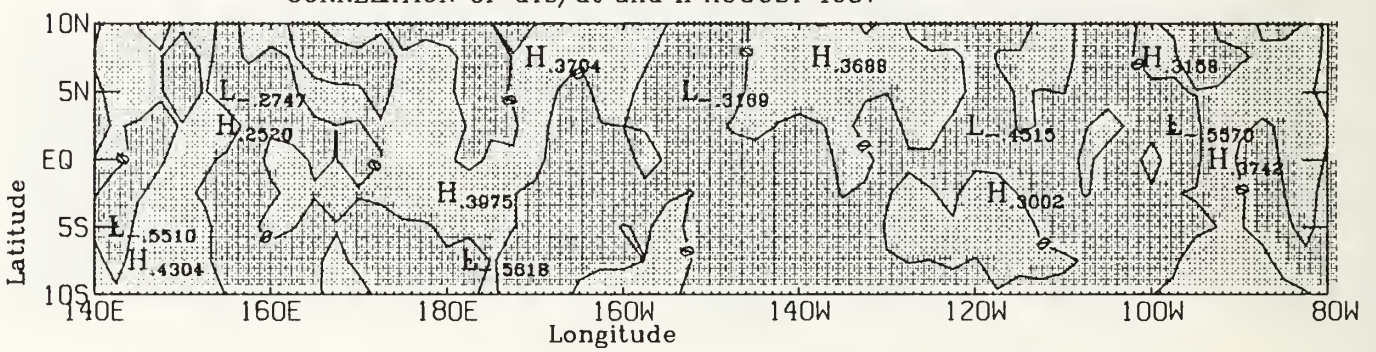
CORRELATION OF dTs/dt and h AUGUST 1987
10N
5N
EQ
5S
10S
Latitude
140E
160E
180E
160W
140W
120W
100W
80W
Longitude
H .3794
H .3688
H .3168
L -.2747
L -.3169
H .2520
L -.4515
L -.5570
H .3975
H .3002
L -.5510
H .4304
L -.5618

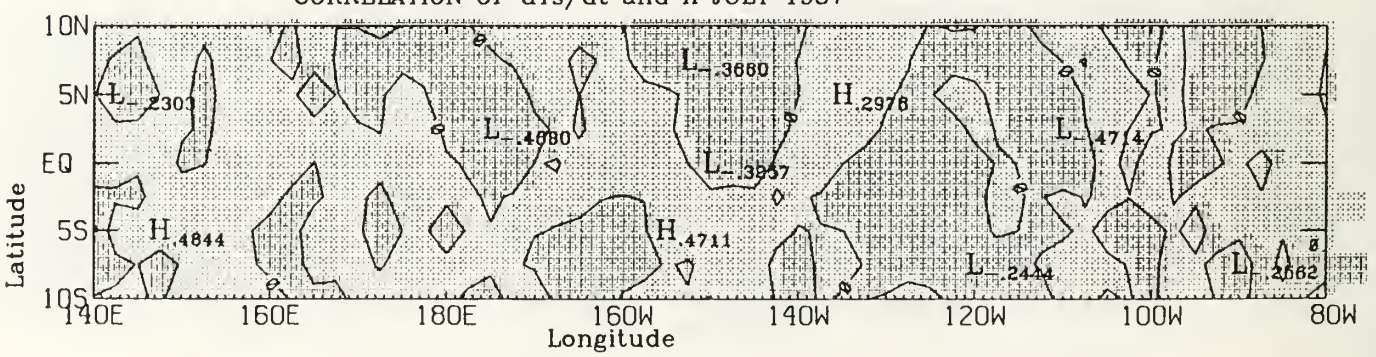
CORRELATION OF dTs/dt and h JULY 1987
10N
5N
EQ
5S
10S
Latitude
140E
160E
180E
160W
140W
120W
100W
80W
Longitude
L -.3660
H .2976
L -.2303
L -.4080
L -.4714
L -.3957
H .4844
H .4711
L -.2444
L -.2662

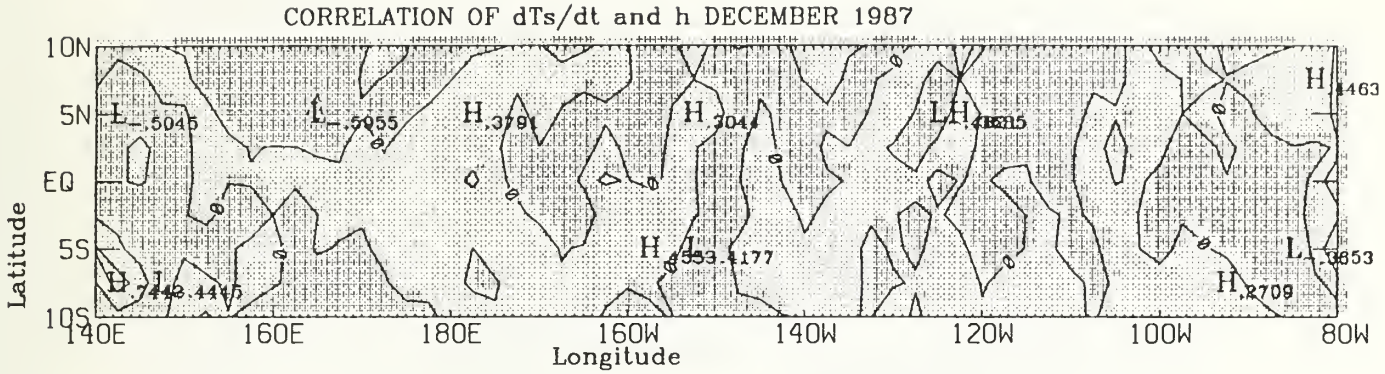
CORRELATION OF dTs/dt and h DECEMBER 1987
10N
5N
EQ
5S
10S
Latitude
140E
160E
180E
160W
140W
120W
100W
80W
Longitude

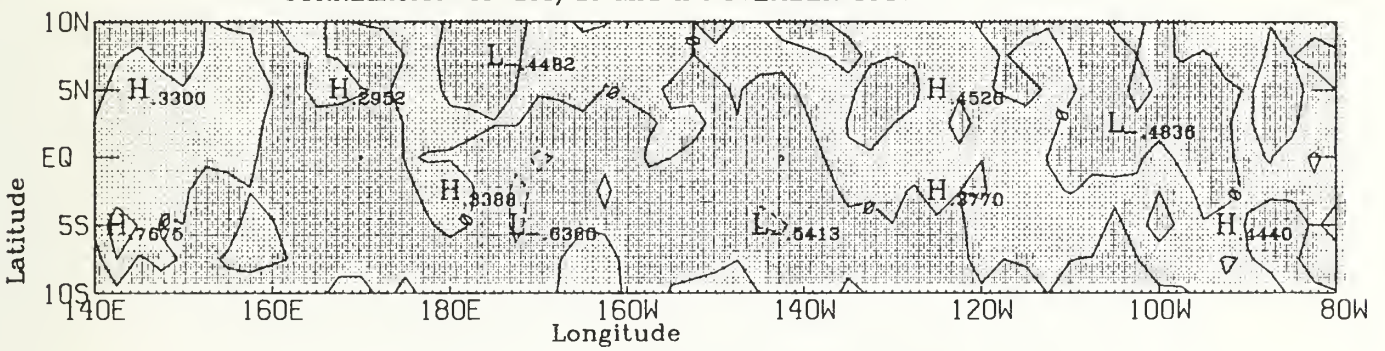
CORRELATION OF dTs/dt and h NOVEMBER 1987
10N
5N
EQ
5S
10S
Latitude
140E
160E
180E
160W
140W
120W
100W
80W
Longitude

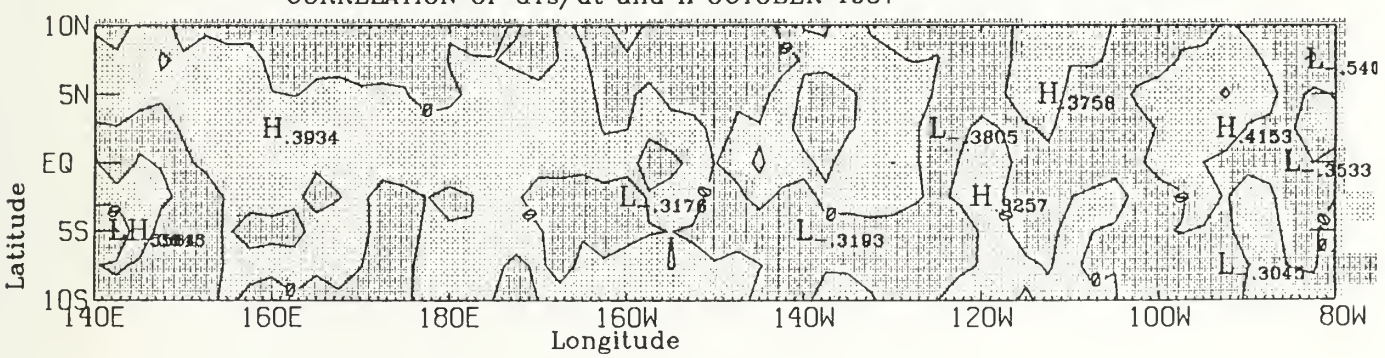
CORRELATION OF dTs/dt and h OCTOBER 1987
10N
5N
EQ
5S
10S
Latitude
140E
160E
180E
160W
140W
120W
100W
80W
Longitude

INITIAL DISTRIBUTION LIST

		No. Copies
1.	Attn: Library, Code 52 Naval Postgraduate School Monterey, CA 93940-5000	2
2.	Superintendent Attn: Chairman, Department of Oceanography (Code OCCo) Naval Postgradute Monterey, CA 93940-5000	1
3.	Superintendent Attn: Associate Professor P. C. Chu (Code OCCu) Naval Postgraduate School Monterey, CA 93940-5000	1
4.	Superintendent Attn: Professor R. W. Garwood (Code OCGd) Naval Postgraduate School Monterey, CA 93940-5000	1
5.	Commanding Officer Naval Research Laboratory Stennis Space Center, MS 39529-5000	1
6.	Defense Technical Information Center Cameron Station Alexandria, Virginia 22314-6145	2

Thesis
S6782 Steadley
c.1 Thermodynamic air/ocean
feedback mechanisms in
the equatorial Pacific.